Development and optimization of high intensity solid state - excimer hybrid laser systems and their application for short pulse material processing

Dissertation

towards the PhD degree

by

József Békési

University of Szeged

Department of Experimental Physics

Szeged

2003

The experimental results presented by the author were reached as a member of the Department of Experimental Physics at the University of Szeged (Szeged, Hungary) at the Laser Laboratorium Göttingen (Göttingen, Germany) in the scope of a collaboration work between the two institutes.

Supervisor: **Dr. Péter Simon**

Internal Consulent: **Prof. Sándor Szatmári**

Table of Contents

1. Introduction

Over the last years a revolution has occurred in our ability to produce high power and extremely high intensity pulses using more and more compact laser systems. The key parameters for an immense increase of intensity are the short pulse duration and the short wavelength. The short radiation time allows us to transfer relatively high-energy pulses in very short time intervals and so to reach high peak powers. If additionally the given power can be concentrated over a very small area, production of intensities up to 10^{21} W/cm^2 becomes possible. This is the point where short wavelength systems have ultimate advantages, because the minimum achievable irradiated spot size scales with the wavelength.

The ability to reach high intensity short pulses with a small-scale laser system opens the way to study a plenty of new areas of physics also in small laboratories. Such areas can be fusion research, relativistic plasma physics, higher harmonics generation or a new regime of laser matter interaction etc. in the tera- or petawatt region. It is fascinating to think, that such environments can be re-created in university laboratories, which usually can only be found in stellar interiors (At around 10^{21} W/cm^2 intensity the field strength is in the order of TV/cm which is about 100 times the Coulombic field binding the ground state electron in the hydrogen atom.), switching the role of the scientist from observer to actor. Already at relatively moderate intensities application of short pulses opens new possibilities also for high precision material processing studies, where the advantages of short wavelength sources are specially pronounced.

Nowadays the used short pulse lasers are predominantly solid-state systems operating in the infrared (IR) spectral region. The reason for the fast development of short pulse solid state lasers was the appearance of the chirped pulse amplification (CPA) technique (invented for the optical spectral range by Gerard Mourou in 1985), solving the nonlinearity problems for short pulse duration in the high saturation energy density solid state active media (more detailed in 2.1). Only relatively moderate scientific forces were concentrated on the development of table-top ultraviolet (UV) systems. In numerous applications, however, high intensity fs pulses in the UV wavelength region have ultimate advantages compared to longer wavelengths. The most powerful candidates are hybrid dye – excimer or solid state – excimer

laser systems (because of the difficulties of ultrashort pulse generation in the UV). In the beginning dye laser front-end systems dominated this field. However, the fast development of reliable solid state sources opened the way for the development of compact and reliable solid state - excimer laser systems, taking over the task of dye lasers used before.

The aims of the present work are to develop compact and reliable short pulse UV systems, optimizing them for the requirement of different applications and the study of possible applications specially concentrating on the field of short pulse micromaterial processing. According to these aims the dissertation is organized as follows. After the present introduction a brief description of the techniques and theories related to the scope of this work is given as a scientific background in chapter 2. A summary of the present state of the art of high power short pulse laser systems together with a historical overview of the development of short pulse lasers is given in 2.1. The next two sessions (2.2 and 2.3) deal with the fundamentals of short pulse amplification in excimers, the limitations of such systems and possible solutions of the problems using different optical arrangements like off-axis amplification (2.3.1) or interferometric multiplexing (2.3.2). Closing the circle of the introduced theories, a brief description of short pulse ablation models is given in 2.4, focused on the differences between long and short pulse ablation processes. The 3rd chapter gives a detailed description of the recent achievements in the development and optimization of short pulse solid state – excimer (and dye – excimer in 3.4) hybrid laser systems. The basic concept of short pulse hybrid laser systems has been described in 3.1. The used front-ends and the frequency tripling unit are introduced in 3.2. In 3.3 and 3.4 experimental results of the application of two different optical setups are described obtained with a modified excimer amplifier module, where optimized operation was maintained for the requirements of different front-ends. Systems delivering output energies of over 50 mJ (3.3) up to 100 mJ (3.4) in a single subpicosecond UV pulse are reported here with some 10 Hz repetition rates. In numerous applications (specially in industrial environment) however moderate intensities but a large number of pulses are required. In 3.5 a newly developed high average power solid state – excimer hybrid short pulse UV source is introduced. This is the point, where solid state front-ends are favorable not only because of their stability and reliability but also because of their high repetition rate. A system consisting of a Ti:Sa front-end and a modified excimer module capable to operate up to 300-350 Hz (NovaLine, Lambda Physik) is described here.

Making use of the unique possibilities of the above described laser systems various results in different application fields like the generation of efficient XUV pulses, investigation of short pulse ablation properties of different materials, metal deposition on silicon and polymer surfaces, application of diffractive phase elements at 248 nm, generation of gratings with grating periods down to 300 nm, and drilling of submicron-size holes on practically all kind of solids etc. becomes possible. Investigations dealing with such application possibilities of short UV pulses are presented in the 4th chapter. In 4.1 investigation results on the short pulse ablation properties of different metals and semiconductors are shown. In 4.2 an amplitude mask imaging technique - for the generation of holes in the micrometer and submicrometer region – is described. Application of mask imaging techniques based on interferometric methods like the imaging of diffractive amplitude- or phase-masks can results in even smaller ablated structure sizes and opens new possibilities to improve the efficiency of the process (4.3). Possibilities of the ablation of submicron-size patterns using diffractive amplitude masks with Fourier filtering and diffractive phase elements (DPE) are discussed in 4.3.1 and 4.3.2, respectively. The fabrication of diffractive phase elements for 248 nm is quite difficult, because of the necessarily low absorption of the usually applied fused silica substrate material at 248 nm. A possible solution for this problem is described and compared with other techniques in 4.4. A newly developed method for the design of DPE´s is discussed in 4.4.1 and a single step laser ablation technique is introduced in 4.4.2 for the mask fabrication process applying 193 nm ArF laser pulses.

2. Scientific background

2.1 High power short pulse laser systems

Since the invention of lasers in 1960 the achievable maximal peak power has been increased by more than 12 orders of magnitudes. The fastest development of the peak power was always in connection with the reduction of the pulse duration. The first lasers were free running devices with pulse durations in the μs range delivering some kW peak powers. The first significant increase in the peak power was reached by modulating the laser cavity quality factor (Q-switching), allowing ns pulse duration, and through the concentration of the pulse energy in a shorter time period pushing the peak power around 3 orders of magnitudes higher. In 1964 with the help of mode locking the picosecond region has been reached and after a very short period the first lasers with GW peak powers appeared. At that point the intensity inside the laser cavity became so high that the refractive index (n) of the materials was not any more constant for different intensities (I) but a linear function of the intensity (2.1):

$$n = n_0 + n_2 I \,. \tag{2.1}$$

This nonlinear reaction of the matter resulted in severe distortions of the beam quality at high power levels. The reason for that is, that the intensity-dependent refractive index produces a nonlinear phase retardation (also called as B integral) given by (2.2)

$$B = (2\pi / \lambda) \int_0^l n_2 I(x) dx \,, \tag{2.2}$$

where λ is the wavelength of the radiation traveling through the medium, n_2 is the nonlinear component of the refractive index, I the intensity in a given point of the medium and l is the propagation length. This nonlinear phase retardation results in wavefront distortion and strong filamentation, which causes damage to the gain medium [1]. To circumvent this problem the only possibility was to increase the beam diameter. This, however, results in other type of problems like difficulties of producing good quality optics, cooling problems, tremendously

increasing sizes and costs and decreased repetition rates. It is well known from numerous investigations [2,3], that for efficient energy extraction a fluence (energy density) level in the order of the saturation energy density (E_{sat}) is required (for details see 2.2). This means that to keep the power density inside the gain medium below the GW/cm^2 level and providing good energy extraction at the same time is only possible, if inferior energy storage materials with some mJ/cm^2 saturation energy density (typical for dye or gaseous active media) for short pulse amplification are used. This fact restricted the circle of applicable active media to dyes and gases. Also here the small E_{sat} indicates the need of large active volumes for high output energies, and so relatively large systems, compared to solid state ones. But since the gaseous active media are easily scalable and the nonlinearities are also much smaller here, they still presented a big potential for short pulse amplification. In the field of solid state lasers no further significant increase of the peak power has been reached until the middle 80ies. At that time the so-called chirped pulse amplification (CPA) technique has been applied the first time for light waves (CPA is an adaptation of the technique of chirped radar in the microwave wavelength range). In CPA the pulse is first stretched (elongated in time) and then amplified, before finally being recompressed [4]. This way a high fluence (energy per unit area) level can be provided keeping the intensity (fluence per unit time) at a moderate value, where no disturbing nonlinearities occur. The combination of ultrashort pulse generation and CPA techniques has been the driving force in the development of terawatt level high peak power solid state laser systems. Most of the systems based on the above mentioned principles are operating in the infrared (IR) spectral range between 800 nm and 1100 nm and the active media are usually some kind of doped glass (like Ti:Sa, Nd:glass or Cr:LISAF) materials.

In the last years, because of the big possibilities of solid state lasers only moderate efforts have been made to develop compact and reliable short-pulse laser systems operating in the ultraviolet (UV) part of the spectrum. In numerous applications, however, high intensity fs UV pulses have ultimate advantages compared to longer wavelengths. Already before the appearance of the solid state lasers using CPA, several concepts have been developed to use the very desirable and promising properties of rare gas - halogen excimer gain media. In the middle 80ies a cascade dye laser system has been developed by Szatmari et al. and was successfully used as a front – end for UV excimer amplifiers [5,6]. As a result of the enormous development of solid state front-ends in the last few years, compact, reliable, easy-

to-handle systems with high average powers and repetition rates become available. These achievements opened the way for the development of solid state - excimer laser systems, where solid state laser features like compactness and reliability can be combined with the advantages of excimer lasers. These advantages are the easy scalability, low nonlinearities, and the ease of amplification even for short pulses without the use of any stretching and compression technique at short wavelengths in the UV, providing nearly diffraction limited beam quality and high optical resolution.

2.2 Fundamentals of short pulse amplification (SPA) in excimers

Short pulse amplification in excimer lasers - especially in KrF modules - has been investigated by different groups [2,7-9]. Several models have been developed to describe the propagation of picosecond and subpicosecond pulses in excimer amplifiers. In an early treatment of the problem by Frantz and Nodvik [8] they obtained a closed-form solution to the photon transport equations describing the growth of the pulse in an amplifying medium similar to that of excimers. Their model gives an exponential growth of the normalized laser energy vs. the total gain at input energies much less than the saturation energy density. In the case of input energy densities in the range or larger than the saturation energy density of the active volume a linear dependence can be obscured. A big disadvantage of this model is that even at very high energy densities a steadily growing amplification is estimated what is not in agreement with the results of high intensity experiments. In an improved model of Tilleman and Jacob the solution of the Franz-Nodvik equations in the presence of absorption is presented and discussed [2]. The equations including absorption are given by

$$\frac{\partial \Phi}{\partial t} + c\frac{\partial \Phi}{\partial x} = c\Phi(g - \alpha), \tag{2.3}$$

$$\frac{\partial g}{\partial t} = -\frac{g\Phi}{\varepsilon_{sat}}, \tag{2.4}$$

$$\frac{\partial \alpha}{\partial t} = -\frac{\alpha\Phi}{\varepsilon_{s\alpha}}, \tag{2.5}$$

where ε_{sat} and $\varepsilon_{s\alpha}$ are the saturation energy density for the gain and for the absorption, respectively, $\Phi = \Phi(x, t)$ is the photon flux, $g = g(x, t)$ is the laser gain, and $\alpha = \alpha(x, t)$ is the absorption coefficient. In (2.3) the photon flux transport is described, (2.4) and (2.5) describe the photon creation and extinction rates due to gain and absorption, respectively. Taking into account that $\varepsilon_{s\alpha} >> \varepsilon_{sat}$, which means that the absorption is nonsaturable, equations (2.3)-(2.5) can be written as

$$\frac{d\bar{\varepsilon}}{dx} + \alpha\bar{\varepsilon} + g_0 e^{-\bar{\varepsilon}} = g_0 , \tag{2.6}$$

where $\bar{\varepsilon} = \left(\int_{-\infty}^{t} \Phi(x,t')dt' \right) / \varepsilon_{sat}$ is the normalized laser energy density at position x and g_0 is the small signal gain. In the limit of no absorption (2.6) can be integrated giving the results presented by Frantz and Nodvik. Introducing nonsaturable absorption as it is taken into account in (2.6) the one dimensional ordinary differential equation there is only numerically integrable. Numerical solutions for different $\overline{\varepsilon_{in}}$, g_0, α, and $L = x_{max}$ values show [2], that an excimer amplifier is working with "positive gain" just until the point, where the energy density inside the active medium reaches a critical value defined by g_0/α (see also in Fig. 2.1). At $\bar{\varepsilon} = g_0/\alpha$ the energy density cannot be further increased, the absorption losses will just be compensated by the amplification. In case of an incoming beam with $\overline{\varepsilon_{in}} > g_0/\alpha$ the device will act as an attenuator until $\overline{\varepsilon_{in}} = g_0/\alpha$ is reached. This result can be obtained from (2.6) by solving it in the limit of $\bar{\varepsilon} > 1$ yielding

$$\overline{\varepsilon(x)} = \bar{\varepsilon}_0 e^{-\alpha x} + \frac{g_0}{\alpha}\left(1 - e^{-\alpha x}\right), \tag{2.7}$$

which predicts the asymptotic limit for $x \to \infty$ as

$$\lim_{x\to\infty} \bar{\varepsilon} = g_0/\alpha . \tag{2.8}$$

Based on (2.6) a further important parameter of the amplifier can be derived which is called the local extraction efficiency (η(ε)). The local extraction efficiency expresses the ratio of the derivative of the normalized pulse energy for a unit amplifier length and the small signal gain as

$$\eta\left(\bar{\varepsilon}\right)=\frac{1}{g_0}\frac{d\bar{\varepsilon}}{dx}=1-e^{-\bar{\varepsilon}}-\frac{\alpha}{g_0}\bar{\varepsilon}\,. \tag{2.9}$$

In case of no absorption and saturated amplification η(ε) = 1, which means, that the complete stored energy is extracted from the amplifier. In a realistic case the extraction efficiency is always smaller than 1 (see Fig. 2.1). The integral of the local extraction efficiency for the whole amplifier length is the overall extraction efficiency, which can be obtained as

$$\langle\eta\rangle=\frac{1}{L}\int_0^L\eta dx=\left[\overline{\varepsilon_L}-\overline{\varepsilon_{in}}\right]\cdot\left(g_0L\right)^{-1}, \tag{2.10}$$

where L is the length of the excited active medium (practically the length of electrodes). From (2.6) and (2.9) the ε value for the maximum extraction efficiency condition can be obtained by differentiating (2.9) with respect to $\bar{\varepsilon}$ and looking for the solution of $\bar{\varepsilon}$ at $\frac{d\eta}{d\bar{\varepsilon}}=0$:

$$\frac{d\eta}{d\bar{\varepsilon}}=\frac{d}{d\bar{\varepsilon}}\left(1-e^{-\bar{\varepsilon}}-\frac{\alpha}{g_0}\bar{\varepsilon}\right)=0\Rightarrow\bar{\varepsilon}=\ln\left(g_0/\alpha\right). \tag{2.11}$$

These results show that the maximum achievable energy density is proportional to g_0/α and can be calculated according to (2.12). If optimized operational conditions are desired, the output energy density of the laser must be around the value given in (2.13)

$$\varepsilon_{out,\max}=\varepsilon_{sat}\cdot\left(g_0/\alpha\right), \tag{2.12}$$

$$\varepsilon_{out,opt.\eta}=\varepsilon_{sat}\cdot\ln\left(g_0/\alpha\right). \tag{2.13}$$

This makes it clear that the saturation energy density, small signal gain coefficient and absorption coefficient define a theoretically achievable maximal and optimal value of the

output energy density for an excimer laser module. According to the importance of these parameters several groups tried to determine these values experimentally [3,7,9-12]. The results show that the saturation energy density for KrF active medium is around 2 mJ/cm^2 for optical pulses with subpicosecond pulse duration [7,12,13]. For g_0/α values between 6 [9] and about 20 [11] has been measured, obviously depending on the gas mix and other device characteristics. Here, values between 10-15 seem to be most reasonable. Substituting these values into (2.12) and (2.13) the optimal output energy density (providing optimal energy extraction efficiency) is about 4.6-5.4 mJ/cm^2 reaching its maximum at around 20-30 mJ/cm^2. By optimizing the operational conditions of a power amplifier high output energy with good energy extraction efficiency and high signal-to-noise ratio are necessary to reach. Since in many applications the signal-to-noise ratio is of comparable importance to the extraction efficiency (given in (2.9) and (2.10)) the amplifiers must be optimized both parameters. The development of the signal-to-noise ratio during amplification can be described by the gain contrast (C) and its local quantity that is called gain contrast coefficient (c), given in (2.14) and (2.15), respectively.

$$C = G/G_0\,, \tag{2.14}$$

$$c = g_{eff}/(g_0 - \alpha). \tag{2.15}$$

In these equations $G = \varepsilon_{out}/\varepsilon_{in}$ is the actual gain, $G_0 = e^{g_0 L}$ is the small signal gain (L is the length of the amplifying medium), g_0 is the small signal gain coefficient, and $g_{eff}(x) = \lim_{\Delta x \to 0} \frac{1}{\Delta x} \ln \frac{\varepsilon_{x+\Delta x}}{\varepsilon_x}$ is the effective gain coefficient (which is defined similar to g_0, but also including the effect of saturation and absorption). C gives the signal-to-noise ratio at the output compared to the input, because (taking into account that the energy density of the noise is much smaller during the complete amplification process than the saturation energy density of the given active medium). the noise will be amplified with the small signal gain and the signal will see only a fraction of that amplification, defined by the actual gain. The importance of the contrast (C) is specially pronounced in the case of UV systems because of the lack of a practicable saturable absorber [14,15]. The simplest method for keeping the signal-to-noise ratio on a low level is to operate the amplifier at optimized condition where C

is close to 1. In Fig. 2.1 the local extraction efficiency (η) and the gain contrast coefficient (c) are plotted.

In Fig. 2.1 it is visible, that the local extraction efficiency first increases quite fast with increasing $\bar{\varepsilon}$, reaches its maximum at $\bar{\varepsilon} = \ln(g_0/\alpha)$, and then starts to decrease. At $\bar{\varepsilon} = (g_0/\alpha)$ the value of η will again reach zero, which means that the energy density cannot be further increased, the maximum value has been achieved. From the figure it is also visible, that both parameters cannot be kept on the optimum at the same time, a trade-off for the different requirements of pre- and power amplifiers has to be made. It has been also shown by numerical calculations, that these parameters can be well controlled during the amplification process applying different solutions for the different problems.

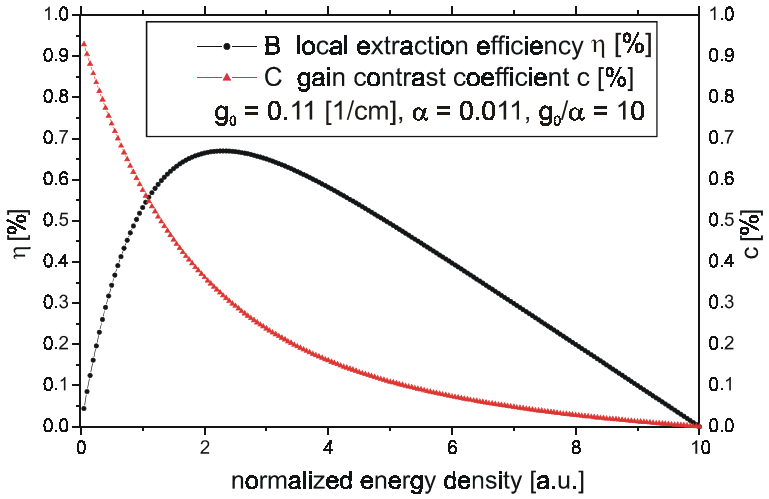

Fig. 2.1: Local extraction efficiency (η) and gain contrast coefficient (c) vs. normalized energy density ($\bar{\varepsilon}$) in a KrF amplifier

2.3 Limitations of SPA in excimers and possible solutions

The application of excimers for short pulse amplification has unique advantages like ease of operation at short wavelengths or the low nonlinearities of the active volume etc., still there are some problems to solve mainly in connection with the fast saturation and short energy storage time of the active medium.

The advantage of the small saturation energy density (ε_{sat}) of dye and excimer active media for short pulse amplification partially turned into a drawback after the invention of the CPA with the appearance of stretcher arrangements to very large stretching ratios, solving a big part of the nonlinearity problems related with the propagation of high intensity pulses in the gain medium. The saturation energy density of excimers is in the mJ/cm^2 range in contrast to solid-state media, where ε_{sat} is usually several J/cm^2. Fig. 2.1 shows that the energy density in the amplifying medium has to be kept on a relatively low value (in the range of the saturation energy density), in order to reach optimized operation. However, this means that it is necessary to apply large active volumes to reach high output energies with excimer lasers. Although, the gaseous excimer media are easily scalable, still there are some difficulties arising by scaling up the excited volume.

The reasons can be listed as follows. It is very difficult to design a discharge with large, stable and homogenous cross section, imposed by the stringent requirements on the inductance of the discharge loop of the laser head [10]. The above mentioned limitation on the cross section forces to increase the length of the discharge, resulting in a pencil like discharge geometry of excimers. Consequently, the width of the discharge will be too small, but too long, causing strong saturation. A simple technique addressed to solve this problem can be the application of the so-called off-axis amplification scheme, which is basically an optical method to change the length and cross section of the discharge seen by the amplified beam, using a geometrical transformation [3,10,16,17].

The second problem arising by amplifying short pulses in a gaseous active medium is the low energy extraction capability caused by the short energy storage time of excimers. The energy storage time of excimers is only a few ns [7]. This means, that a short pulse has only access to that part of the stored energy of the amplifier, which has been accumulated within the last few ns before the arrival of the short pulse. Compared to the excitation time of the discharge (which is typically 15-20 ns) the energy storage time is still about 5-10 times shorter. Dynamics measurements [7,12,13] showed that the relaxation time, the time necessary to built up the population inversion after a short pulse has traveled through the active medium of excimers is also in the 2-3 ns range. Consequently, a short pulse could be efficiently amplified every 2-3 ns within the gain window of the amplifier. The energy, which can be extracted from an amplifier with a long (practically 15-20 ns) optical pulse can be defined as the whole

stored energy (E_{tot}), and similarly, for short pulses - due to the short storage time of the active medium of excimers - the momentarily stored energy (E_{st}). The whole stored energy is given by (2.16), where T is the gain window and τ is the recovery time of the gain.

$$E_{tot} = E_{st} \cdot T / \tau . \tag{2.16}$$

T/τ is determined by physical and electrical properties of the given gas mixture and the amplifier module, and as discussed before in the case of commonly used KrF amplifiers its value is around 5-10. This means that the momentarily stored energy of an excimer module is relatively small compared to the total stored energy. A short optical pulse in a single pass has only access to a small fraction of the whole energy stored in the excited medium. The only way to have access to the whole stored energy of the amplifier is successive replenishment of the momentarily stored energy (E_{st}).

A possible solution would be to amplify a train of short pulses within the time window of the discharge, and the "only" task is to recombine the subsequent pulses after amplification. The best candidates to manage this task in case of femtosecond pulses are different variants of the so-called interferometric multiplexing technique [18].

2.3.1 Off-axis amplification

The off-axis amplification is a multiple pass amplification technique. In this arrangement the seed pulse is not sent through the amplifying medium parallel with the longitudinal axis of the discharge (on-axis) but the direction of propagation is enclosing an adjustable angle (off-axis angle) with the longitudinal axis of the discharge, in the plane of the electrodes. Such a scheme is visible in (Fig. 2.2), where a conventionally used 3 pass version of the off-axis arrangement is shown.

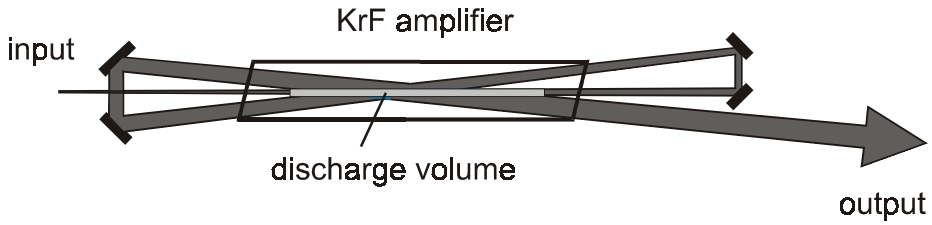

Fig. 2.2: 3 pass off axis arrangement

As it is visible in the figure, the off-axis amplification allows amplifying a short pulse in subsequent steps, fitting the operational conditions to the optimum values in each pass. This is possible by changing the size and the off-axis angle of the beam. Especially in case of KrF amplifiers the optimal value for the energy density inside the active volume can only be varied in a relatively narrow range between around 0.5 ε_{sat} and 3 ε_{sat} (see Fig. 2.1). The reason for that is the strong dependence of the efficiency and contrast on the energy density (already discussed in 2.2), the presence of a relatively wide nonsaturable absorption range, and the lack of a well applicable saturable absorber. Additionally, it is very difficult to keep the energy density in this range because of the high overall gain in a single pass, caused by the pencil-like discharge geometry of excimers. This problem can be partially solved by applying an optical method that changes the effective length and cross-section of the discharge seen by the seed pulse.

For on-axis amplification the length and width of the gain medium is practically the length (L) and width (W) of the discharge. For off-axis amplification the effective length and width of the discharge can differ from L and W as it is shown in Fig. 2.3.

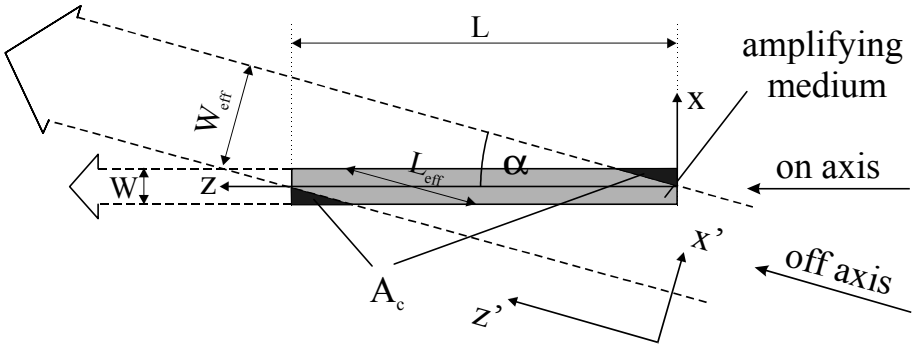

Fig. 2.3: Off-axis geometry

The off-axis arrangement changes the effective length (L_{eff}) and width (W_{eff}) of the discharge seen by the pulse if

$$\alpha > arctg(W/L), \tag{2.17}$$

where α is the off-axis angle of the beam. This is the practically important case (otherwise the effective L and W values will not change significantly), and for these angles the new values of L_{eff} and W_{eff} can be calculated as

$$L_{eff} = W/\sin\alpha, \tag{2.18}$$

and

$$W_{eff} = LW/L_{eff} = L\cdot\sin\alpha\,. \tag{2.19}$$

The left side of (2.19) means that this transformation leaves the active volume of the amplifier unchanged. (The right side is obtained by substituting (2.18) into (2.19).) From Fig. 2.3 it is visible that this assumption is fairly good for a pencil like excimer discharge geometry. Calling the real used volume as V_{eff} the ratio of V_{eff} and V (discharge volume) can be given as

$$\frac{V_{eff}}{V} = \frac{(L\cdot W - 2A_C)\cdot D}{L\cdot W\cdot D} = 1 - \frac{W}{L}\cdot\frac{1}{4tg\alpha}, \tag{2.20}$$

where D is the electrode distance (not shown on Fig. 2.3), and A_C is the area of the corners of the discharge, not used by off-axis amplification. For usual discharge parameters like L = 100 cm, W = 20 mm, and $\alpha = 2°$ a ratio of V_{eff} / V ~86 % is obtained.

It is visible from (2.19) that by changing the off-axis angle L_{eff} and W_{eff} can be controlled. This allows us to fit the energy density of the desired values in the subsequent amplification passes. It is possible by changing the propagation angle of the beam or by changing the size of the beam between the amplification passes, applying telescopes or in an even simpler way by sending a divergent beam through the amplifier. (At first sight it would also be possible to send a divergent beam through the amplifier in on axis mode. It is mostly not the case because in on-axis operation the effective width of the discharge is equivalent with the real discharge width, and consequently too small to support the amplification of a beam with the desired

divergence. That is why only elongated output beams (usually with height – width ratios over 3 or 4) - with much smaller cross section - can be efficiently amplified that way.)
This also means, that the beam cross-section (A) can be significantly increased in the off-axis amplification arrangement, which is a very important feature, taking into account that the theoretically achievable maximum output energy (E_{out}) scales with the beam cross-section. As a consequence of (2.13), for optimized operation E_{out} is defined by ε_{opt} and A, and can be calculated as

$$E_{out} = \varepsilon_{opt} \cdot A . \tag{2.21}$$

2.3.2 Interferometric multiplexing

Optical multiplexing is basically a multiple beam technique. By taking special care of the proper delays of the subsequent multiplexed pulses the same amplifying medium can be used also in multiple pass arrangement, opening the way to combine the advantages of multiple pass and multiple beam arrangements, reaching even higher output energies. The main idea of optical multiplexing is, that the seed beam is split into equal parts and sent into the amplifier with different delays. The pulse train is recombined again after amplification, forming a single output beam. The key point of any kind of multiplexing is how accurately the recombination can be performed. In the conventional multiplexing schemes (Fig. 2.4 a) recombination is far from that of interferometric accuracy, imposing severe limitations on the temporal reconstruction of the partial beams and on the resulting focusability. Satisfactory demultiplexing has been reached only for longer than picosecond pulses [19-21]. For femtosecond pulses a generally applicable interferometric beam recombination method has been described in [18]. In the arrangements presented there the above mentioned shortcomings of the conventional multiplexing methods are eliminated by using the same optical element for multiplexing and demultiplexing, so that the divided beams have exactly the same optical path, allowing an automatic, phase-locked synchronization of the partial beams (Fig. 2.4).

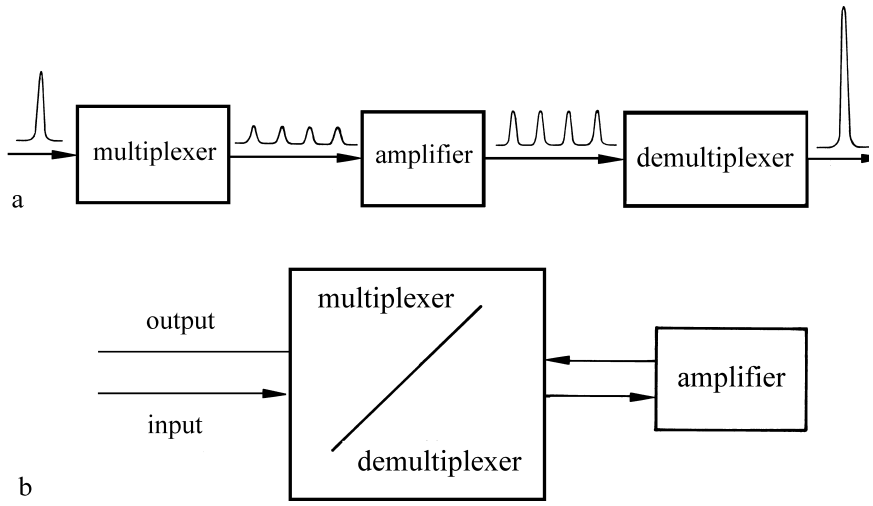

Fig. 2.4: The principles of (a) optical multiplexing and (b) interferometric multiplexing methods [18]

The multiple beam arrangements gives the possibility to divide the input beam into several parts, amplify them one after the other and recombine them after amplification, outside the amplifying medium. This way the energy density inside the active medium can be kept around the optimum value, and still higher output energy densities (and therefore higher output energies) can be reached outside the active volume. Multiplexing allows efficient extraction of the stored energy of amplifiers of short storage time by the use of a train of pulses of about the same intensity.

In [18] several arrangements have been investigated like on-axis and off-axis arrangements, 2 and 4 beams evaluations, geometrical and polarization splitting techniques or the combination of them. The arrangements are based on Sagnac interferometer's principle. Applying this technique it is possible to multiply the output energy extractable from the same module with a single short pulse. Combining the multiplexing with the off-axis amplification technique allows to make use of the advantages of both arrangements, changing the effective cross section and gain length of the amplifier through the off-axis angle of the beams, applying for several beams at the same time. In an arrangement where a 2 beam variant is applied for the same excimer module, the maximum achievable output energy is about 2 times the value, which can be theoretically reached in an off-axis arrangement (2.21).

2.4 Short pulse material processing

Laser micro-machining of solids is nowadays a well accepted technology for the manufacturing of components in electronics, aerospace, optics, medical and photovoltaic industries. Also laser etching of sub-micron-sized features in dielectric materials is a widely used technique in photolithography for the fabrication of microelectronic devices. Usually the laser devices used for these applications are standard CO_2, Nd:YAG, Ar^+ or excimer lasers with nanosecond or longer pulse durations [22-27]. In case of some of the materials (e.g. polymers), generation of submicron structures with relatively simple laser sources is possible and was experimentally demonstrated by several groups [28-32]. For the machining of another group of materials (e.g. special polymers, metals, semiconductors, ceramics and biological tissues) application of short laser pulses is necessary to achieve the required ablation quality. Picosecond and femtosecond laser ablation has been proved to be a powerful technique for the patterning of highly conducting (thermally) and wide-bandgap materials. Both lateral spreading of the absorbed energy outward from the irradiated zone and screening of the incident laser light can be diminished or even ignored with femtosecond pulses, enabling the creation of micron size structures, and allowing very localized material removal with much less irradiated energy. Good results on short pulse ablation of various targets have been reported in [33-40]. However, to reach submicron resolution with IR sources is hardly possible. These are the applications where UV femtosecond sources have ultimate advantages not only because of their short pulse duration but also for the high optical resolution at this wavelength and the high absorption coefficient of most materials in the UV. In the case of materials highly transparent in the VIS and IR, laser direct writing of submicron-size structures is only possible with ultra short UV laser pulses [41-44].

The results of ablation studies on highly conducting materials show, that the size of the heat affected area can be characterized by the thermal diffusion length L_{th} [45], given as

$$L_{th} = \sqrt{2\kappa\tau}\ , \tag{2.22}$$

where κ is the thermal diffusivity of the material, and τ is the laser pulse duration. For Ni the value of κ is 0.19 cm^2/s [46], which means that L_{th} is about 1 μm for laser pulses longer than

15 ns. On the other hand, the penetration depth of the radiation at 248 nm is in the nm range because of the strong absorption (for Ni α^{-1} = 8 nm at the KrF wavelength [46]). Although the energy of the laser pulse will be absorbed in a thin surface layer, it will be transferred in deeper regions through thermal conduction, because of the long interaction time (some ns). In this way, a material layer will be damaged in the form of different heating and melting effects, with a thickness of around 100 times larger then the optical penetration depth. This is, in principle, the origin of the molten zones occurring around the ablated structures applying ns or longer pulses. Intuitively, it is expected that the limiting effect of the heat conductivity can be neglected, if $L_{th} \leq \alpha^{-1}$ with α^{-1} being the penetration depth of the laser radiation. In the case of Ni this is the case for pulses shorter than 1.5 ps. It was demonstrated by several groups, that by applying laser pulses shorter than a picosecond the size of the damaged zone can be drastically reduced [35,38,41,45]. Additionally, short pulses have the advantage, that during the complete penetration of the pulse into the material there is no time for the development of a plume, which would otherwise cause significant energy losses through absorption of the trailing edge of the pulse. This advantage, together with the much lower losses through heat conduction provide around 2 orders of magnitude lower ablation thresholds in case of metal targets for short pulses compared to the long pulse ablation thresholds. A further advantage is that getting rid of disturbing plume effects the imaging quality can be kept constant good during the ablation process [41]. In contrast to nanosecond pulses, the ablation rate for femtosecond pulses is found to be independent of the irradiated spot diameter [47]. Another difference was reported in the case of metal film targets, where the ablation rate was found to be independent of the film thickness, as far as the optical penetration depth is larger than the thermal diffusion length (d > 100 nm) [46], which is in contradiction with the results of nanosecond ablation experiments indicating basic differences between the two processes.

An effective optimization of the applied parameters is much easier with the complete understanding of the ablation mechanisms. Especially the dynamics of the single steps from the absorption of the laser pulse until the formation of the ablated structure is of increased interest. Time-resolved measurements yield fundamental information on the dynamics of the ablation process. In particular, they permit one to determine the importance of multiphoton processes, the lifetime of excited states, the latent time between the incident laser pulse and

the ejection of species from the surface, the influence of plasma shielding effects, etc. Among the various techniques employed are acoustic methods, time resolved reflectivity and beam deflection measurements, and various types of spectroscopic techniques.

Based on theoretical considerations and experimental results, a relatively new theory of the short pulse ablation mechanism has been developed in the last years. Although the main principles of the process are similar for different materials, still there are some differences in the ablation behavior of metals and semiconductors, mainly because of the different material properties.

In case of metals the penetrated pulse energy is almost exclusively absorbed by free-free electron transitions in the conduction band. As a first step the short pulse will be absorbed in a relatively thin surface layer (skin depth) of the irradiated material. The absorbed radiation will excite the free electrons through inverse Bremsstrahlung [48,49]. Thermalization between the electron subsystem and the lattice is usually much slower, typically of the order of 1 to 100 ps, depending on the strength of the electron-phonon coupling ($\Gamma_{e\text{-}ph}$). This way the femtosecond laser pulse generates a hot electron gas and temperatures over several thousand Kelvin will be reached in the electron system. During this time temperature of the lattice will not be significantly over the room temperature. As a result we can define two different temperatures of these two systems. To describe this state of the matter a two-temperature model has been invented by Anisimov et. al. [50] and was later further developed by Allen [51]. The transient non-equilibrium between hot electrons and the lattice can be described by temperatures T_e and T, which can be calculated from the corresponding heat equations. For a laboratory system these coupled equations for femtosecond and, in good approximation, also for picosecond pulses can be written as

$$C_e \frac{\partial T_e}{\partial t} = \nabla(\kappa_e \nabla T_e) - \Gamma_{e-ph}(T_e - T) + Q\,, \tag{2.23}$$

and

$$C \frac{\partial T}{\partial t} = \Gamma_{e-ph}(T_e - T)\,, \tag{2.24}$$

where C_e and C are the heat capacities per unit volume of the electron and lattice subsystem, respectively.

This model describes the heat transport between the electron and phonon system, and builds the theoretical base for the different investigations in this field. The experimental demonstration of the temperature difference between the electron and phonon system become first possible in the middle of 80ies, parallel with the fast development of short pulse laser systems. Eesley [52,53], Fujimoto et al. [54] and also Elsayed-Ali et al [55] were able to demonstrate the mentioned temperature difference experimentally through photoelectrons [54] and thermomodulations spectroscopy by irradiating copper samples with short laser pulses. During the excitation of about 100 fs the Fermi-Dirac energy distribution of the electron system will be reached through electron-electron collisions. The strongly overheated electron system gives the energy to the lattice within a few picoseconds through the electron-phonon coupling [56]. It has been found that beside the energy coupling to the phonon system, also the heat transport inside the electron system plays a very important role in the energy relaxation [57-60]. Usually the heat transport dominates the process in the first 500 fs, and later the electron-phonon coupling plays the more important role [61].

In case of semiconductors the optical excitation generates electron-hole pares by pushing electrons from the valence band to the different electronic energy bands. However, the photon energy has to be at least as big as the bandgap energy [49]. In less than 120 fs the energy distribution will be thermalized through Coulomb-collisions [62]. Also in this case strongly different temperatures for the electron and the phonon structure can be observed. This temperature of the charge carrier particles will be equaled through collisions between electrons and holes and partially through Auger-recombination in the first picosecond after irradiation [63,64]. The relaxation of the temperature difference between the charge carrier system and the lattice has a constant in the few picosecond range [48]. The process can be described as follows: The energy coupling into the phonon system and material melting can be observed within the first 100 fs [65], although high resolution measurements show that the melting is inhomogeneous on this time scale [66]. Within the first picosecond a homogeneous molten zone will be reached [67]. After around 5 ps material evaporation has been observed [66,68], combined with cluster formation in a 100 ps time scale [66]. After few nanoseconds the complete resolidification of the surface can be detected.

The ablation dynamics description above is a summary of the most important steps, that has been observed by several research groups after irradiating metal or semiconductor probes with

high intensity laser pulses. The dynamics of the processes depend on the material properties, the microscopic state of the probe [69,70], and the energy density, repetition rate, accumulation effects, etc. However, for energy densities higher than the ablation threshold of the given material the global effects (heating, melting, evaporation) are very similar for all kind of investigated materials [49].

Another field of application of ultrashort pulses is the patterning and micromachining of materials for which the photon energy of conventional lasers is not high enough either for direct (single-photon) bandgap excitation or for efficient defect generation. Such materials are fused silica, fluoride crystals, diamond, sapphire, teflon, etc, having only little absorption in the UV part of the spectrum. Subpicosecond UV lasers can be new tools for the precise micro-machining of these materials. Ultrashort pulses generate extremely high peak powers (~TW/cm^2) already at moderate energies. At such high power levels multiphoton processes become dominant establishing the condition for the concentration of the irradiated energy in a thin surface layer necessary for precise machining. At the same time, the relatively low energy of the pulse ensures that little or no optical damage occurs to the adjacent zones or to the bulk material.

A further very important feature of the complete system used for micromachining is the high optical resolution. In material processing, especially if high precision is required, it is the minimal achievable focal spot size, which is considered to be the major figure of merit for the performance of the laser system. This is where the better focusability of short wavelength gas lasers plays a very important role [71-78]. Fabrication of feature sizes below one micron is hardly possible with lasers operating in the infrared. However, the short UV wavelength results in an around 3 times smaller theoretically achievable minimal focal spot size, compared to an IR system running at around 800 nm. The gaseous active medium of excimers also introduces less optical distortions [72-74,76,77]. As a result of the combination of these effects, a typically 10-100 time smaller focal spot area is reachable for excimer lasers compared to high intensity solid state systems [17]. This significantly relaxes the requirements also for the peak power necessary to reach a given focused intensity. The most important advantages of such a system for submicron machining are the small penetration depth of the radiation, the small thermal diffusion length and a high optical resolution. The high peak power ensures a small penetration depth through multiphoton absorption and

consequently well defined ablation depths. Additionally the short pulse duration provides a small thermal diffusion length and through that prohibits the lateral spreading of heat into the surrounding regions, ensuring the creation of small lateral structures. Operation with UV pulses provides the necessary high spatial resolution because the minimum achievable irradiated spot size scales with the wavelength. Further advantage of the short wavelength is the increased absorption of most of the materials in the UV region. This relaxes further the system requirements even for hardly machinable, in the IR and VIS wavelength region transparent materials. As a result of all these advantages practically all kind of materials can be machined with submicron precision, applying UV femtosecond pulses.

3. Short pulse hybrid laser systems

3.1 Basic concepts of short pulse hybrid laser systems

To date there is no effective way to generate ultra short pulses directly in the UV. So far the most attractive scheme for the control of the temporal, spatial, energetic, and spectral properties of short UV pulses consists of three well-defined stages. These stages are the seed pulse generation in the IR or visible wavelength range, followed by a spectral conversion stage, where the frequency of the primary radiation is up-converted into the amplification band of an excimer gain medium. The final part is the power amplifier stage, which is based on excimer module(s) with a properly chosen optical arrangement. For the short pulse generation different front ends can be used, e.g. frequency tripled seed beams from a Ti:Sa solid-state laser or frequency doubled pulses of a short pulse dye laser system. In earlier experiments the dye laser front-end [6] was used and successfully applied in numerous laboratories all over the world. Actually, such a front-end is used in the polarization multiplexing experiments, described in details in 3.4. However, thanks to the recent achievements of solid state laser technique, there are some features (reliability, simplicity, possibility of high frequency operation), that make the solid state front-ends more preferable in a big part of the applications. After a brief description of the used front-end systems and the frequency tripling arrangement in 3.2, the achieved results on the development of hybrid laser systems are enumerated in the following sessions (3.3-3.5) of this chapter.

3.2 The different front ends and the frequency tripling unit

There are several possibilities to generate ultrashort pulses in the visible or the IR spectral range. One promising way is to use a hybrid dye-excimer system for the generation of ~500 fs pulses tunable over a wide spectral range between 400 and 600 nm. For amplification in KrF, the lasing wavelength of the DFDL (distributed feedback dye laser, which is the key

component of the system) is tuned to 497 nm, being twice the 248.5 nm KrF wavelength. The experimental arrangement of such a dye laser front end is shown in (Fig. 3.1).

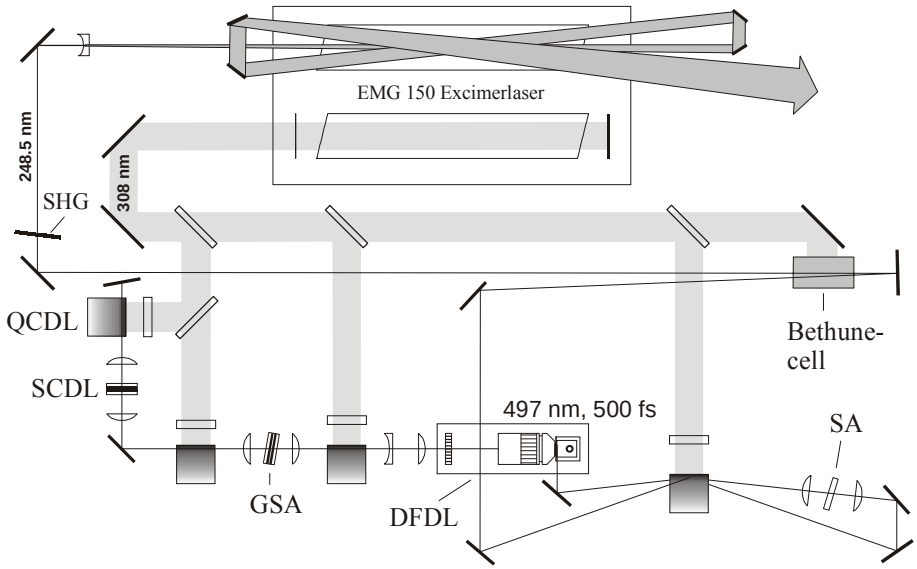

Fig. 3.1: Szatmári-type cascade dye laser system

This system is based on a cascade of dye laser and amplifier stages, pumped with an exciter laser delivering ~15 ns pulses at 308 nm. The pulse is shortened step-by-step (QCDL, SCDL, GSA), applying different shortening techniques [79], reaching a pulse duration of ~0.5 ps after the DFDL. These pulses are amplified again and frequency doubled in a single BBO crystal, reaching the desired 248.5 nm wavelength. The applied excimer module is an EMG 150 laser, consisting of an oscillator and amplifier tube. The frequency doubled pulses can be amplified in the second tube up to ~10 mJ. Such a system is ideal as a front end if relatively high energy input pulses are desired, offering some energy reserves even if e.g. spatial filtering or compressor stages are necessary to use before further amplification. A further advantage of the arrangement is that the twin tube excimer module automatically solves the synchronization. Disadvantages are the complicated alignment procedure of the cascade dye stages and the low repetition rate (in the range of 10 Hz).

Alternative candidates to solve the above mentioned problems arising from the dye laser system are short pulse solid state lasers. Our choice was a commercially available Ti:Sapphire

solid state laser system (Spectra-Physics Lasers, Inc., CA) shown in (Fig. 3.2), generating around 150 fs pulses at 745 nm with a repetition rate up to 1000 Hz [80,81].

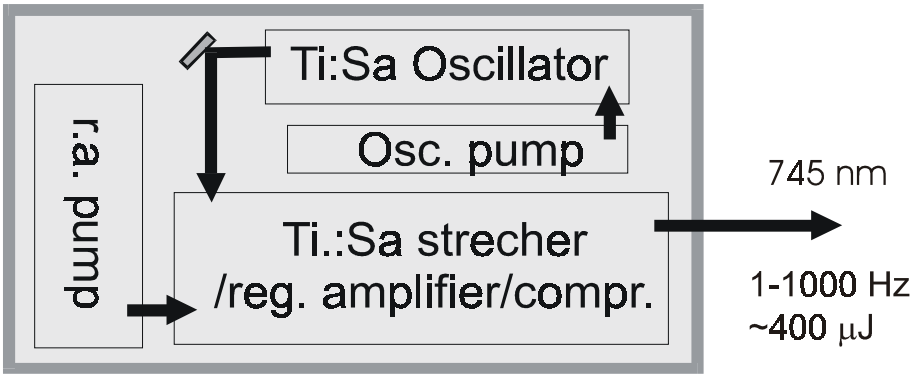

Fig. 3.2: The short pulse Ti:Sa laser system

The system consist of a quasi cw mode-locked master oscillator providing a broadband seed radiation centered normally at around 800 nm with ~90 fs pulse duration. A slit placed into the cavity allows tuning the laser to the desired 745.5 nm wavelength. The seed pulses are stretched, and then amplified in the regenerative amplifier (RA). The frequency of the Q-switched pump laser for the RA can be varied between 1-1000 Hz, determining the repetition rate of the amplified pulses. After amplification the beam is compressed again to about 130-150 fs, carrying an energy of ~400 μJ. These pulses can be frequency converted in a frequency-tripling unit. To provide absolutely hands off operation, the tripling unit was built in a linear arrangement, placed into a sealed box flushed by argon.

The frequency upconversion was realized in two main steps [80,81]. First a second harmonic (2ω) signal was generated in a nonlinear medium with around 40 % efficiency. After the necessary correction on the polarization and timing of the ω and 2ω beams sum-frequency mixing was used to generate the desired third harmonic (3ω) radiation. The details of this arrangement are as follows. To generate the 2ω radiation at 372.7 nm a 7×7×0.8 mm thick polished BBO crystal was used as nonlinear medium with type I phase-matching condition with $\theta = 31{,}4°$ and $\phi = 0°$ cutting angles. To compensate the group velocity delay after frequency doubling a 1.1 mm thick polished MgF_2 wave plate was used. The operation of the wave plate is based on the birefringence of MgF_2. The polarization of the fundamental and the

second harmonic radiations are orthogonal, as a consequence of the type I phase-matching in the doubling crystal. By proper choice of the cutting angle relative to the optical axis allows us to roughly define the required refractive indices ($n(\lambda)$) of the MgF_2 wave plate seen by the different wavelengths. Rotating the normal of the crystal surface relative to the incoming beams a fine-tuning of the optical path lengths and the refractive indices for the different beams is realized allowing to adjust the required group delay. This way the optimal temporal overlap of the ω and 2ω waves on the tripling crystal can be ensured. To reach parallel polarization between the fundamental and the second harmonic wave on the second BBO crystal we used a 2 mm thick MgF_2 retardation plate (dual wave plate with AR/AR coating for 400 and 800 nm from Alphalas GmbH Göttingen), placed right behind the wave plate. In the second main step sum-frequency mixing also in type I phase-matching condition was used. The 0.24 mm thick second BBO crystal (polished, 7×7×0.24 mm thick, $\theta = 49°$ and $\phi = 0°$ cutting angles) mixed the remaining IR (ω) and the second harmonic (2ω) near-UV light to produce the third harmonic (3ω) radiation at 248.5 nm. The crystals together with the wave and retardation plates were placed into a sealed box, filled with Ar gas to protect the crystals against humidity, ensuring long lifetime of the optical components. The maximal efficiency for the tripling was around 8%. Although this is not the highest possible conversion efficiency, the linear arrangement provides absolutely hands off, “no tweak” operation of the tripling unit, making the arrangement more reliable.

3.3 Description of a 50 mJ system

In the first experiments a solid state Ti:Sa system set to 745,5 nm wavelength was applied with ~30 μJ energy seed pulses. These pulses were amplified up to over 50 mJ. For the amplification a specially designed wide-aperture KrF excimer module was used in a three-pass off-axis arrangement [80].

As it is described in details in 2.3.1, the off-axis amplification allows to use a KrF module in multiple pass operation, fitting the operational conditions of the amplifier to the gain requirements in each pass by changing the size and the off-axis angle of the beam. The

theoretically achievable maximal number of passes is around 5-10, however, the overall gain lifetime and the length of the discharge limits the number of amplification passes to a practical maximum of 3.

In the experiments an EMG 201 Lambda Physics excimer laser was used, and it was specially modified for short pulse amplification. The length of the discharge was 930 mm, with 36 mm electrode separation. The charging circuit, the capacitor banks, the magnetic switch, the peaking capacitors, the electrode profile and the preionization geometry were also fitted to these parameters. The main goal of the modifications was to increase the momentarily stored energy (E_{st}) of the amplifier. After modification of the amplifier E_{st} was measured experimentally. In case of a short pulse amplifier E_{st} can be theoretically calculated from (3.1)

$$E_{st} = E_{sat} \cdot g_0 \cdot L \cdot W \cdot D\,, \tag{3.1}$$

where E_{sat} is the saturation energy density, g_0 is the small signal gain coefficient, L is the length of the discharge, W is the width of the discharge and D is the electrode separation. For the measurement of the stored energy (3.2) can be used

$$E_{st} = E_{sat} \cdot (g_0 L_{eff}) \cdot W_{eff} \cdot D\,, \tag{3.2}$$

where both the gain length product ($g_0 L_{eff}$) and the effective width of the discharge (W_{eff}) are measured values. In such a measurement a small diameter femtosecond probe beam was sent through the spatial maximum of the gain (in our case enclosing an angle of 1.5° with the longitudinal axis a_y of the amplifier) and the energy of the amplified output beam was measured, scanning through the effective width of the discharge (W_{eff}) in lateral direction (Fig. 3.3).

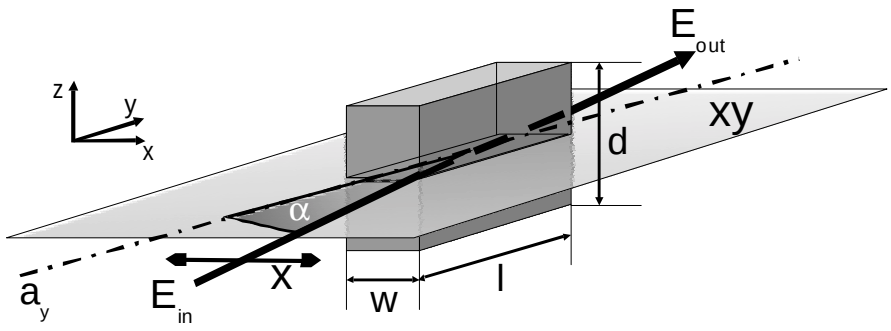

Fig. 3.3: Setup for the stored energy measurements. In the picture the discharge volume is visible where W is the width, L is the length and D is the height of the discharge (electrode separation). E_{in} and E_{out} represent the measured input and output energies, a_y is the longitudinal axis of the amplifier, α = 1.5° is the angle enclosed by the beam and a_y, and x is the direction of the scan in the xy plane.

The input signal was strongly attenuated in order to avoid saturation of the amplification during the whole measurement. By measuring E_{in} and calibrating the attenuation factor it is possible to calculate the gain length product for each measured point according to

$$g_0 L_{eff} = \ln(E_{out}/E_{in}). \tag{3.3}$$

The other measured value W_{eff} can be defined as the FWHM of the measured amplification curves.

For our specially developed discharge module a momentarily stored energy (E_{st}) of as high as 100 mJ was found. For the calculation we used the values E_{sat} = 2 mJ/cm^2, D = 36 mm and the measured maximal values for $\ln(E_{out}/E_{in}) = g_0 L_{eff} = 5.3$ and W_{eff} = 25 mm (width of the discharge seen by a femtosecond probe pulse at an off axis angle of 1.5° around the spatial maximum of the gain).

We used this newly developed amplifier in combination with the frequency-tripled output of a Ti:Sa system (delivering 40 μJ energy at 248 nm) in a 3 pass off-axis arrangement (see Fig. 2.2 in 2.3.1). In order to ensure a proper timing an active delay control unit (EMG 97 or LPA 97, Lambda Physik) was used to trigger the excimer module. This means that the maximal gain in the excimer active medium has to be continuously adjusted in time relative to

the seed pulse. The active delay control unit manages to keep a constant delay between an external trigger pulse and the discharge in the amplifier. After adjusting the correct time delay the frequency-tripled signal was directed into the amplifier at an angle of 1.1°. The proper divergence was reached by a negative lens placed in front of the amplifier. The beam diameter at the input was 6 mm. In the first pass it is not a necessity that the beam fills the entire discharge cross section because the extracted energy in this pass is small compared to the momentarily stored energy of the amplifier. The angle of the first pass was chosen quite small to boost up the energy into the mJ range, corresponding to an amplification factor of ~70. The energy density of the beam right after amplification is about 1.2 times ε_{sat} (2 mJ energy in an around 10 mm diameter beam), which is close to the determined optimum for pre-amplifiers. The small angle provides the high amplification factor, however also causes stronger ASE coupling. In order to suppress the amplified spontaneous emission we applied a spatial filter after the first pass. To keep the arrangement relatively compact we applied here a relatively short spatial filter. This way it was easier to build a stable optical arrangement and to stay within the middle region of the time window of the maximal gain. The drawbacks of the short filter are mostly in connection with the use of short focal length focusing optics. This way the focal spot size is very small generating high intensities in the focus and consequently faster deterioration of the used pinholes. Additionally the introduced pulse front distortions are also higher this case. The beam was focused with an f = 180 mm fused silica lens. In the focus position a quartz pinhole with 50 μm diameter was used, placed into an evacuated tube. The whole vacuum tube was mounted on an xyz micrometer translator stage, allowing precise positioning of the pinhole. For collimation an f = 350 mm quartz lens was used not only collimating but also introducing an around 2 times magnification of the beam. After the spatial filter the beam diameter was about 25 mm delivering about 1-1.5 mJ energy. For the 2nd and 3rd passes the divergence was aligned so that the beam at the output filled the aperture of the amplifier. The angles were adjusted to 2° and 2.4°, respectively. After the 2nd pass about 1.8 times the saturation energy density was reached (beam diameter around 30 mm) corresponding to an amplification factor of ~20. In the third pass a large off-axis angle was adjusted providing a small amplification factor (about 2) but still the biggest amount of extracted energy (~20-30 mJ). The measured output energy was 50 mJ with less than 5% energy fluctuation. The pulse length was measured to be ~530 fs (shown in Fig. 3.4), using a

homemade UV autocorrelator, based on multiphoton ionization in NO [82]. For the calculation of the pulse width a gauss fit was used, the measured FWHM value was 760 fs corresponding to 532 fs pulse duration.

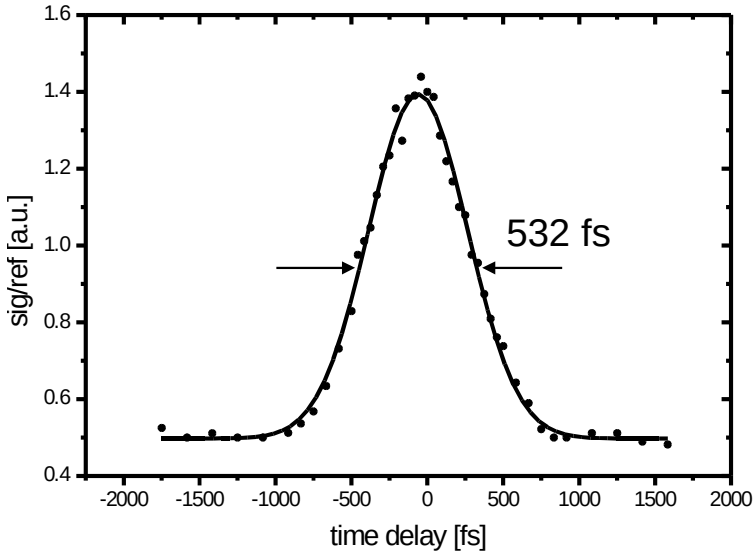

Fig. 3.4: Measured autocorrelation curve, the half with of the fitted gauss curve was 760 fs corresponding to 532 fs pulse length

The pulse-width broadening (~340 fs) relative to the pulse duration of the frequency tripled seed beam (~190 fs) can be explained by the group velocity dispersion (GVD) of the window materials using the equation given in (3.4).

$$\Delta T = \frac{l_Q}{c} \cdot \Delta\lambda \cdot \left(dn_g / d\lambda\right)_{Q,\lambda=248nm} + \frac{l_{CaF_2}}{c} \cdot \Delta\lambda \cdot \left(dn_g / d\lambda\right)_{CaF_2,\lambda=248nm}, \qquad (3.4)$$

where ΔT is the temporal broadening of the pulse, l_{mat} is the length of the material, $\Delta\lambda$ is the pulse bandwidth and $dn_g/d\lambda$ is the GVD coefficient of the given material at 248 nm. Using the values $l_Q = 36$ mm (quartz lenses in the off-axis arrangements and windows for the tripling box and for the vacuum pinhole), $l_{CaF_2} = 48$ mm (6 times the 8 mm thick CaF_2 window), $c = 300$ nm/fs, $\Delta\lambda = 0.7$ nm, and $dn_g/d\lambda = 1.334 \cdot 10^{-3}$ 1/nm and $2.104 \cdot 10^{-3}$ 1/nm for CaF_2 and fused silica (at 248 nm), respectively, the temporal broadening estimated to be ~330 fs, which is within the measurement error.

The focusability of the amplified output beam was measured in a simple arrangement, where the full diameter beam was focused with a 1 m nominal focal length fused silica lens (f was measured to be 1105 mm, partially because of the divergence of the beam) and the focal spot was imaged with a 10x microscope objective onto a CCD. The focal distribution was investigated using a beam analyzing system. (The results of a similar measurement are shown in Fig. 3.10 measured for the same amplifier but in a different optical setup.) For a square shaped output beam the diffraction limited focal spot size (FWHM) can be calculated as

$$x \approx \frac{\lambda \cdot f}{d}, \tag{3.5}$$

where λ is the wavelength of the radiation, f is the measured focal length and d is the beam size on the focusing element. For $d = 45\text{mm}$, $f = 1105$ mm, $\lambda = 248\text{nm}$ the calculated diffraction limited focal diameter would be $x = 6.1$ μm. The measured FWHM values were 12.5×14.5 μm corresponding to a 2.4×2.1 times diffraction limited beam.

The reached 50 mJ output energy is quite close to the theoretically estimated maximum extractable energy for our amplifier. In this arrangement the discharge parameters of our modified excimer module support a maximal output beam size of around 36x36 mm^2. From (2.19) $W_{eff} = L\sin\alpha \sim 37$ mm calculating with $L = 970$ mm discharge length and $\alpha = 2.2°$ off axis angle. Taking the optimal energy density value for a power amplifier (from [17]), the achievable maximal output energy can be calculated according to (2.21). Using the values $\varepsilon_{sat} = 2$ mJ/cm^2, $\varepsilon_{opt} = 2.2\ \varepsilon_{sat}$ and $A = 3.6^2$ cm^2 the maximal output energy is ~60 mJ. This means that using the off-axis amplification scheme operational parameters close to the theoretically achievable optimum have been found for our modified module. For further increase of the output energy excimer modules with even larger amplification cross sections or tricky optical arrangements have to be used. Such a powerful candidate is the so-called polarization multiplexing technique.

3.4 Description of a 100 mJ system

In this section a polarization multiplexing method (based on Sagnac interferometer's principle) is described and investigated to increase the extractable energy out of the same excimer module applied in 3.3. The modified KrF amplifier device (the same as the one described in 3.3) was tested in a 2-beam variant of the polarization multiplexing scheme, and 100 mJ maximum output energy pulses in a single subpicosecond beam at 248 nm were reached and characterized [80].

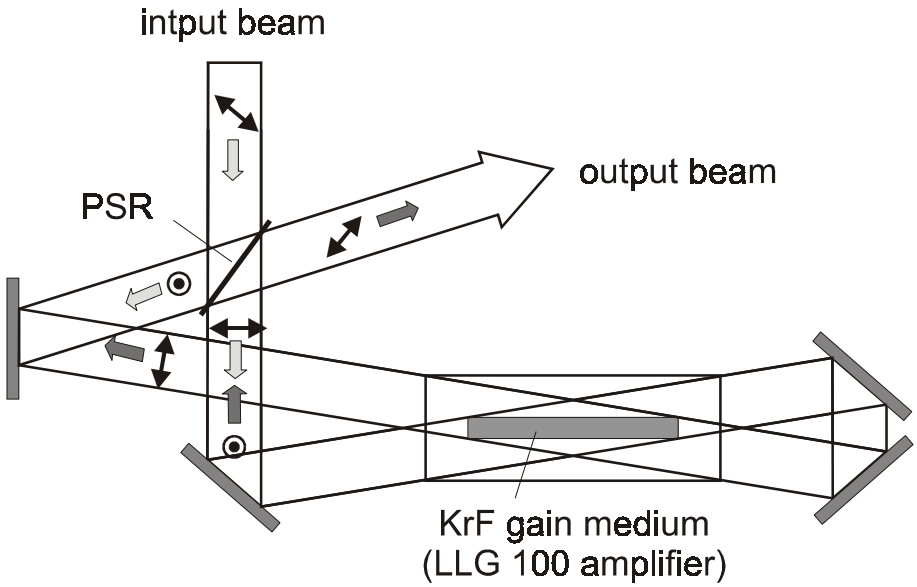

Fig. 3.5: Two-pass polarization multiplexing scheme, the key component is the polarization sensitive reflector (PSR)

It was shown by theoretical considerations that our modified wide aperture KrF amplifier can be used to amplify femtosecond UV pulses in a multiple pass arrangement up to ~60 mJ. In the previous section generation of 50 mJ energy output pulses was demonstrated using a 3 pass off-axis amplification scheme. However, to reach even higher output energies with the same amplifier a multiple beam arrangement (interferometric multiplexing) is needed. Multiplexing allows efficient extraction of the stored energy of amplifiers of short storage time by the use of a train of pulses. For shorter than picosecond pulses a generally applicable interferometric beam recombination method was found, and theoretical studies have already

been made [18]. The shortcomings of the conventional multiplexing methods (detailed in 2.3.2) are eliminated by using the same optical element for multiplexing and demultiplexing, so that the partial beams have exactly the same optical path, allowing an automatic, phase-locked synchronization of the beams (Fig. 2.4 b in 2.3). In the measurements detailed in the followings 2 beams in 2 passes were amplified based on the polarization splitting method (Fig. 3.5).

The most important component of the optical setup is the polarization sensitive reflector (PSR). This splits the input beam into two partial – perpendicularly polarized – beams counterpropagating in the ring, and recombining them again, thus providing a single output. The Sagnac interferometer is considered to be well-aligned, when the two partial output beams have a complete spatial overlap. If the input beam has a plane phase front, the output beams have always parallel phase fronts for any alignment of the interferometer, in which the number of mirrors – taking into account the PSR itself – should be an odd number. This means that neither a parallel shift nor a directional change of an optical component can cause a non-parallelism of the output beams.

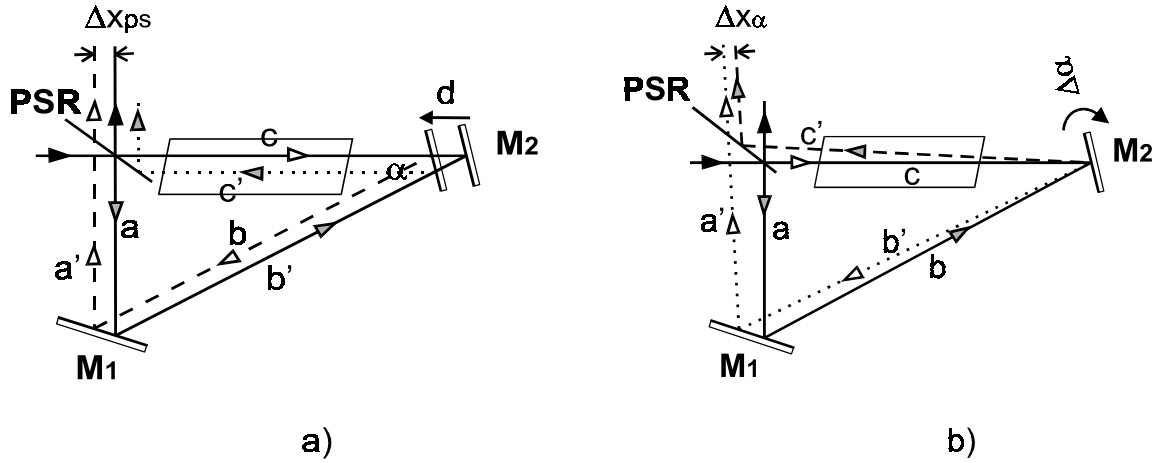

Fig. 3.6: Simplified scheme of interferometric multiplexing based on a Sagnac interferometer, a) misalignment in the case of a parallel shift d of M_2 and b) misalignment caused by $\Delta\alpha$ directional change of M_2 (PSR means polarization sensitive reflector, M_1 and M_2 are dielectric mirrors)

However, as displayed in Fig. 3.6 a, a parallel shift of d causes a lateral shift of the two outputs which is given by (3.6)

$$\Delta x_{ps} = d \cdot \sin\alpha . \tag{3.6}$$

Directional change of a component causes not only a parallel shift but also a phase shift (Fig. 3.6 b). The parallel shift can be calculated as (3.7)

$$\Delta x_{\alpha,\varepsilon} = (a+b-c)\sqrt{\sin^2(2\Delta\alpha)+\sin^2(2\Delta\varepsilon)}, \tag{3.7}$$

where $\Delta\alpha$ and $\Delta\varepsilon$ are the directional misalignment of a component in a plane parallel and perpendicular to that of the interferometer, respectively, and a, b and c are the optical pathways between the components of the setup. The phase shift of the two beams is given by

$$\Delta s_{\alpha,\varepsilon} = 2(a+b-c)\sqrt{\sin^4\Delta\alpha+\sin^4\Delta\varepsilon} . \tag{3.8}$$

Using the assumption $\Delta\alpha \approx \sin\Delta\alpha$ with $(\Delta\Psi/2)^2 = \Delta\alpha^2 + \Delta\varepsilon^2$ and D=a+b-c, (3.7) and (3.8) can be simplified as

$$\Delta x_{\alpha,\varepsilon} = D \cdot \Delta\Psi, \tag{3.9}$$

and from the relationship $1/2(\sin^2\alpha+\sin^2\varepsilon)^2 \le \sin^4\alpha+\sin^4\varepsilon \le (\sin^2\alpha+\sin^2\varepsilon)^2$ one obtains for Δs:

$$1/8 \cdot D \cdot \Delta\Psi^2 \le \Delta s \le 1/2 \cdot D \cdot \Delta\Psi^2 . \tag{3.10}$$

Here $\Delta s = 1/8 D\Delta\Psi^2$ if $\Delta\alpha = \Delta\varepsilon$, and $\Delta s = 1/2 D\Delta\Psi^2$ if $\Delta\alpha = 0$ or $\Delta\varepsilon = 0$.

From Fig. 3.6 D = a+b-c is the optical delay of the two beams and assuming only small misalignments $\Delta\Psi$ is the angle deviation of the outputs from the original direction caused by the misalignments $\Delta\alpha$ and $\Delta\varepsilon$ of an optical component. In case of excimer amplifiers where D is around 1 m, assuming $\Delta\Psi$ = 0.5 mrad - which can easily be realized without special care - Δx = 0.5 mm and 31.25 nm $\le \Delta s \le$ 125 nm. This means that it is possible to reach an

alignment, where the lateral displacement can be neglected compared to the beam size and the phase matching accuracy is better than $\lambda/2$.

The multiplexing arrangement requires input energies, in the mJ range. The reason for this is the absence of a similar pass like the first one in e.g. a 3 pass off-axis arrangement, where the energy is boosted up into the mJ regime. For this purpose we used the output of a femtosecond dye-excimer laser system. A further amplifier stage for the Ti:Sa system which would be able to provide ~1 mJ frequency tripled seed pulses was not available in our institute. The output of the dye - excimer laser system (see in Fig. 3.1) was sent through a 3 m long spatial filter where the beam was cleaned up from the ASE. At this point the focused intensity is already so high that special care had to be taken to design the filter. In order to elongate the lifetime of the pinhole we used a long focal length lens to get a bigger focal spot diameter (2r) and through that a decreased power density in the focus (power density in the focus ~ $1/r^2$). We used home-made CaF_2 and MgF_2 pinholes as filtering elements because of the much smaller two photon absorption coefficient and hence higher damage threshold of these materials. After the spatial filtering the beam was collimated and sent into the Sagnac interferometer. Its first component is the polarization sensitive reflector (PSR). The PSR is a special mirror, which has 100 % reflectivity for s-polarized 248 nm radiation and 100 % transmittance for the p-polarized 248 nm radiation at Brewster angle. In order to get two beams with the same intensity, it is necessary to have a completely linearly polarized seed radiation and the polarization of the input beam has to be set so that it encloses an angle of 45° with the plane of incidence of the PSR. This results in a reflected and a transmitted beam with roughly the same intensity, one beam with s- and the other with p-polarization. Then, the reflected beam was delayed by 3.5 ns – which is in the range of the relaxation time of a KrF amplifier [7] - and both were sent through the amplifier. At the other end of the amplifier a delay of 7 ns was adjusted for both beams in order to obtain complete relaxation of the amplifier before the beams re-enter it for the second pass. Through this delay line the beams were sent back to the amplifier to retrace the same beam path. After subsequent amplification the two beams reach the PSR at exactly the same time, thus yielding a recombination with interferometric precision. The beam, which was totally reflected, will be totally reflected again and the opposite holds for the transmitted beam, resulting in only a small leakage back

to the spatial filter. The applied off-axis angle of 2.2° was the highest allowed by the clear aperture of the amplifier windows.

Fig. 3.7 shows calculated values of the overall contrast (C calculated as in (2.14)), overall extraction efficiency (<η>, given in(2.10)) and the output energy ($E_{out} = \varepsilon_{out}A$) as a function of the input energy (E_{in}) for different off-axis angles (α) in our amplifier calculating with two passes of the same off-axis angle. This is the case for the multiplexing setup assuming that the delays were defined so that the population inversion in the active medium is totally recovered between each amplification step.

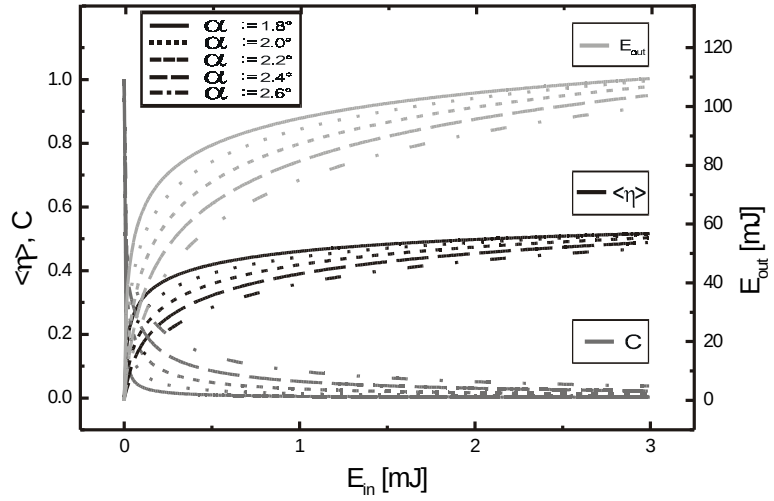

Fig. 3.7: Calculated values of the overall contrast (C), overall extraction efficiency (<η>) and the output energy (E_{out}) as a function of the input energy (E_{in}) for our amplifier assuming two passes with the same off-axis angles

It is seen from Fig. 3.7, that by increasing the input energy the output energy increases fast and saturation is reached quite soon. At larger off-axis angles the output energy increasing slowlier, however because of the faster saturation at smaller angles the difference will be very small already at the end of the measured region. The overall extraction efficiency seems to be quite insensible in the whole plotted region after a fast increasing period. In contradiction with that the contrast decreases fast with increasing input energies and a very strong depencence on the off-axis angle is visible. For larger angles the drop is significantly slower than for smaller ones. Altogether, high output energies can be reached with only small inputs,

although at larger off-axis angles this value is somewhat lower. However, small off-axis angles will result in a bad contrast. A trade-off can be reached using 1-2 mJ input energy and large off-axis angles reaching high output energy and good extraction efficiency at relatively good contrast values.

By constructing the PSR we had to consider two very important features. One of them was two-photon absorption of the PSR substrate material, the other is a reflection from the non-coated surface of the polarizer. There are different possibilities to place the polarizer, which had to be considered (Fig. 3.8).

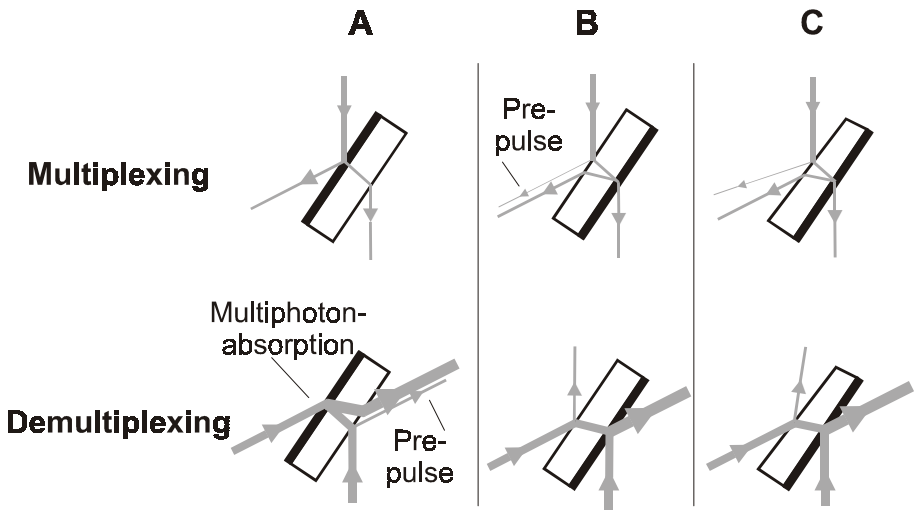

Fig. 3.8: Different possibilities to place the polarizer into the beam-path, the most critical properties: appearance of pre-pulses and multiphoton-absorption

If the input beam hits the reflecting surface first, no difficulties at the multiplexing process occur, however, upon demultiplexing the recombination of the two beams will take place before the beam passes the substrate material. This way the high-energy beam has to propagate through the substrate material causing higher losses by nonlinear absorption or color center formation. In addition, a small reflection (1-2% of the total energy) can occur from the substrate surface by any misalignment from the Brewster-angle, causing a pre-pulse at the output few picoseconds before the main pulse (corresponding to the optical path in the substrate material), which is not tolerable in many experiments (Fig. 3.8 A).

The other possibility is to place the PSR so that the input beam first reaches the non-reflecting surface. In this case the recombined beam will not pass the substrate but a pre-pulse is

injected into the amplifier and can deplete it before the main pulse enters the amplifier (Fig. 3.8 B). To eliminate this problem we tried to use antireflection coatings but for such a special case no practicable AR-coating is available and even with the use of a special colloid AR-coating the transmission is only around 98-99% for the critical polarization, which is still not satisfactory. To solve this problem we used a wedged substrate with a wedge angle of 20', which causes about 1° deviation at Brewster-angle incidence (Fig. 3.8 C). Such deviation results in a lateral shift enough to get rid of the pre-pulse on the > 2 m way up to the amplifier. Because of the wedge the polarizer is working like a prism, causing some limitations for the focusing and temporal properties of the output beam through angular dispersion.

In the following this limiting effect will be evaluated and it will be shown that it can be neglected. The effect is different for the transmitted and reflected parts. The reflected part will see the PSR as a prism with $\varepsilon_p = 20'$ prism angle two times, first by entering the interferometer and for the second time by leaving it. The polarizer will introduce the same deviation in both cases that have to be added. For the reflected part the PSR will act as a prism with $\varepsilon = 2\varepsilon_p$ prism angle but only once, by entering the interferometer. As it is known a single dispersive element with a given angular dispersion introduces negative GVD (group velocity dispersion), and therefore a spatially evolving negative chirp [83,84]. The introduced chirp is a function of the angular dispersion ($d\Theta / d\lambda$), wavelength (λ) and spectral bandwidth ($\Delta\lambda$) of the laser pulse and the optical path of the beam (l), according to

$$\Delta T = \frac{l \cdot \lambda}{c \cdot n} \cdot \left(\frac{d\Theta}{d\lambda} \right)^2 \cdot \Delta\lambda, \tag{3.11}$$

where c is the speed of light, n the absolute refractive index in air ($n \approx 1$), and $d\Theta/d\lambda$ can be derived from (3.12)

$$\Theta(\lambda) = \alpha_1 + \arcsin\left[n(\lambda) \sin\left(\varepsilon - \arcsin\left(\frac{1}{n(\lambda)} \sin\alpha_1\right) \right) \right] - \varepsilon, \tag{3.12}$$

where α_1 is the incident angle of the beam and ε is the apex angle of the prism. Substituting the values l = 7,3 m, λ = 248.5 nm, c = $3 \cdot 10^8$ m/s, $\Delta\lambda$ = 0.6 nm, $\alpha_1 = 56°$, and $\varepsilon_p = 20'$ into

(3.11) and (3.12), the calculated temporal broadening of the pulse is –0.084 fs and –0.323 fs for the transmitted and reflected beam, respectively. It is evident that this effect is fully negligible, the spatially evolving chirp practically does not influence the pulse length and will not cause any difficulties at recombination.

A further effect is that the introduced angular dispersion will cause a lateral walk-off of the different spectral components inside the beam and also influence the minimal focal spot size. Using $l = 7$ m, and $d\Theta/d\lambda = 4.92 \cdot 10^{-6}$ rad/nm the calculated lateral misalignment inside the interferometer is ~20 and 40 μm for the transmitted and reflected beam so it is around 3 orders of magnitude smaller compared to the beam size therefore it can be neglected. The lateral separation of the different spectral components in the focal plane, which is caused also by the angular dispersion of the prism, can be calculated as

$$\Delta x = f \cdot \frac{d\Theta}{d\lambda} \cdot \Delta\lambda \,. \tag{3.13}$$

The calculated deviation in the focal plane is 4.3 μm for the multiplexed beam, using the values $f = 750$ mm (focal length of the focusing lens), $\Delta\lambda = 0.6$ nm (spectral bandwidth) and 9.65×10^{-6} rad/nm angular dispersion for our PSR when its material is CaF_2 and the prism angle is $2\varepsilon = 40'$. This is about 0.7 times the size of a diffraction-limited focus for these parameters.

Using CaF_2 as substrate material instead of quartz can significantly decrease the losses caused by nonlinear absorption. It is well known from the literature that for fused silica the losses are mainly caused by two-photon absorption while for CaF_2 by three-photon absorption [15]. In the 10 GW/cm^2 intensity range – which is reached for a 500 fs long pulse if 100 mJ energy in concentrated in a 36 mm size square like beam – this allows around 66.8% transmission for fused silica and 99.7% transmission for CaF_2 calculating with 8 mm material thickness (which is necessary to reach good mechanical stability and surface polish for the PSR). The other parameters used in this calculation are: 58° incidence angle, 9×10^9 W/cm^2 input intensity, $n = 1.508$ and 1.468 refraction index for fused silica and CaF_2 and $\beta = 5.8 \times 10^{-11}$ cm/W two-photon absorption coefficient for quartz and $\gamma = 3.8 \times 10^{-23}$ cm^3/W^2 three-photon absorption coefficient in the case of CaF_2 as it is given in [15]. These calculations show that CaF_2 is a

much better choice for substrate material, allowing higher transmission with minimized losses even at output energies in the 100 mJ region.

Under optimized conditions output pulses with 100 mJ energy were obtained in a single beam. The intensity distribution of the output beam after demultiplexing is shown in Fig. 3.9 with and without amplification. For this measurement a fluorescing glass plate was placed into the beam path whose surface was imaged onto a CCD camera.

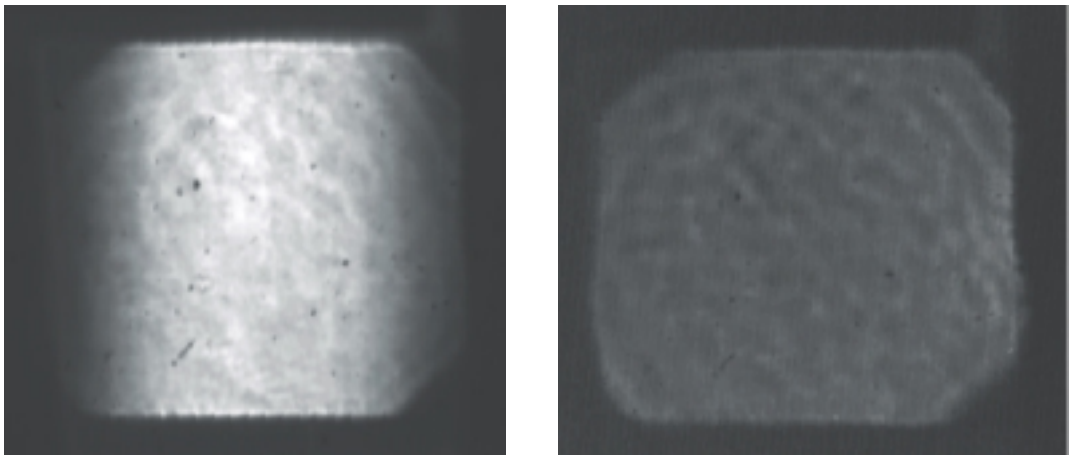

Fig. 3.9: Measured beam profile of the multiplexed output made by imaging the whole beam onto a CCD camera (on the left: amplifier on, on the right: amplifier off)

For an assessment of the focusability the output beam was focused with an f = 750 mm focal length lens and a magnified image of the focal spot was observed by the CCD-camera (Fig. 3.10), recorded and analyzed with a beam analyzing system (MrBeam, LLG).

The size of the beam was 36 × 36 mm, the calculated diffraction limited focal spot size is 6.3 μm. The measured values were 14.88 × 12.86 μm for the not amplified beam and 13.96 × 12.40 μm in the case of the amplified output, corresponding to a 2.36 × 2.04 and 2.22 × 1.97 times diffraction limited beam, respectively.

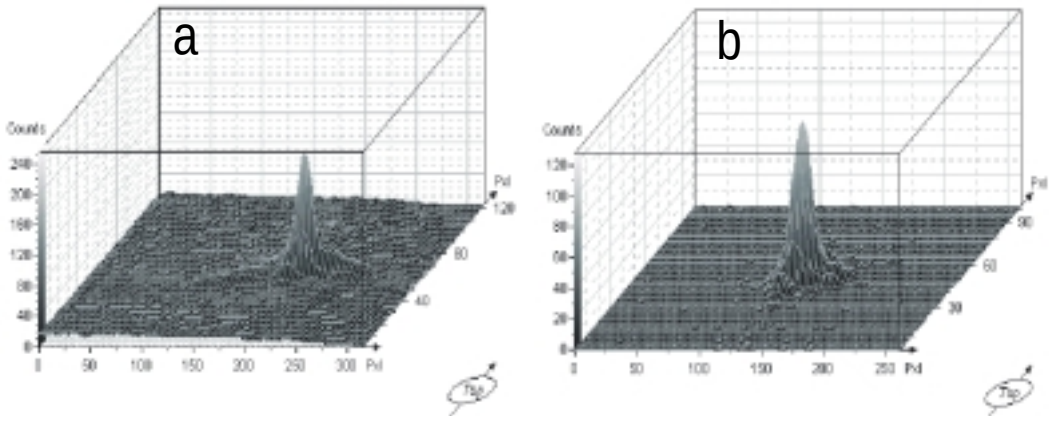

*Fig. 3.10: Focal distribution of the output beam **a** without amplification and **b** with amplification. The beam was focused with a 750 mm focal length fused silica lens and was imaged onto a CCD camera with a 10x magnification quartz objective*

Such a high power table-top femtosecond laser system operating in the UV region at 248 nm and delivering 100 mJ output energy in a single beam facilitates the generation of about 1.7×10^{19} W/cm^2 of focused intensity with the use of high quality focusing optics (f = 70 mm off-axis parabolic mirror). These intensities allow the investigation of high intensity processes and plasma-physics experiments for many laboratories with the use of such a small-scale excimer laser system. On the other hand for high precision material processing this intensity level is higher than necessary. In numerous applications it is more desired to make the process faster, most effectively by increasing the repetition rate. Solid state front-ends are able to operate at several kHz repetition rate, more difficult task is to solve the problem for excimers. It necessitates the development of high repetition rate excimer modules as short pulse amplifiers.

3.5 Description of a 9 W system

Thanks to the dynamic development of short pulse solid state laser sources [85-88], nowadays a new potential occurred to push the repetition rate up to the limit of the excimers in solid state excimer hybrid systems, in contrast to dye laser sources used before. There the

maximum repetition rate was restricted to the 10 Hz range. Front-end devices with high repetition rates open the way to the development of high average power femtosecond UV laser systems. This research line was followed by the group of S. Watanabe [89-91]. Recently, they reported on a solid state Ti:Sa-excimer system delivering 50 W output power at 200 Hz with 248 nm femtosecond UV pulses [89]. The significant increase in the output power was achieved by splitting the seed pulse into 4 parts and than amplifying them resulting in 4 output beams with 12.5 W power each delayed by 2.5 ns. Without recombination of the pulses – which is practically impossible – the applicability of such an arrangement with a 4 beam pulse train is restricted to specialized experiments. (A multiple pulse structure can not be tolerated in experiments like e.g. formation of a plasma channel for multikilovolt x-ray generation [92], study of hot electron production [93], etc.) Moreover, a rather complex, home made front-end was used in [89], thus strongly limiting the applicability of such an arrangement in industrial environment e.g. for material processing.

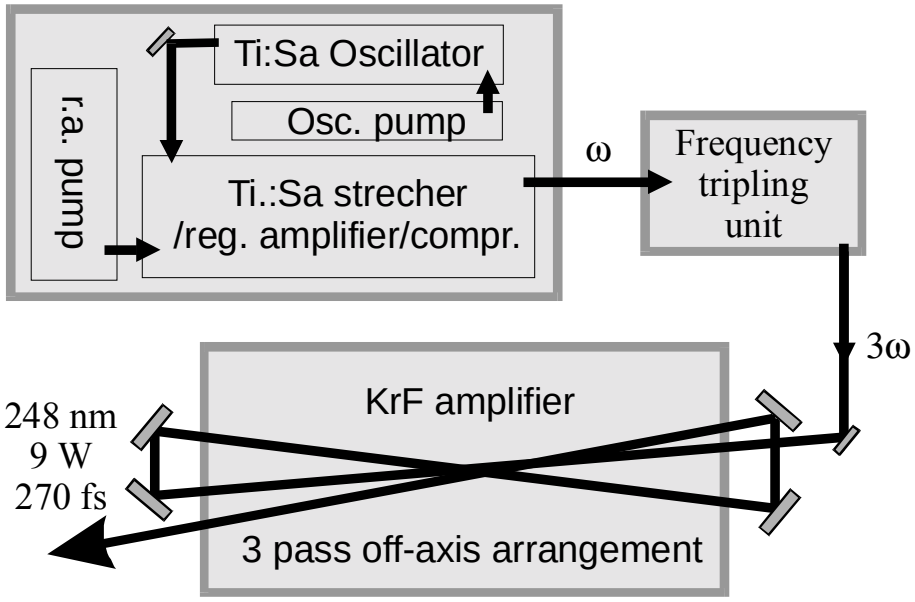

Fig. 3.11: Femtosecond laser system consisting of a Ti:Sa solid state front-end, a frequency tripling stage and an excimer amplifier in a three pass off-axis arrangement

The system developed in our group is a compact table-top UV femtosecond system based on the combination of a Ti:Sa laser-system, and a newly developed wide-aperture, discharge-pumped KrF amplifier [81]. Frequency tripled seed pulses of the Ti:Sa system were amplified

in an excimer module using a 3 pass off-axis scheme. The device was specially modified and carefully optimized for short pulse amplification. Measurements of the stored energy as a function of gas pressure, repetition rate and peaking capacitance were carried out. At optimized operational conditions the laser system delivers 270 fs pulses at 248 nm with an average power of more than 9 W at 300 Hz in a single output. The compactness and reliability of the system would, in principle, allow industrial application of the apparatus.

In Fig. 3.11 the 3 main parts of the system is shown. The first part is a commercially available Ti:Sapphire solid state laser system (Spectra-Physics Lasers, Inc., CA) followed by a frequency tripling unit being the second part. Both of them were already detailed in 3.2. After frequency tripling a telescope was used to adjust the proper divergence for subsequent amplification. After the telescope the 248 nm pulse was directed into a specially modified wide aperture, discharge pumped excimer module based on a LP NovaLine laser. The length of the discharge was 970 mm with an electrode separation of 25 mm. The excimer module was used in a 3 pass off-axis arrangement in order to reach the optimal conditions for the amplification of femtosecond pulses [16]. The divergence was adjusted so that the beam entirely fills the clear aperture of the amplifier at the end of the 3rd pass (25x25 mm). The chosen off-axis angles were 1°, 1.5° and about 2° for the three passes, respectively.

	laser param.	$\ln(E_{out}/E_{in})$	w´ (mm)	E_{st} (mJ)
repetition rate	25 Hz	5.701	21.6	61.6
	100 Hz	5.531	22.0	60.8
	250 Hz	5.559	23.2	64.5
	300 Hz	5.647	21.9	61.8
pressure	1.9 bar	4.813	23.5	56.6
	2.3 bar	5.109	23.4	59.8
	2.8 bar	4.877	24.1	58.8
	3.3 bar	5.647	21.9	61.8

Tab. 3.1: Measurement of the stored energy depending on the repetition rate and gas pressure. $\ln(E_{out}/E_{in})$ and W' are measured values, E_{st} is the calculated momentarily stored energy.

After modifications of the discharge frame, the windows and the window holders, stored energy measurements were carried out to characterize the module and to fit the operational conditions to the requirements of short pulse amplification (see also in 3.3). First the dependence of the stored energy on the repetition rate and gas pressure was measured and the results are displayed in Tab. 3.1.

The measurements on the repetition rate dependence were carried out at 3.3 bar pressure with 43 nF capacitance of the peaking capacitors. The results show that our amplifier's stored energy is practically independent of the repetition rate in the measured range.

It is also known that at high repetition rates the stored energy can strongly depend on the pressure because of insufficient circulation of the gas in the discharge volume. To investigate this behavior of the given amplifier E_{st} has been measured at 300 Hz and different pressures, and the results are displayed in Tab. 3.1. (measured with 43 nF peaking capacitance). It is seen, that E_{st} is optimal at the highest pressure allowed in the chamber (3.3 bar).

In further measurements we applied 3.3 bar pressure in the amplifier and measured the dependence of the stored energy on the peaking capacitance. By optimizing the number of capacitors it was possible to reach an increase of about 14% in the stored energy compared to the original value. This best case was achieved by decreasing the number of capacitors by about 34% (Tab. 3.2).

peaking capacitance (nF)	$\ln(E_{out}/E_{in})$	w´ (mm)	E_{st} (mJ)
43	5.647	21.9	61.8
35	5.732	23.2	66.5
28.5	5.779	24.3	70.2
20.5	5.686	23.1	65.7

Tab. 3.2: Measurement of the stored energy dependence on the peaking capacitance

The values in these measurements were recorded at 300 Hz repetition rate at a total pressure of 3.3 bar. For the further experiments we set the number of capacitors to the measured optimal value and built up the 3 pass off-axis arrangement that was very similar to that described in 3.3. The frequency tripled beam from the telescope (with a given divergence) propagates through the amplifier three times. After each pass a delay line is applied because

of the ~2-3 ns recovery time of the amplifying medium. In the 1st pass the energy is boosted up to the mJ region. In the second pass the energy reaches the 10-15 mJ region. The energy density is around 2-2.3 times the saturation energy density (E_{sat}) of KrF in an about 17×17 mm beam. In the last pass the beam reaches the 25×25 mm size (which is the maximum allowed by the electrode separation) with pulse energy of around 30 mJ at an off-axis angle of 2° (the highest allowed by the windows and the off-axis frame we used). This results in an output energy density of around 2.4 times E_{sat}, which is in the optimal region for a power amplifier [3,17]. The measured ASE content was around 15% in the case of maximal gain but by reducing the gain to 80 % of its original value it was possible to reduce the ASE level to below 4-5 %. These signal-to-noise ratios represent an upper limit, since they were calculated as the ratio of the output power without seed and with seed pulse, however the real ASE content is smaller in the presence of the short pulse because the gain is depleted by the femtosecond pulse preventing ASE generation in the presence of the short pulse [89].
The dependence of the output power on the repetition rate has also been measured. The results show a linear dependence through the measured region with a gradient of 1, which means that the output pulse energy is practically independent from the repetition rate (as it was already found by measuring the stored energy). The measured values can bee seen in Fig. 3.12.

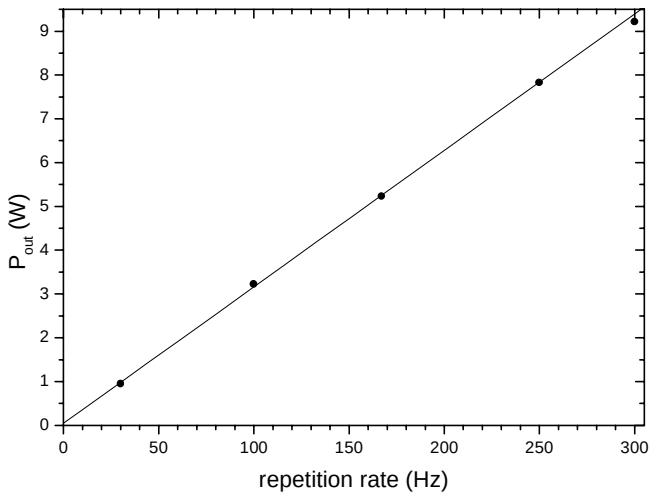

Fig. 3.12: Measured output power as a function of the repetition rate.

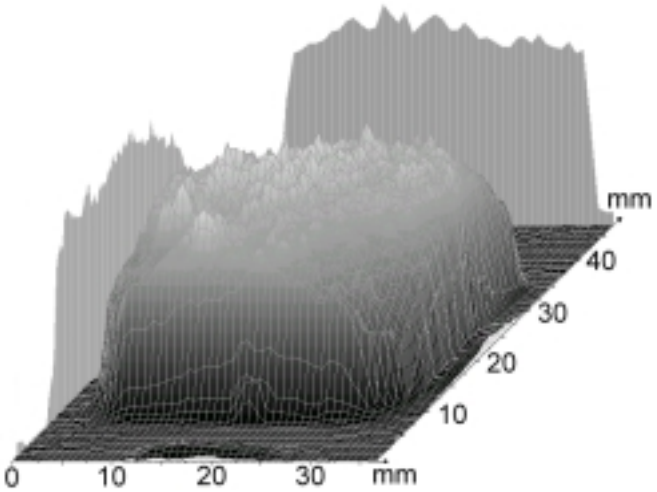

Fig. 3.13: Measured 3D near-field beam profile recorded by a CCD camera and processed with a beam profiler system.

A 3D graph of the output beam profile shown in Fig. 3.13 was recorded by a CCD camera and than processed with a home built beam profiler system. A relatively flat-top beam profile is visible.

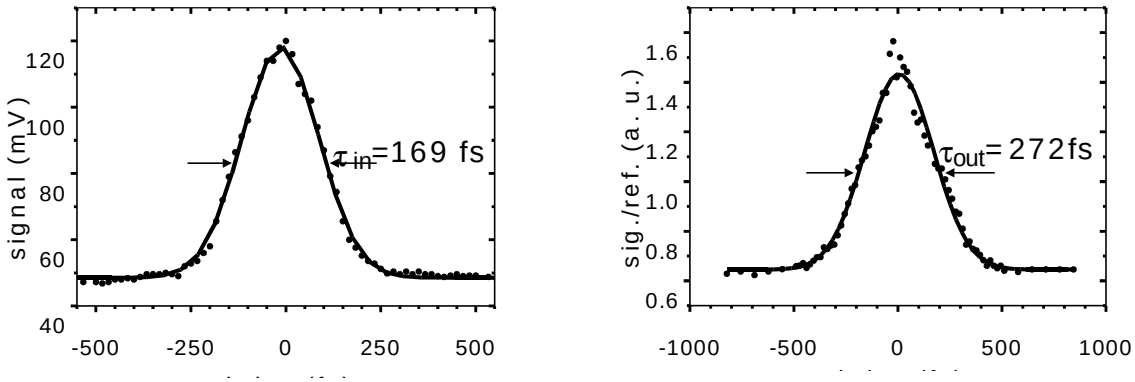

Fig. 3.14: Autocorrelation curves and calculated pulse widths of the seed (a) and the amplified (b) pulses. τ_{in} and τ_{out} are the calculated pulse lengths for the applied gaussian fits.

We also measured the pulse length of the seed pulse and the amplified pulse. In Fig. 3.14 autocorrelation measurement of the seed pulse (a) and the amplified output pulse (b) is visible. The autocorrelation widths for the two pulses were found to be 241 and 388 fs for the

incoming and the amplified beam, respectively, corresponding to 169 and 272 fs pulse lengths, calculating with gaussian pulse shapes.

The values demonstrate a temporal broadening of 103 fs. Calculations show that the measured temporal broadening is mainly caused by the GVD in the window materials. The total broadening caused by $n_g(\lambda)_{248nm}$ of the window materials (6 mm thick CaF_2) was calculated (using $\Delta\lambda = 0.65$ nm and $(dn_g/d\lambda)_{CaF_2,248nm} = 1.334 \cdot 10^{-3}$ 1/nm) and found to be 104.5 fs, which is in good agreement with our experimental results.
Combining the advantages of a solid state front-end with those of an excimer KrF amplifier and with optimized operational conditions it was possible to reach over 30 mJ output pulses in a single beam. The repetition rate could be increased up to 300 Hz reaching an average output power of over 9 W in a single 270 fs UV pulse. To our knowledge, at this repetition rate, this system generates the most powerful UV femtosecond pulses ever obtained.

4. Applications

The unique possibilities of the laser systems described above open new ways to investigate new application fields. Because of the relatively short history of the short pulse techniques, the study of the ablation process for different materials is still not completed. With reducing pulse duration higher and higher resolution in time can be reached, concentrating significant scientific forces onto this field. Improvement of the spatial resolution is another strong motivating force. This is resulting in a worldwide trend of decreasing the wavelength of the irradiating sources. Up to date the applied wavelength in the industry for IC fabrication is 248 and 193 nm, but the first prototypes operating at 157 nm are running. To further decrease the wavelength, the generation of efficient XUV pulses through frequency tripling of 248 nm pulses is a powerful candidate, delivering 83 nm wavelength subpicosecond XUV radiation [94,95], getting closer to the ultimate aim of 13 nm [96]. Because of physical and practical reasons, the shortest wavelength at which energetic subpicosecond pulses can be obtained is 248 nm, and so short pulse systems operating at that wavelength are the best candidates for the different material processing studies up to date. Belong the numerous application possibilities these are investigation of metal deposition on silicon [97] or generation of submicron-size metal ant metal oxide dots on different surfaces with the laser-induced forward transfer (LIFT) technique [98]. Also the application of diffractive phase elements at 248 nm [99], generation of gratings with grating periods down to 300 nm, and drilling of submicron sized holes on practically all kind of solids [94,99-102] has been investigated. Some of these possibilities are detailed in the following sessions.

4.1 Subpicosecond ablation studies

As it is discussed in (2.4 and references there) the duration of the laser pulse plays a very important role in the ablation process, especially if materials with high thermal conductivity are necessary to machine with high spatial resolution. To verify the theoretical predictions, morphology changes as a function of pulse duration has been investigated [102].

The limiting effect of the heat conductivity can be neglected, if the penetration depth of the laser radiation is less than L_{th} (see equation (2.22)). For most metals (and semiconductors) this condition is fulfilled for pulses shorter than a couple of picoseconds. The ablation of sub-micron structures at 248 nm on copper and silicon representing the material classes of metals and semiconductors has been demonstrated. Periodic line structures with a line-spacing below 400 nm, and individual holes with diameters below 500 nm have been produced on the sample surface by single laser shot exposure (Fig. 4.1) and the pulse duration was varied for the different measurements between 500 fs and 50 ps.

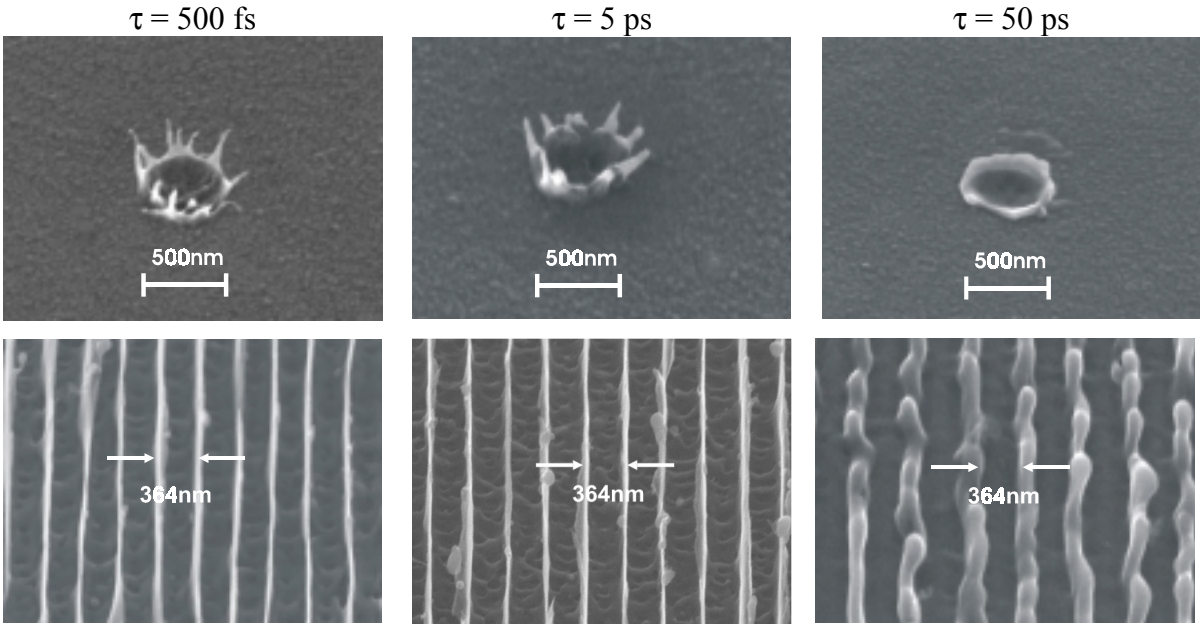

Fig. 4.1: Holes (1.2 J/cm^2) and grating structures (0.6 J/cm^2) ablated in copper with single pulses at 248 nm with different pulse durations.

The observed ablation morphology for metals can be explained as follows. Irrespective of the mechanism of the primary ablation process (evaporation) there will be a melt zone with a depth defined by the pulse duration, the electron-phonon relaxation-time, and the thermal diffusivity. This melt is affected by the recoil of the evaporated material and moves to the edge of the irradiated area forming rims or droplets. The shape of these structures depends on the driving force of the melt expulsion (recoil pressure) and the duration of heating and subsequent cooling. Fast cooling leads to rapid solidification causing sharp burrs and small

droplets in case of short pulses, and to broad, smooth rims for longer ones. It is readily seen from Fig. 4.1 and Fig. 4.2 that both for metals and for semiconductors the quality of the resulting structures deteriorates at pulse durations exceeding 5 ps.

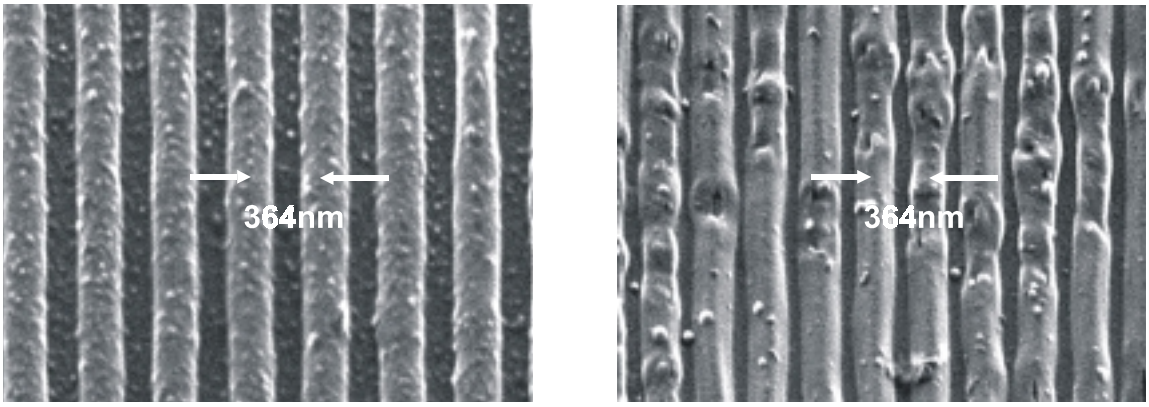

τ = 5 ps τ = 50 ps

Fig. 4.2: Grating structures ablated on silicon (0.2 J/cm^2) with single pulses at 248 nm with different pulse durations(5 ps and 50 ps, respectively).

The influence of the applied pulse duration on the morphology of various materials has been studied, however, the processes involved are not yet completely understood. In particular, knowledge of the dynamic evolution of the processes, starting with the absorption of the laser energy, continuing with melting followed by ablation and resolidification, is of crucial importance. In order to learn more about the dynamics of the ablation process, pump-probe measurements of the temporal evolution of sub-micron structures can be performed [102-104].

It has been shown, that the morphology of the ablated structures is significantly different for short pulses. But not only morphological differences can be measured using femtosecond pulses but also differences in the ablation thresholds and ablation rates. Ablation properties of metals, semiconductors have already been investigated by several groups [41,42,103,105]. However, novel materials like nanoparticle layers - to our knowledge - have not been investigated so far.

That is why basic ablation properties (like ablation thresholds and rates) of nanoparticle layers have been investigated [106]. Based on a newly developed inert gas evaporation and deposition technique [107], thick films of ultra-fine gold particles were prepared. This

deposition method is designed for creating isolated nanocrystals and nanocrystal films with well-defined narrow-band log-normal particle size distribution of (7 ± 1) nm [108]. These nanoparticles are of high purity because they are "distilled" in a high-purity inert gas atmosphere. Furthermore, they are formed under conditions of quasi-thermal equilibrium. Therefore they have very good crystallinity and have a well-controlled and reproducible mean size ranging from 3 – 100 nm. The ablation properties of the same material with different atomic structures like in the case of conventionally evaporated layers and nanoparticle structures, can react differently with short laser pulses, similarly to the numerous differences in other material features like flexibility and hardness (10 times higher for nanoparticles than for vacuum evaporated layers), annealing temperature (above 700 °C for nanogold [109]), resistance against oxidation (e.g. in the case of iron and aluminum) or electronic properties [110], caused mainly by the defect-free nature of nanoparticles. That is why UV laser ablation of gold nanoparticle films on glass substrates using femtosecond pulses was investigated and compared with the ablation properties of conventionally evaporated gold layers. The pulse length of the laser was 500 fs at 248 nm wavelength. Ablation thresholds, ablation rates at different fluxes, and the morphology of the ablated structures were measured and explained by taking into account the energy transport properties of nanocrystalline and conventionally evaporated gold films [106].

The generation process of the nanogold films used in the experiments can be described as follows. Gold was evaporated from a carbon crucible by induction heating and condensed in an inert (He) gas atmosphere at pressures of 250, 500, and 750 mbar (Fig. 4.3).

A selection of nanocrystals was fed into the deposition chamber as a jet flow via the transfer pipe and a special "nozzle" having a special inner shape and an end diameter of 500 μm. The temperature of the molten metal was kept ~100 K above the melting point to obtain optimal vapor pressures. In the deposition chamber the pressure was kept below 10^{-1} mbar. The substrate was cold (50 °C) glass, cleaned and degassed previously by standard techniques.

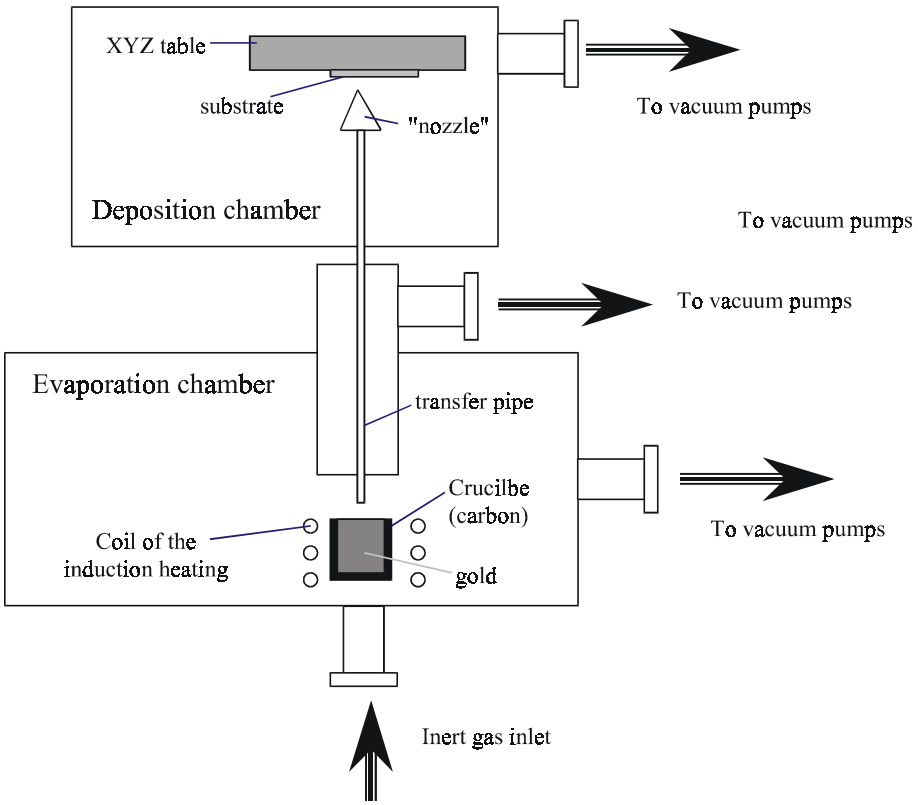

Fig. 4.3: Experimental setup for nanoparticle film production by the inert gas deposition method

Ablation experiments were performed with a short-pulse, hybrid Ti-sapphire-KrF laser system delivering 50 mJ energy output pulses at 248 nm with pulse duration of about 500 fs (described in 3.3). Irradiation was carried out in a mask projection setup. In this arrangement a 4.5 mm diameter circular aperture was placed into a homogeneous part of the laser output beam and was imaged onto the sample surface with a 200 mm focal length lens, resulting in irradiated spots of 250 μm diameter. The laser fluence was varied between 80 and 300 mJ/cm^2 by a variable attenuator. In order to avoid air breakdown in the focus the sample was located in a vacuum chamber. Ablation depths were measured by a Dektak 3030 Auto II stylus profilometer and by optical microscopy. The morphology of the ablation holes was investigated using a scanning electron microscope (Zeiss DSM 962).

During laser ablation of metal samples melting of the surface occurs and governs the process even in the case of subpicosecond UV pulses [42]. Theoretical and experimental investigations have demonstrated the key role of electron–phonon coupling in the fast ablation

processes [111,112]. As a first step the optical excitation generates hot electrons in the metal sample whose energy will be converted into the lattice through electron–electron scattering and electron–phonon relaxation within a couple of ps. The rates of these processes are different for nanocrystalline films, which cause differences in the ablation mechanisms. Besides their mechanical and chemical stability, the resistance of thin films to laser irradiation is of crucial importance in some important applications. Such properties of layers can be investigated in laser ablation experiments. However, in the case of metal films with high heat conductivity, rapid spreading of the absorbed optical energy during the laser pulse prohibits the evaluation of such measurements. The only way to circumvent this problem is to apply ultra-short laser pulses with pulse duration below the electron–phonon relaxation time of several ps. Moreover, applying ultraviolet laser pulses ensures a very short penetration depth of the radiation, thus further reducing any influence of the substrate on the laser heating of the film itself.

In the case of conventional vacuum-deposited films an ablation threshold of 145 mJ/cm^2 is obtained (Fig. 4.4 a). This is in good agreement with former results of other groups [41,103]. In the case of nanoparticle films the measured ablation thresholds were different for samples deposited at different inert gas pressures (250–750 mbar).

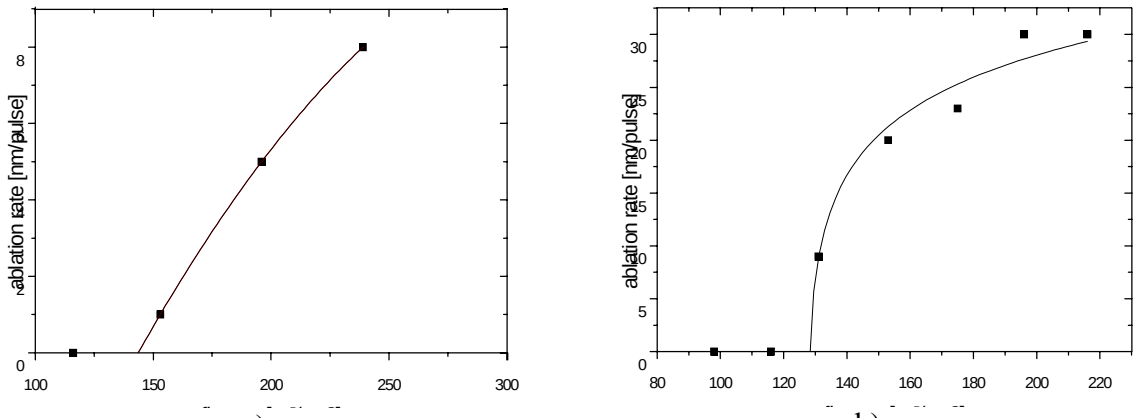

a) b)

Fig. 4.4: a) Ablation depth vs. laser fluence for evaporated gold and b) for nanocrystalline gold film (results derived after 20 laser shots, ν =5 Hz, E =200 μJ in the image plane with a diameter of 250 μm)

Fig. 4.4 b shows the ablation rate vs. laser fluence for a nanoparticle film evaporated at 250 mbar. From the data an ablation threshold value of 128 mJ/cm^2 is obtained. The measured thresholds increased with increasing pressure. For films made at 750 mbar the ablation threshold increased to the same value obtained for conventional vacuum-deposited films. Güdde et al. showed that by applying the two-temperature model the energy transport after absorption of a fs laser pulse is mainly determined by diffusion of hot electrons [113]. In agreement with this model the somewhat smaller ablation threshold for nanoparticle films can be explained by the irregularities at the borders of nanocrystals, because they can decrease the electron conductivity, keeping the energy in a smaller volume. These borders also act as "weak points" in the structure of the film. The higher pressure during the evaporation process promotes better bounding of nanoparticles, which determines the increase in the ablation threshold in the case of samples made at higher pressures. Comparing Fig. 4.4 a and b one can also see a difference in the ablation rates of the two kinds of samples. The almost five times higher ablation rate of the nanoparticle films can be explained by a difference in the ablation process. Presumably during ablation of nanoparticle films whole nanocrystals or nanocrystall agglomerates (with a size in the region of 30 nm) are removed. Although inside the crystals – because of their defect-free nature – the ablation threshold can be higher than for normal gold films, between them the binding forces are smaller. So for ablation we must deposit an amount of energy that is enough to break the connections between the nanocrystals to a depth the size of one nanocrystal. This theory is supported by the data in Fig. 4.4, where the measured rates were integer multiples of 7 nm, which is the particle size of our samples, and the saturation of the ablation rate is in the range of the agglomerates' size (about 30 nm). This would mean that the ablation threshold and rate of the nanoparticle films should depend on the particle size of the nanocrystals. At smaller crystal sizes the ablation thresholds and rates expected to be smaller than in the case of larger ones.

Fig. 4.5 a and b indicates that the morphology of the ablated structures is similar in the case of nanoparticle and conventional gold films. For this comparison both types of film were only partially removed by 20 pulses at laser fluences slightly above the ablation threshold (132 mJ/cm^2 and 156 mJ/cm^2, respectively). In both cases well-defined edges and very similar structures of the ablated areas are visible.

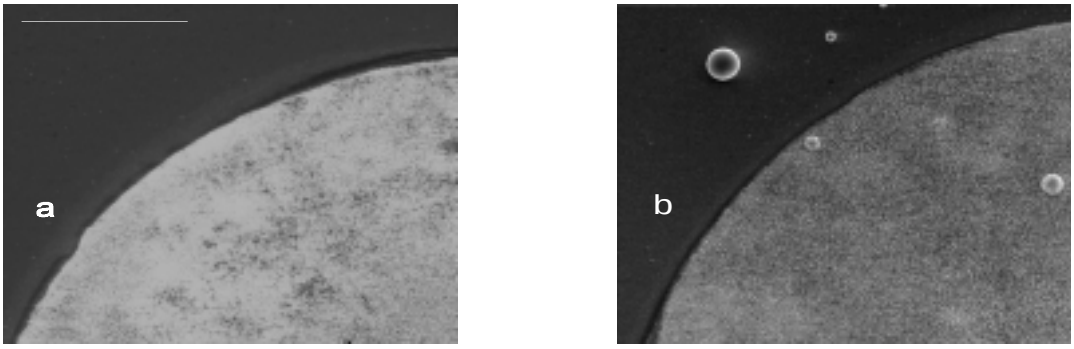

Fig. 4.5: SEM pictures of a) ablated evaporated and b) nanoparticle gold layers. The holes are 250 μm in diameter, irradiated at a fluence of 156 mJ/cm^2 in the case of conventional gold film and 132 mJ/cm^2 in the case of the nanoparticle layer. In both cases the number of shots was 20. The white line represents 10 μm

4.2 Submicron-size hole drilling

In case of materials with high thermal diffusion length (like metals and semiconductors) the creation of submicron sized structures is only possible by applying pulses shorter than a couple of picoseconds. Generation of submicron period gratings or sub-μ diameter holes requires high spatial resolution in addition to the short pulse duration. Such resolution can usually be achieved by using short wavelength sources. The combination of short pulse duration and short wavelength supposed to be a superior tool to create submicron-size holes on the surface of highly conducting materials. These possibilities are demonstrated and discussed in the followings [94,100,101].

As it is shown in 2.4, by applying femtosecond laser pulses (even for materials with high thermal conductivity) the size of the heat-affected zone is in the submicron region, allowing the creation of small lateral structures, with negligible heat affected zone, at lower ablation thresholds in the absence of plasma shielding effects. However, the short pulse duration itself does not predestinate the necessarily high optical resolution enough to reach the submicron region. Applying fs pulses at 800 nm wavelength, ablated structures down to the some μm range are reported [114,115] The theoretical limit for the achievable smallest spot size is defined by the numerical aperture (N.A.) of the imaging optics and the wavelength (λ) of the

laser radiation. This gives us two possibilities to increase the resolution of the used optical system. Increasing the numerical aperture the resolution will be increased, however a maximum practical value will be reached quite soon at around 1. Further increase of N.A. can only be reached by applying complicated immersion optics, introducing unacceptable losses in ease of operation and efficiency, too. By decreasing wavelength the optical resolution becomes higher, making laser sources emitting in the UV region more powerful tools. The theoretical limit of the spatial resolution at the KrF laser wavelength (248 nm) is over three times higher than that of a solid state Ti:Sa laser (usually operating around 800 nm) supposing the same optical setup and diffraction limited beams. Although it was demonstrated that making use of the threshold like properties of the ablation process and the gaussian focal distribution of the Ti:Sa lasers the generation of submicron-size structures in the infrared (IR) wavelength range is possible, creating much smaller size ablated structures than the focal spot diameter [116,117]. The application of these kind of techniques is strongly restricted by the extremely high requirements on the energy stability of the pulses. Based on this threshold-like property of the removal process the size of the ablated structures is a sensitive function of the pulse energy, in contrast to imaging techniques, where the energy fluctuation does not influence the size of the structures but only the ablation rate. Using short wavelength UV radiation facilitates the application of imaging techniques and the creation of submicron-size structures above the ablation threshold for the complete irradiated area.

This capability of our UV fs system was demonstrated applying a mask imaging setup. First a simple imaging setup based on quartz singlet or achromatic lenses was tested. This way generation of holes of several micron size in steel samples was possible. Such a pattern is shown in Fig. 4.6, where 10 μm diameter holes were ablated with 60 shots (per hole) in steel samples. In the experiments an f = 100 mm focal length achromatic lens was used to image a circular aperture onto the sample surface.

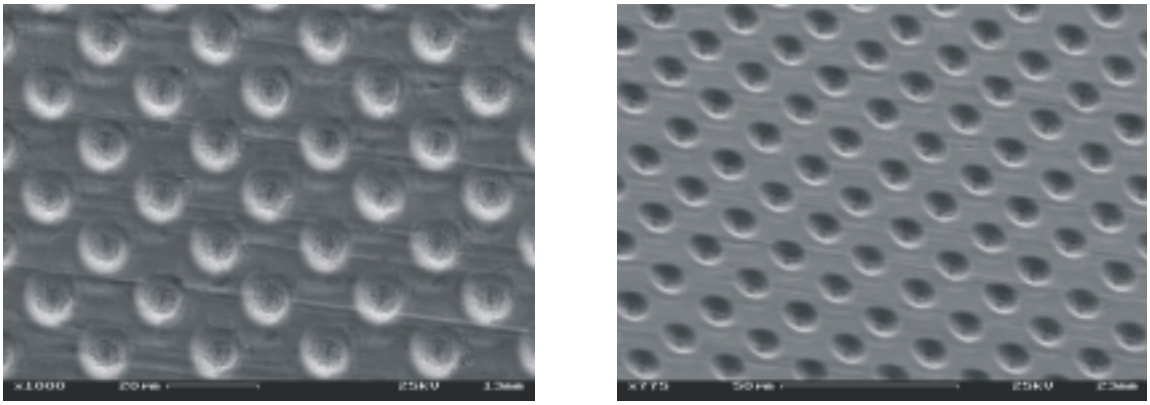

Fig. 4.6: Ablated 10 µm diameter holes (60 shots per hole) in steel samples using an f = 100 mm focal length achromatic lens.

For the creation of holes in the sub-micrometer range the optical resolution of a single lens is usually not high enough anymore. Severe distortions caused by multiphoton absorption, self-focusing, chromatic and spherical aberrations of the lens material prohibit the application of such optical schemes.

In the experiments investigating sub-µm structuring of various solids a Swarzschild-type reflective objective was used for mask projection (Fig. 4.7). In multishot experiments the beam passed a rotating λ/2 plate to rotate the polarization of the beam shot to shot eliminating the consequences of undesired polarization effects [118]. After the polarization plate a field lens was used to increase the energy density on the mask. The mask was a 25 µm diameter pinhole and was imaged onto the surface of the steel foil samples. The focal length of the field lens and the diameter of the mask were chosen so that the diffracted beam entirely covered the aperture of the Swarzschild-type objective. The demagnification of the objective was 36x with a numerical aperture of 0.3. Because of the small depth of field of the objective a monitoring system for online controlling of the image plane was used. For this purpose a He-Ne laser beam was directed onto the mask and after reflection from the sample surface, it was coupled out with a pellicle beam splitter and was imaged onto a CCD camera (Fig. 4.7).

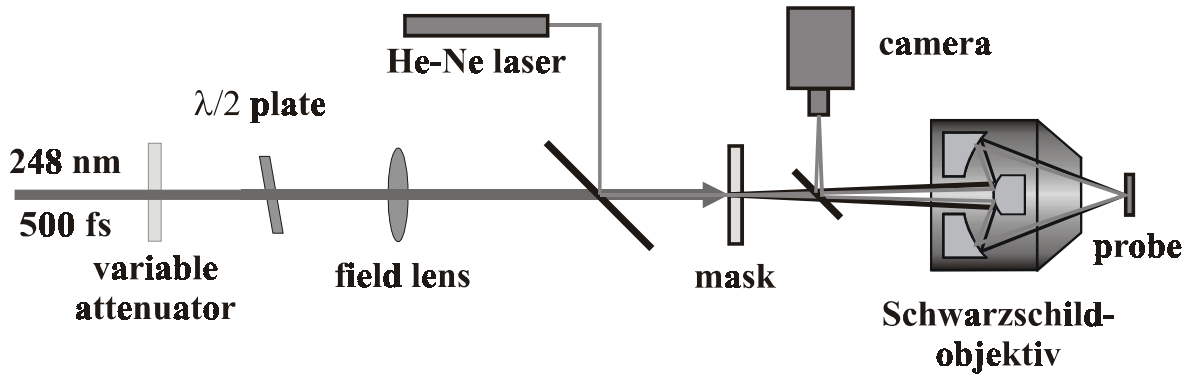

Fig. 4.7: Optical arrangement based on a Schwarzschild-type reflective objective

This setup made it possible to find the image plane practically online also in case of samples with uneven surfaces. Before irradiation of the given sample, the surface has been adjusted to the image plane of the optical setup, using the calibrated He-Ne beam. (First in a separate measurement the image plane of the He-Ne arrangement has been adjusted to be coincident with the UV setup.) In the first experiments with the use of moderate intensities and a few number of shots we were able to ablate submicron sized holes into stainless steel plates.

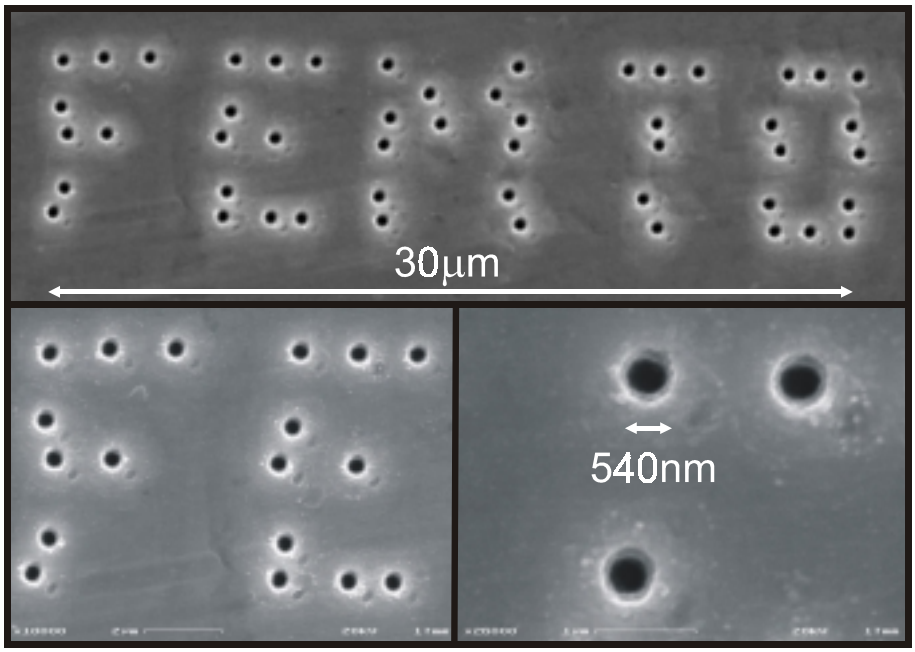

Fig. 4.8: Sub-micron sized holes on stainless steel plates.

In Fig. 4.8 holes on steel samples with diameters of around 600 nm are shown. The number of shots was 50. A good reproducibility and precise edges with minimum ablation debris are readily seen.

In further experiments we tried to drill through steel foils of different thicknesses preserving the submicron diameter of the holes. Our results showed that the limit is around 5 μm [100]. Over this thickness it was not possible to drill through the samples without deteriorating the ablated structures on the irradiated side. Because of the high N.A. and in connection with that the small confocal parameter of the optical arrangement (based on the Schwarzschild objective with N.A. = 0.4, Rayleigh length = 7.2 μm), generation of structures with high aspect ratios is not possible. A solution could be to move the sample compared to the image plane during irradiation, however, severe damage of the surface region was observed this case. This way presumably caused by the significantly different intensity distribution outside the image plane. Channeling effects similar to that, reported in numerous drilling experiments [119] has not been observed to be significant.

Using a similar setup like Fig. 4.7 and higher number of pulses, stainless steel foils with 5 μm thickness were perforated with 4000 pulses. Fig. 4.9 a and b shows such through holes with a diameter of around 600 nm at the exit side, and a detailed high magnification SEM picture, respectively.

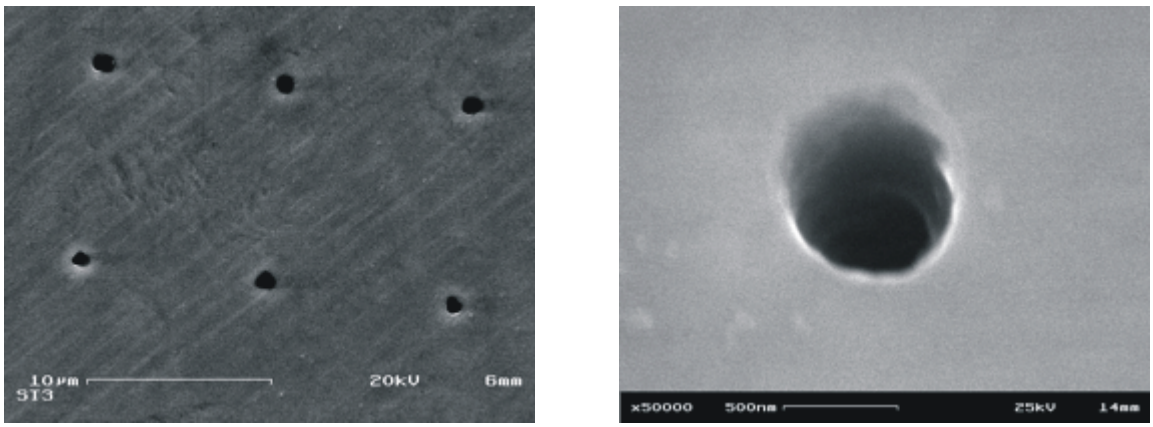

a) b)

Fig. 4.9: Sub-μm holes in 5 μm thick steel made by fs-UV-laser

Perforation of foils above this limit is only possible by applying complicated pre-drilling processes. Combining this process with conventional methods (e.g. precision mechanical

drilling or “macro” hole drilling with lasers) can facilitate the fabrication of sub-µm holes in thicker steel plates (Fig. 4.10), applying a more complicated multiple step process.

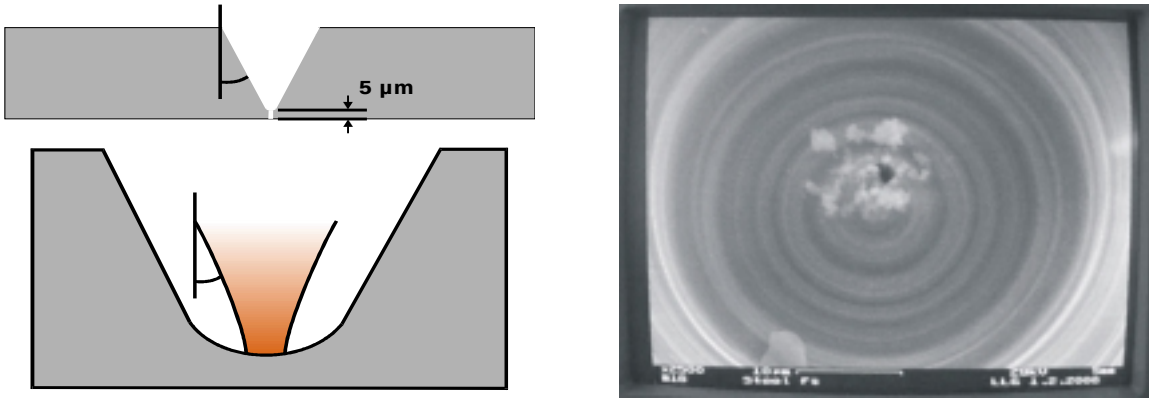

Fig. 4.10: Predrilled holes and macro blind hole with submicron sized hole in the middle

A possible multiple step solution can be described as follows. First a “macro” blind hole can be made with a conventional method, so that the thickness of the remaining material is small enough (few µm) to drill it through with fs laser pulses. At the end we have a sub-µm hole drilled through the center of the macro hole. Such holes can be used in several applications, e.g. in high pressure or vacuum systems or in the automotive industry as special nozzles. The “macro hole” shown in Fig. 4.10 was made by applying a special, high precision mechanical milling technique. This technique allows drilling blind conic holes with some 100 µm diameter on the surface and only ~50 µm on the bottom so, that the remaining bottom thickness is only a few microns. Another possibility can be the application of laser pulses for the predrilling, specially optimized for its requirements. Because of the lack of an adequate system and while the principle scope of this work is the generation of small structures, this line was not followed in more details.

The results of different investigations show, that it is possible to texture surfaces individually, using a precise positioning system in combination with a UV fs laser source and a high quality imaging system. However, if fabrication of a large number of features over an extended area is needed the large number of points can prohibit the application of single hole processing techniques. In these cases it would be reasonable to apply other optical setups where many holes could be drilled simultaneously. A possible solution is the application of a

special interferometric technique that produces a 2D periodic intensity pattern on the sample surface [120].

4.3 Ablation of submicron-size patterns

Excimer laser ablation for surface patterning is performed in most cases by mask projection. The mask is illuminated by a flat-top beam profile, and by using an appropriate optical system an (in general strongly demagnified) image of the mask is formed on the surface of the workpiece. In the simplest case a circular aperture (a small hole on a plate) can be used to create submicron-size holes. The fabrication of these masks is quite simple and problems like low damage threshold of the mask materials can be solved and high transparency can be reached. In this case, however, sequential machining of individual holes makes the process time consuming and inefficient especially if complex patterns with large number of holes are required. In these cases more complicated masks are necessary to use. Such amplitude masks are usually transparent substrates (fused silica), patterned with an opaque layer (Cr). Mask shops provide them with high accuracy and resolution. But there are several disadvantages of them: first, they are easily damaged at high fluences; therefore dielectric layers are used in some high power applications [121]. Second, for applications with a small filling factor of the mask (large opaque areas with only a few transparent regions) a large amount of laser radiation is lost at the mask and the process becomes rather inefficient.

For efficient texturing of large surfaces we developed and experimentally tested two different methods for different assignments. The first arrangement is based on the projection of amplitude gratings combined with a Fourier filtering technique. It is reasonable to use these masks to generate dense patterns, e.g. crossed lines or for instance densely packed holes. This way highly reproducible periodic line structures with a line-spacing below 400 nm have been produced on the sample surface by single laser shot exposure or hole matrices on metal surfaces with individual hole diameters of 300 nm were generated. For the generation of surface patterns with small filling factor a second method was tested, based on DPE's (diffractive phase elements). Applying this technique hole-arrays with 1 - 2 μm diameters were fabricated.

4.3.1 Application of diffractive amplitude masks with Fourier filtering

Application of a relatively simple projection technique, where amplitude gratings are illuminated and imaged onto the sample surface after Fourier filtering allows the generation of various submicron patterns. This way highly reproducible submicron sized periodic line structures or individual holes down to 300 nm diameters were generated. [94,99,101,102].

The optical setup consists basically of a diffractive optical element, a beam selector placed into the Fourier plane of the optical arrangement and a Schwarzschild objective. The diffractive optical element splits the beam into several parts. Applying the beam selector in front of the objective allows to select arbitrary beam parts. After this filtering the beams are overlapped in the image plane of the objective, forming the desired intensity distribution. By properly choosing the diffractive beam splitter and the beam selector, different sub-μm patterns can be generated over the entire interference region.

The simplest diffractive amplitude mask can be an amplitude grating, consisting of alternating highly transitive and reflective zones. Using the grating as a mask and imaging it onto the sample a periodic intensity distribution with submicron period can be created on the surface. By blocking the 0^{th} order the period can be halved further decreasing the size of the ablated structures. With the help of this simple filtering technique a perfect sinusoidal grating can be generated. This simple one step process is a powerful candidate to replace complicated multiple step processes used before in numerous applications. Highly reproducible periodic line structures with a line-spacing below 400 nm have been produced on the sample surface by single laser shot exposure on metal and semiconductor surfaces (see Fig. 4.1 and Fig. 4.2).

Besides metals and semiconductors, we have also investigated dielectric materials having relatively high heat conductivities. One of them, $LiNbO_3$, has attracted accentuated interest in integrated optics applications. Optically pumped $LiNbO_3$–based distributed Bragg reflector (DBR) waveguide lasers hold great promise in optical communications technology. The key component of these devices, the narrow band Bragg reflector gratings, were fabricated by holographic exposure and a set of dry etching techniques. This fabrication technology is time consuming and expensive. Recently, however, it has been shown that applying 248 nm subpicosecond pulses, grating structures with periods of about 360 nm can be created on

$LiNbO_3$ with single exposure [43]. As can be seen in Fig. 4.11, a smooth and homogeneous sinusoidal modulation profile has been achieved.

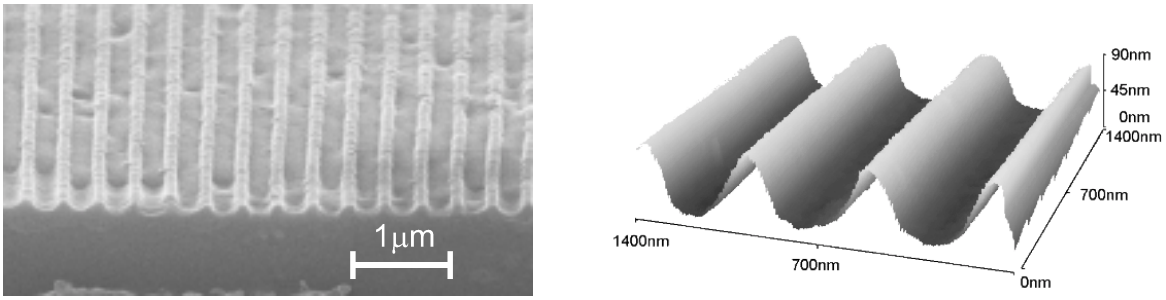

a) b)

Fig. 4.11: SEM picture (a) and an AFM record (b) of a periodic structure ablated in LiNbO3 with a single 500 fs UV pulse.

Another important material in various areas of optical technology is Ta_2O_5. Due to its good transparency and the high refractive index ($n > 2.2$ in the visible range) it is often used for multilayer dielectric mirrors or masks and also for planar waveguides in optical communications technology and in integrated optical sensors. Due to the high thermal conductivity of Ta_2O_5 fabrication of sub-μm structures has only become possible with 248 nm subpicosecond pulses. In a recent work similar results to that of $LiNbO_3$ were demonstrated [122].

Using more complicated diffractive elements with Fourier filtering, not only periodic lines, but also various surface patterns can be generated on the samples. A possible way is to use an amplitude mask consisting of crossed lines and spaces. Such a mask can also be created by using 2 amplitude grating masks in crossed position (the lines are perpendicular to each other), pushing the coated surfaces together. By blocking the 0^{th} order together with the higher orders (2^{nd}, 3^{rd}, etc.), a sinusoidal crossed grating structure can be generated. The ablated structure looks like small hemispheres packed densely in a matrix structure, as is shown in Fig. 4.12.

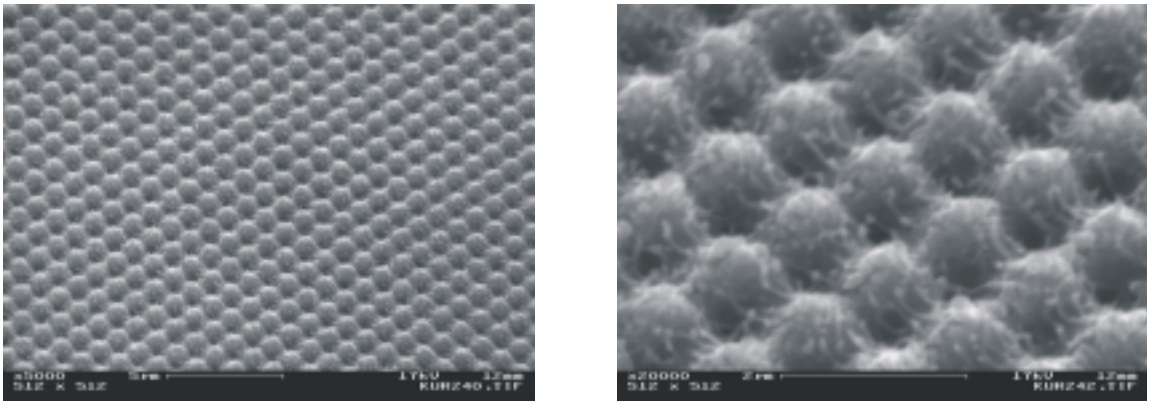

Fig. 4.12: Ablated cross-gratings with 1mm period in Ni samples using simple transitive amplitude gratings as DPE mask.

Playing around with the beam selector and selecting only the 4 principal first order beams out of the diffraction pattern, an even more interesting intensity distribution will be generated in the image plane of the objective [120,123].

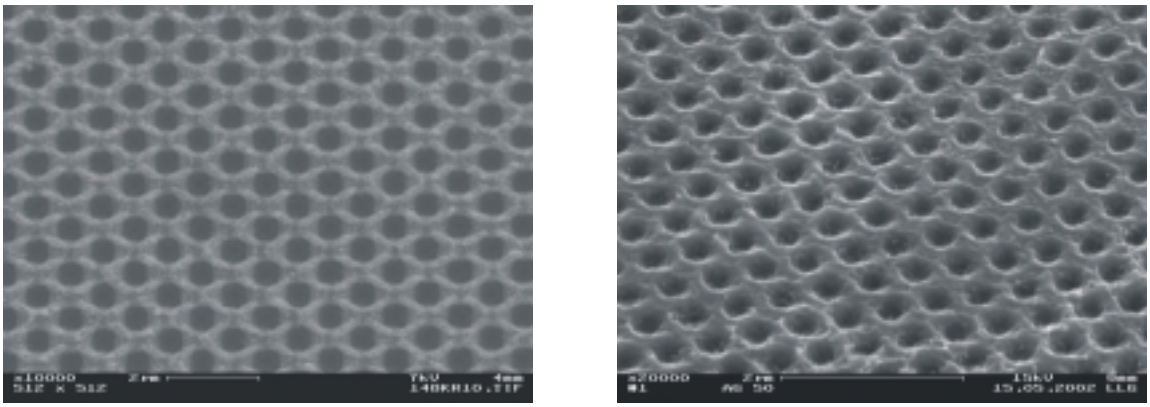

a) b)

Fig. 4.13: Submicron sized hole patterns in Ni (a) and Ag (b) films generated with interferometric projection technique.

Such distribution is shown in Fig. 4.13 and Fig. 4.14. In such an experiment a Cr-mask consisting of crossed lines and spaces was imaged with a Schwarzschild objective on steel and copper surfaces resulting in a dense pattern of holes. In this way two dimensional large area patterns consisting of individual holes with diameters down to 300 nm were fabricated (Fig. 4.13).

Although the setup was not optimized for large area irradiation, it was possible to create patterned areas with a size of 60×60 μm. In the presented example the surface was irradiated with 15 shots creating around 7000 holes with a depth of ~300 nm.
Similar results have also been reached on other metal surfaces like stainless steel, copper silver etc. In Fig. 4.14 holes made by applying 20 pulses with 0.9 J/cm^2 are shown.

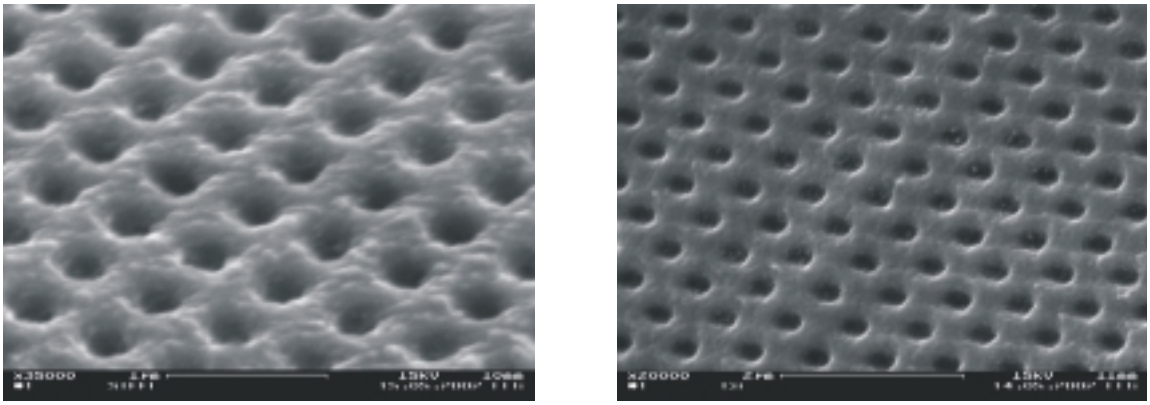

Fig. 4.14: Hole grid pattern in (a) stainless steel and (b) copper made by projection of an amplitude mask. Laser parameters: λ = 248 nm, τ = 300 fs, Φ = 0.9 J/cm^2, n = 20 pulses.

The demonstrated techniques facilitate the fabrication of large surfaces in short time, opening the way for industrial applications in high quality submicron machining, without the use of complicated lithographic or chemical processes.
Combining this technique with our newly developed high repetition rate UV femtosecond laser system [81] - delivering 30 mJ pulses up to 300 Hz repetition rate - it would be possible to machine large surfaces also in industrial environments. In applications where the generation of small holes in a periodic matrix arrangement is desired our technique could be a powerful tool.

4.3.2 Patterning with Diffractive Phase Elements (DPE)

Applying specially designed diffractive phase elements (DPE) generation of micron size hole matrices on different metal surfaces has been demonstrated. Using these special masks individual (not necessarily periodical) structures can be generated with high efficiency [99].
For making more efficient use of the laser photons in case of masks with small filling factor, in some cases diffractive optical elements are used to distribute the laser light only in those areas of the mask that contain the transparent features [124]. In this case the amplitude mask still defines the precise pattern and in addition suppresses stray light, which may originate from the imperfections of the DPE. In a further step, if it is possible to precisely define the desired pattern by the DPE, there is no need for an amplitude mask any more. The workpiece can be directly positioned in the signal plane of the DPE (the element is called Fresnel-DPE, if the signal plane has a finite distance from it), or it is positioned in the focal plane of an additional lens, which transfers the signal of a Fraunhofer-DPE from infinity into its focal plane. This latter case offers more flexibility, because various signal sizes can be realized depending on the lens. Especially for creating high resolution patterns this method is preferable, because otherwise the pixel size of the DPE strongly limits the achievable resolution.

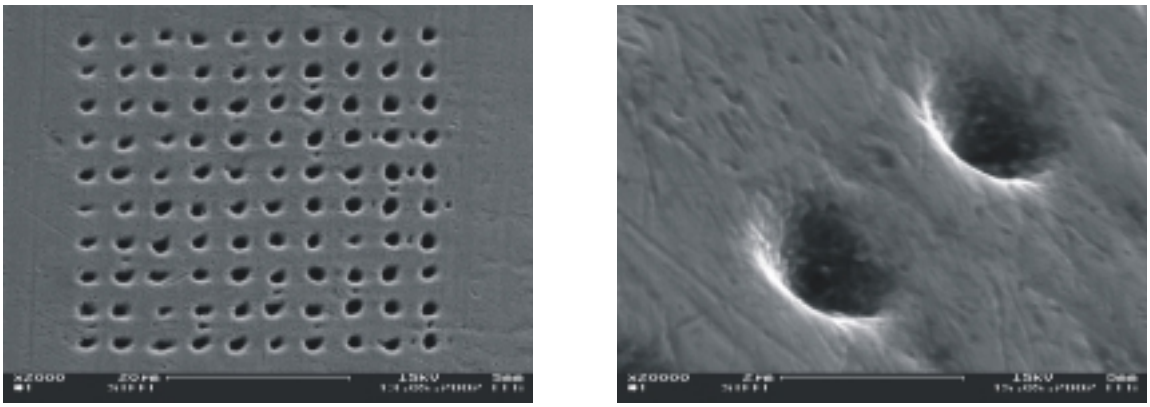

Fig. 4.15: Hole pattern in stainless steel made by the DPE shown in Fig. 4.17 and Fig. 4.18. Laser parameters: λ = 248 nm, τ = 300 fs, n = 100 pulses, Φ_M = 54 μJ/cm^2 on the mask, and Φ = 780 mJ/cm^2 on the sample.

An experimental demonstration of the operation of the DPE was performed applying our short pulse UV laser as the illumination source. A 25x Schwarzschild (N.A. = 0.4) objective was used to create the necessary high resolution. The use of a high quality achromatic optical system is essential to avoid pulse front distortions, which would deteriorate the signal pattern. This kind of processing was applied to various metals. A scanning electron micrograph (SEM) of the full 10 x 10 hole matrix ablated in stainless steel and a strongly magnified section of the pattern are shown in Fig. 4.15.

Ni Ag

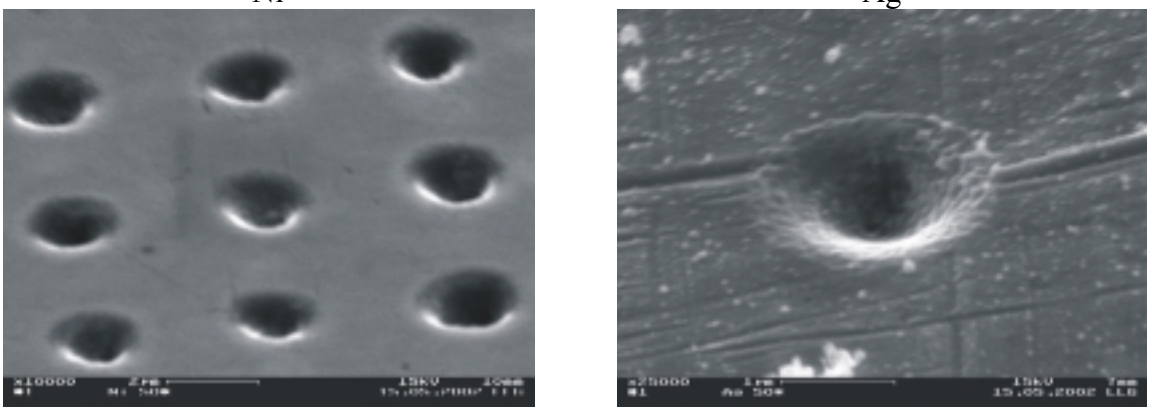

Fig. 4.16: Hole pattern metals made by the DPE shown in Fig. 4.17 and Fig. 4.18 in (a) nickel and (b) silver surfaces. Laser parameters: λ = 248 nm, τ = 300 fs, n = 100 pulses, Φ_M = 36 $\mu J/cm^2$ on the mask, and Φ = 520 mJ/cm^2 on the sample.

The pattern was made by 100 laser shots with a fluence of 54 µJ/cm² on the mask corresponding to 780 mJ/cm² on the sample. Further examples are shown for nickel as well as for silver in Fig. 4.16 a and b.

4.4 Design, generation and fabrication of two level DPEs

For the fabrication of the diffractive phase elements a one-step method was developed based on ns excimer laser ablation using ArF operating at 193 nm. I also developed and successfully tested a new method to decrease the stringent restrictions for the pixel-depth of the DPE. Immersion liquid has been used to set the refractive index difference of the mask substrate

and the ambience and to reach optimized operation of the DPE for the given surface relief step height [99].

4.4.1 Design and computer simulated reconstruction of DP masks

Design and fabrication of DPE's has been investigated. Using an Iterative Fourier Transform Algorithm (IFTA) for the design and a simple one-step ablation process for the fabrication process it was possible to create diffractive phase masks on quartz plates.
As a demonstration of this technique a DPE was designed to generate an intensity distribution consisting of a matrix of 10 x 10 spots. The calculation was performed with an iterative Fourier transform algorithm (IFTA) [125] and resulted in a two level DPE represented by a 128 x 128 binary bitmap.

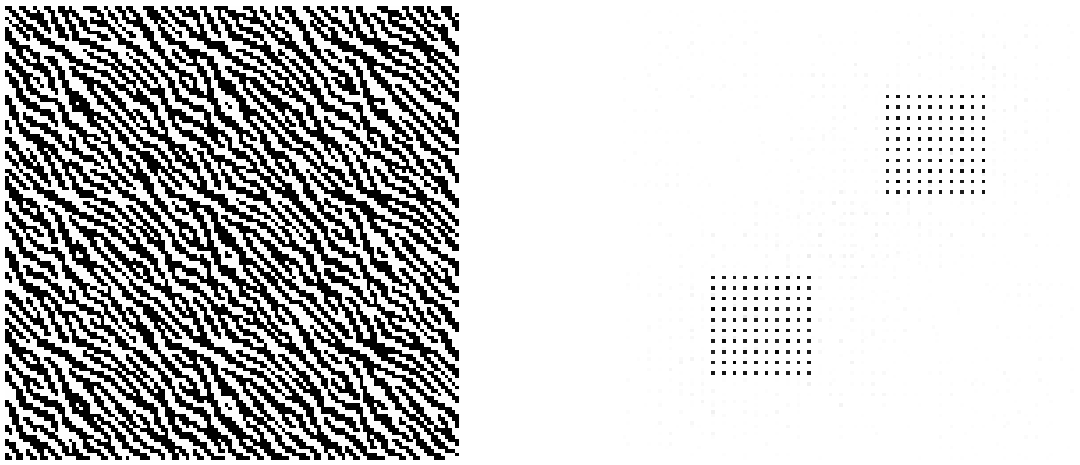

Fig. 4.17: (a) IFTA-designed binary bitmap of the DPE and (b) computer simulated reconstruction of the intensity distribution in the signal plane.

Fig. 4.17 (a) shows the bitmap code of the phase distribution of the DPE and (b) displays the simulated reconstruction. We also developed a fabrication method for the realization of the DPE mask according to the simulations. The appropriate mask materials are quite difficult to machine at 248 nm because of the high transmission at this wavelength. That is why alternative solutions have to be found, as it is detailed in 4.4.2.

4.4.2 Mask fabrication process based on ArF excimer laser ablation

The fabrication of quartz is usually quite complicated, especially if shallow holes with a few nm depth precision and a very smooth bottom are required. For the generation of efficient phase masks for 248 nm operation, the surface relief step height has to be ~244 nm (for fused silica substrate material in air ambience). The generation of such a quartz mask required complicated etching processes so far. In order to relax the stringent restrictions for the hole depth a new technique has been developed using immersion liquid in front of the mask. This way the necessary pixel depth can be controlled by changing the refractive index difference of the immersion liquid and the substrate material. This technique was successfully tested on the phase elements fabricated with ArF excimer laser pulses at 193 nm.

Whereas Cr-masks are easily available with any desired pattern, DPEs for high power applications are not available as standard components. Especially for UV applications they have to be made of fused silica, so that a highly complex fabrication procedure including lithographic and reactive ion etching steps is required [126]. Alternatively, the required surface relief can be made by laser ablation. This process has been demonstrated for DPE in plastics [127-129], dielectrics [130-132] and diamond [133]. Excimer laser ablation of fused silica has been investigated for various laser wavelengths [105]. For this highly transparent material it is not easy to obtain precise, high quality surface structure. Whereas from the issue of laser-material interaction, 157 nm is the most promising wavelength [134], from the point of view of practicability (processing in air, availability of optics) 193 nm is very attractive for this task and was used here. Though fused silica tends to form cracks after several pulses when ablated with 193 nm, well defined excisions can be made by applying only one or two pulses per position.

The calculated phase level distribution in bitmap form (as shown in Fig. 4.17 a) was transferred into a surface relief on fused silica (suprasil 1) by ablating pixel by pixel. With a pixel size of 12.5 µm x 12.5 µm the total size of the DPE is 1.6 mm x 1.6 mm. To be used efficiently at a wavelength λ, the relief step height has to be $d = \lambda/(2(n_r-n_0))$, if n_r is the refractive index of the DPE-material and n_0 the refractive index of the environment. For a reconstruction wavelength of $\lambda = 248.5$ nm and fused silica ($n_r = 1.508$) in air ($n_0 = 1$) the required step height is $d = 244$ nm. As the ablation behavior of fused silica near the threshold

is rather complex (incubation, influence of surface), this step height cannot be reached with sufficient reproducibility. A larger depth is reached more easily. Therefore for each pixel to be ablated, two pulses of about 19 J/cm² were applied to reach an ablation depth of 900 nm (Fig. 4.18). Then, if the surface profile is immersed in water ($n_0 = 1.37$), the step height condition is matched quite well, in this case the theoretically optimal step height is 900.4 nm. Before application the surface was cleaned from ablation debris by slightly polishing it with window cleaning powder.

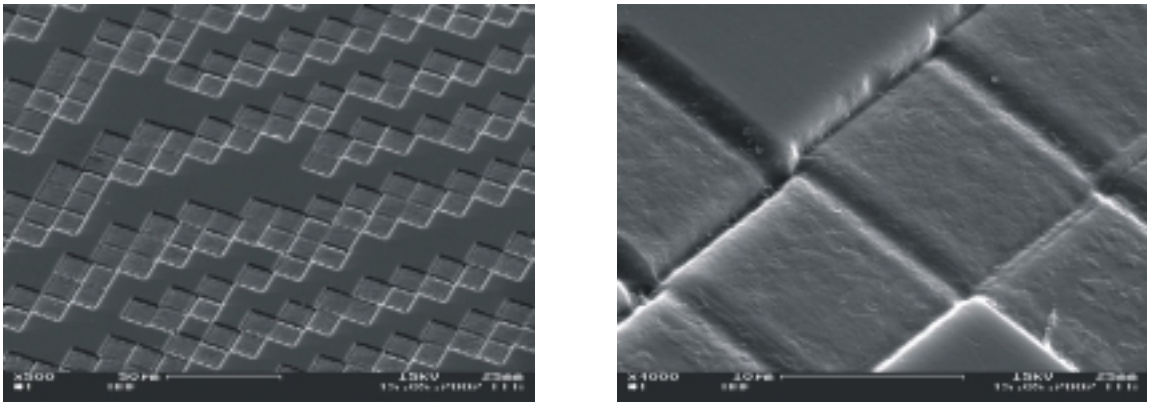

Fig. 4.18: Two level DPE made by ablation at λ = 193 nm in fused silica, according to the design of Fig. 4.17, n = 2 pulses per pixel, Φ = 19 J/cm^2 on the sample.

5. Summary

Thanks to the advantages of the well-known chirped pulse amplification (*CPA*) technology, solid state laser systems operating in the infrared (*IR*) region are widely used as compact high brightness sources, and in fact dominate this field. Only moderate efforts have been made to develop compact and reliable short-pulse laser systems operating in the ultraviolet (*UV*) part of the spectrum. In numerous applications, however, high intensity fs pulses in the UV wavelength region have ultimate advantages compared to longer wavelengths. In most of the high intensity experiments, it is the minimal achievable focal spot size, which is considered to be the major figure of merit for the performance of the laser system. This is where the better focusability of short wavelength gas lasers plays a very important role. The short wavelength results in an around 3 times smaller theoretically achievable minimal focal spot size, compared to that of solid-state systems operating around 800 nm. The gaseous active medium of excimers also introduces less optical distortions. As a result of the combination of these effects, a typically 10-100 times smaller focal spot area is reachable for excimer lasers compared to high intensity solid-state systems.

Since there is no effective way to generate ultrashort pulses in the UV, it is necessary to amplify frequency-converted beams, most effectively in specially designed excimer modules. Different front ends can be used, e.g. frequency tripled seed beams from a Ti:Sa solid-state laser or frequency doubled pulses of a short pulse dye laser system. In earlier experiments the dye laser front-end was used and successfully applied in numerous laboratories all over the world. However there are some features (reliability, simplicity, possibility of high frequency operation), which make the solid-state front-ends more preferable. Because of their enormous development in the last few years compact, reliable, easy-to-handle systems with high average powers and repetition rates are available. The above-mentioned developments opened the way for the development of solid state - excimer laser systems. This line was followed in this work combined with the study of possible applications.

A very important application field of such systems is material processing, especially if high precision is required. The most important advantages of such a system for submicron machining are the small penetration depth of the radiation, the small thermal diffusion length

and the high optical resolution. The high peak power ensures a small penetration depth through multiphoton absorption and consequently well defined ablation depths. Additionally the short pulse duration provides a small thermal diffusion length and through that prohibits the lateral spreading of heat into the surrounding regions, ensuring the creation of small lateral structures. Operation with UV pulses provides the necessary high spatial resolution because the minimum achievable irradiated spot size scales with the wavelength. Further advantage of the short wavelength is the increased absorption of most of the materials in the UV region. This relaxes further the system requirements even for hardly machinable, in the IR and VIS wavelength region transparent materials. As a result of all these advantages practically all kind of materials can be machined with submicron precision, applying UV femtosecond pulses.

My PhD work focuses on the development of reliable and compact high power femtosecond UV laser systems, optimizing the operational conditions and optical setups. My aim was to improve the output parameters like pulse energy, repetition rate or output power and to adept the system to different applications. Among the investigated applications one of the most important field was micromaterial processing. In this part of my work I focused on the development of time effective material processing techniques, allowing the fast machining of large surfaces, also in industrial environment.

In the experiments a big variety of investigation methods and tools have been used. For the development of high intensity solid-state-excimer laser systems a solid state Ti:Sa laser source has been used (*Spectra Physic Inc., USA*) to generate seed pulses at 745 nm wavelength. For the frequency upconversion a frequency-tripling unit was built in a linear arrangement based on BBO crystals (*CASIX, China*) as nonlinear medium. For the amplification of these pulses at 248 nm different excimer modules (*Lambda Physic GmbH, Germany*) were modified and optimized for the different experimental conditions. The investigated optical setups are based on the principles of the off-axis amplification and interferometric multiplexing schemes.

To measure the pulse energies of the amplified and seed pulses at 248 nm and to measure the pulse energies at 745 nm right before frequency tripling Gentec ED100, ED200, ED500 and RJP735 type piezoelectric energy meters were used. To measure the output power of the queasy cw Tsunami master oscillator Spectra Physics power meter (*model 407a*) was applied.

To characterize the output pulse length at 745 nm a Spectra Physic single shot autocorrelator, at 248 nm a multiple shot UV autocorrelator based on multiphoton ionization of NO was used. For the spectral measurements a homemade grating spectrometer in Littrow condition was applied and the spectrum was visualized with a diode array (Hamamatsu) as a detection unit. To control the timing between the different laser units active delay control boxes from Lambda Physik (*LP*) were used. To adjust the optimal delay between the different laser components fast photodiodes (*Hamamatsu R1193U, Alphalas UPD-200-UD*) in combination with a 1 GHz bandwidth analog oscilloscope from Tektronix (*Tektronix 7104*) were used. For the measurements of the beam profile of the amplified UV beams a homemade image processing system was used based on a modified UV sensitive CCD camera and a beam analyzing system (*MrBeam, LLG, Germany*).

In the material processing measurements alternative laser sources as ns mode excimer lasers operating at 157 nm, 193 nm, 248 nm and 308 nm, AR^+ ion lasers at 488 nm, Nd-YAG lasers at 1064 nm and 532 nm were used together with the short pulse UV and IR systems operating at 248 and 745 nm, respectively. Different imaging techniques were tested and compared based on achromatic UV objectives (*Spindler&Hoyer, DUV Retro*), Schwarzschild-type reflective objectives (*Ealing 25x, 36x*) in combination with simple amplitude masks or specially designed and generated diffractive phase elements. For the precise positioning of the samples xyz-translators from PI (*Physik Instruments, M-510.11*) were used in combination with home made online monitoring systems. The morphology of the irradiated samples was investigated with light microscopes (*Zeiss Axioskop*) and with a scanning electron microscope (*Zeiss, DSM 962*), the depth of the ablated structures was measured by a profilometer (*Dektak 3030 Auto II Stylus*) and by atomic force microscopy (*AFM*).

The aims described above were investigated with the help of the listed methods and tools, and the new experimental results of these investigations are listed in the following:

1. *A new solid state – excimer hybrid laser system has been developed, amplifying the frequency tripled output of a solid state Ti:Sa system set to 745 nm delivering up to over 50 mJ energy at 248 nm in the UV wavelength region. For the amplification a specially designed wide-aperture KrF excimer module was used in a three-pass off-axis arrangement [80].*
2. *By applying a 2-beam variant of the polarization-multiplexing scheme in combination with the same excimer module used in point 1, amplification of UV femtosecond pulses up to the 100 mJ region has been realized. Seed pulses with 2-3 mJ energy were used in order to reach optimized operation [80].*
3. *Based on a high repetition rate solid-state front-end a Ti:Sa - excimer system has been developed operating up to over 300 Hz repetition rate, delivering 30 mJ output energy UV pulses. This way an average power of 9 W at 300 Hz repetition rate has been reached in the UV wavelength region [81].*

Making use of the unique possibilities of the above described laser systems various results in different application fields like the generation of efficient XUV pulses [94], investigation of short pulse ablation properties of metals, semiconductors [102] and nanoparticle gold films [106], metal deposition on silicon and polymer surfaces [26,97], application of diffractive phase elements at 248 nm [99], generation of gratings with grating periods down to 300 nm, and drilling of submicron-size holes on practically all kind of solids [94,99-102] etc. can be presented. The most important results are concluded in the following points.

4. *By investigating the ablation properties of materials with high heat conductivity in the picosecond and subpicosecond region. Morphology changes as a function of the pulse duration have been studied, and the result show that the quality of the ablated structures strongly depends on the pulse duration. For metals and semiconductors optimal pulse duration under 5 ps was found to be necessary in order to eliminate undesired melting*

effects. Subpicosecond ablation properties (like thresholds, rates and morphology) of novel nanoparticle layers has also been investigated and compared with that of conventionally evaporated films. For nanoparticle films five times higher ablation rates have been measured. The ablation thresholds and rates were also found to be dependent on the particle size and evaporation pressure [102,106]

5. *Micromachining of different type of metals and semiconductors has been investigated. It has been demonstrated experimentally that even in the case of materials with high thermal diffusion length (like metals and semiconductors) it is possible to create submicron period gratings or sub-μ diameter holes on the surfaces of different materials applying a mask projection setup based on a Schwarzschild-type reflective objective. Using high fluences and some thousands of shots it was possible to perforate 5 μm thick stainless steel foils with 600 nm diameter holes [94,100,101].*
6. *It has been demonstrated experimentally that using a high power femtosecond laser source, the experimental conditions can be optimized for various applications like: a) generation of submicron size periodic surface modulation like normal grating or sinusoidal crossed grating structures, b) simultaneous drilling of large number of holes with diameters down to 300 nm using a special interferometric technique or c) generation of micron size hole matrices on different metal surfaces applying specially designed diffractive phase elements (DPE). Applying different experimental conditions and optimized optical arrangements for the application, significant increase in efficiency can be reached [99,101,102].*
7. *For the fabrication of the diffractive phase elements a one-step method was developed based on ns excimer laser ablation using ArF operating at 193 nm. I also developed and successfully tested a new method to decrease the stringent restrictions for the pixel-depth of the DPE. Immersion liquid has been used to set the refractive index difference of the mask substrate and the ambience and to reach optimized operation of the DPE for the given surface relief step height [99].*

The above listed scientific achievements contribute to a better understanding of the physical properties of KrF amplifiers. The combination of the advantages of solid state lasers with the

ones of UV excimer power amplifiers open new perspectives by providing a simple tool for the investigation of a wide range of physical phenomena. The developed new sources and imaging techniques can open new ways in material processing of practically all kind of materials even for mass production in industrial environment. Alternatively, such a system opens the way for the investigation of high intensity processes even in small laboratories, using a reliable, easy-to-handle small-scale table-top solid state-excimer laser system.

6. Összefoglaló

A jól ismert fázismodulált impulzus erősítés (*CPA: Chirped Pulse Amplification*) technikának köszönhetően kompakt, nagy intenzitású szilárdtest lézerrendszerek széles körben kerülnek alkalmazásra napjainkban, uralkodó szerepet töltve be a felhasználási területek jelentős részében. Ezen lézerrendszerek túlnyomórészt Ti:Sa alapúak, és az infravörös tartományban - 800 nm-es hullámhossz környékén - működnek. Viszonylag kis mértékű tudományos erőfeszítés irányult azonban olyan megbízható és könnyen kezelhető rendszerek fejlesztésére, amelyek az elektromágneses spektrum ultraviola (*UV*) tartományában sugároznak. Számos felhasználás esetében azonban nagy intenzitású UV femtoszekundumos nyalábok alkalmazása jelentős előnyökkel járhat az infravörös lézerek nyújtotta lehetőségekkel szemben. A nagyintenzitású kísérletek többségében például az alkalmazott lézerrendszer legmérvadóbb paramétere a legkisebb elérhető fókuszméret. Összehasonlítva a 800 nm környékén működő szilárdtest lézerek nyújtotta lehetőségeket az UV lézerekével, az utóbbiak esetében - a hullámhossz-különbségből adódóan - kb. háromszor kisebb elméletileg elérhető fókuszmérettel számolhatunk. Ehhez járul hozzá az általában gáz közegű UV lézerek anyagában létrejövő torzulások kisebb aránya. A két effektus kombinációjából adódóan tipikusan körülbelül 10-100-szor kisebb fókuszterület érhető el ilyen rendszerekkel a szilárdtest lézerekhez viszonyítva.

Pillanatnyilag nem ismert olyan eljárás, amelynek segítségével jó hatásfokkal tudnánk nagy energiájú és rövid impulzushosszú UV sugárzást előállítani. A legalkalmasabb módszer e célra frekvencia-többszörözés segítségével előállított rövid UV impulzusokat erősíteni egy speciálisan módosított excimer modulban. A rövid impulzusok előállításához különböző szilárdtest- illetve festéklézer-rendszerek alkalmazhatók. A Ti:Sa alapú szilárdtest lézerek kezelhetőség, megbízhatóság és ismétlési frekvencia tekintetében is előnyösebb tulajdonságokkal bírnak. Egy $\lambda = 745$ nm-re hangolt rendszer esetén frekvencia-háromszorozás után megkapható a KrF aktív közegben történő erősítéshez szükséges 248 nm-es hullámhosszú rövid impulzus, amely ezután különböző optikai eljárások alkalmazásával erősíthető speciálisan módosított excimer modulokban. A napjainkban kereskedelmi forgalomban is kapható megbízható, könnyen kezelhető és nagy ismétlési frekvenciát

biztosító szilárdtest lézerek új utat nyitottak szilárdtest – excimer hibrid lézerek kifejlesztéséhez, lehetővé téve a különféle rendszerek előnyös tulajdonságainak kombinálását. Ezt a fejlesztési irányt követi a jelen dolgozat, kiegészítve a rendszerhez kapcsolódó alkalmazási lehetőségek tanulmányozásával.

A rövidimpulzusú lézerrendszerek felhasználási területei között fontos szerephez jut az egyre szélesebb körben alkalmazott lézeres anyagmegmunkálás, különösen abban az esetben, ha nagy optikai felbontóképesség kívánatos. Nagy precizitású anyagmegmunkálás esetén a legfontosabb követelmények a rendszerrel szemben a rövid behatolási mélység, a rövid hővezetési hossz és nagy optikai felbontás. A nagy intenzitás többfotonos abszorbciót eredményez, ezáltal minimalizálva a behatolási mélységet azon anyagok esetében is, amelyek egyébként az UV tartományban is magas transzmisszióval rendelkeznek. A rövid impulzushossz meggátolja a folyamat során keletkező hő szétterjedését a környező területekre, lehetővé téve kisméretű struktúrák létrehozását. Ezen tulajdonságokat kombinálva a rövid hullámhossz biztosította nagy optikai felbontással a legtöbb (más módszerekkel egyáltalán nem, vagy alig megmunkálható) anyag mikron alatti méretű megmunkálása válik lehetővé.

PhD munkámban célul tűztem ki nagy intenzitású femtoszekundumos UV lézerrendszerek paramétereinek (mint pl. kimenő energia, ismétlési frekvencia, átlagteljesítmény) javítását, illetve a rendszerhez kapcsolódó felhasználási lehetőségek szélesítésének vizsgálatát. Ezek között is kitüntetett helyet foglalt el a rövidimpulzusú szubmikronos anyagmegmunkálás. A kísérletek során különös figyelmet fordítottam azon lézer- és optikai paraméterek optimalizálására, amelyek a mikron alatti méretű felületmegmunkálás szempontjából fokozott jelentőséggel bírnak. Célul tűztem ki továbbá olyan leképezési technikák vizsgálatát, amelyek segítségével nagy optikai felbontás érhető el, a lehető legkisebb mértékű energiaveszteség mellett. Nagy felületek gyors és effektív megmunkálása válik ezáltal lehetővé.

A kísérletek során nagy számú vizsgálati módszert és eszközt alkalmaztam. A nagy intenzitású szilárdtest - excimer rendszer kifejlesztéséhez egy kiloherzes ismétlési frekvenciájú, 745 nm-es hullámhosszon működő Ti:Sa lézerrendszert használtam (*Spectra Physic Inc., USA*) a rövid impulzusok generálására. A frekvencia konverzióhoz olyan háromszorozó egységet építettem, amely igen kis helyet elfoglaló lineáris elrendezésének köszönhetően stabil, mindennapos beállítási eljárást nélkülöző működtetést tesz lehetővé.

Nemlineáris közegként BBO kristályok (*CASIX, Kína*) kerültek felhasználásra. A végerősítő kifejlesztéséhez különböző KrF excimer modulokat (*Lambda Physik GmbH, Németország*) alakítottam át és optimalizáltam a rövid impulzusú erősítés szabta követelményekhez. Az excimer erősítők optimalizálása során használt optikai elrendezések az „off-axis erősítés" és az „interferometrikus multiplexelés" elvén alapulnak. A nyalábprofillal kapcsolatos mérésekhez egy digitális képfeldolgozó rendszert használtam (*MrBeam, LLG, Göttingen*). Az impulzushossz meghatározásához gázok kétfotonos ionizációján alapuló UV autokorrelátor állt rendelkezésre. A Ti:Sa rendszerben működő lézerek teljesítményének mérésére egy Spectra Physics teljesítménymérőt (*model 407a*), a 745 nm-es nyaláb energiájának mérésére pedig Gentec *RJP735* típusú energiamérőt használtam. A különböző energiájú 248 nm-es hullámhosszú erősítetlen illetve erősített lézerimpulzusok energiájának mérésére Gentec *ED100*, *ED200*, *ED500*, vagy *RJP735* típusú piezoelektromos elven működő energiamérőket alkalmaztam. A spektrális vizsgálatokhoz egy házi készítésű Littrow-elrendezésű rácsos spektrográfot használtam. A különböző lézeregységek pontos időbeli szinkronizálását gyors fotodiódákat (*Hamamatsu R1193U, Alphalas UPD-200-UD*) alkalmazva egy nagy sávszélességű (1 GHz) Tektronix (*Tektronix 7104*) oszcilloszkóp segítségével végeztem.

Az anyagmegmunkálási vizsgálatok során különféle hullámhosszú (F_2*: 157 nm, ArF: 193 nm, KrF: 248 nm, XeCl: 308 nm, Ti:Sa: 745 nm*) és különböző impulzusidejű (ns-os, ps-os, illetve fs-os nagyságrendű tartományba eső) lézereket használtam. Különböző leképezési technikákat hasonlítottam össze, különböző típusú és minőségű optikák – pl. egyszerű UV lencsék, akromatikus UV „transzmissziós" objektívek (*Spindler&Hoyer, DUV Retro*) és Schwarzschild típusú „reflexiós" objektívek (*Ealing 25x, 36x*) – felhasználásával. A kísérletek során egyszerű amplitúdómaszkokat, diffrakciós amplitúdómaszkokat vagy speciális módon tervezett és előállított diffrakciós fázismaszkokat (*DFM*) alkalmaztam. A minták nagy pontosságú pozicionálásához xyz-eltolókat (*Physik Instruments, M-510.11*) használtam, saját felépítésű monitoráló rendszerrel kiegészítve. Az ablált felületeket fénymikroszkóp (*Zeiss-féle Axioskop*) és pásztázó elektronmikroszkóp (*Zeiss, DSM 962*) segítségével vizsgáltam. Az ablált minták mélységét egy sekély struktúrák alaki tanulmányozására használható úgynevezett profilométerrel (*Dektak 3030 Auto II Stylus*) illetve atomi erőtér mikroszkóppal (*AFM*) mértem.

A leírt tudományos célkitűzéseket az ismertetett kísérleti módszerek és eszközök segítségével megvalósítva az alább felsorolt új tudományos eredményeket értem el:

1. Kifejlesztettem egy olyan szilárdtest – excimer hibrid lézerrendszert, amely 50 mJ energiájú femtoszekundumos UV impulzusok előállítását teszi lehetővé - 3 erősítési átmenetet alkalmazó - „off-axis" elrendezésben [80].

A rendszerben a rövid impulzusok generálása egy Ti:Sa alapú szilárdtest lézerben történik, az infravörös (*IR*) hullámhossz-tartományban. Az alkalmazott szilárdtest-lézerrendszer egy diódalézerrel (*Millenia*) pumpált Ti:Sa oscillátorból (*Tsunami*) és egy Nd-Ylf (Merlin) lézerrel pumpált regeneratív erősítőből (*Spitfire*) áll, és ~ 400 μJ energiájú impulzusok előállítására képes maximálisan 1000 Hz ismétlési frekvenciával A „kezdeti" 745 nm-es hullámhossztól frekvencia-háromszorozás segítségével juthatunk az UV tartományban lévő 248 nm-es hullámhosszig. A frekvenciakonverzióhoz egy - BBO kristályokat alkalmazó - lineáris elrendezésű háromszorozó egységet építettem, amely lehetővé teszi a frekvencia-többszörözés esetén szokásos mechanikus optikai késleltető karok nélkülözését. Ezáltal az elállítódási lehetőségek túlnyomó részét kiküszöböltem, és ~ 8 %-os konverziós hatásfokot értem el. A kapott kb. 150-180 fs-os UV impulzusokat egy speciálisan módosított nagy apertúrájú KrF excimer modulban erősítettem. Három erősítési átmenetet alkalmazó „off-axis" típusú optikai elrendezésben - amelyben a rövid impulzus a kisülés hosszirányú tengelyéhez képest ferde szögben halad át az erősítő közegen – működtetve az erősítőt, 50 mJ energiájú kimenő impulzusokat detektáltam. Az erősített nyaláb impulzushosszát többlövéses UV autokorrelátorral 530 fs félértékszélességűnek mértem.

2. Az 1. pontban leírt excimer erősítőn a polarizációs multiplexeléses technikának kétnyalábos osztáson alapuló változatát alkalmazva, 100 mJ energiájú impulzusok kibocsájtására alkalmas rövidimpulzusú UV fényforrást építettem [80].

Ez esetben a rövid impulzusok generálásához egy festéklézerekből álló, az elosztott visszacsatolású festéklézerek (*EVFL*) működési elvén alapuló rendszert használtam (*Szatmári-féle festéklézer-rendszer*) az erősítő telítéséhez szükséges kb. 2-3 mJ bemenő energia biztosítására. Az impulzusok háttérsugárzástól való megszűrése érdekében egy 3 m hosszúságú, nagy intenzitású térszűrőt építettem, magas roncsolási küszöbű CaF_2

pinholokat készítve és beépítve a rendszerbe. A Sagnac-féle interferométerek működési elvén alapuló polarizációs multiplexelés segítségével a bemeneten kettéosztott nyalábot két-két „off-axis" átmenetben erősítettem. A nyalábok fázishelyes egyesítésével 100 mJ kimenő energiát mértem az 1. pontban alkalmazott speciális excimer erősítő kimenetén. A vizsgált kétszeresen diffrakciólimitált femtosekundumos nyaláb előimpulzust nem tartalmazott, köszönhetően az elrendezésben használt polarizációs osztó tervezésének. A polarizációs osztó tervezésekor a főbb szempontok a megfelelő mechanikai stabilitás elérése (vastag hodozóanyag), az anyagban fellépő többfotonos abszorbció okozta veszteségek lecsökkentése (különböző hordozóagyagok összehasonlítása), illetve előimpulzusok keletkezésének elkerülése (ékes lap használatának átgondolása, térbeli elhelyezés megválasztására vonatkozó meggondolások) voltak.

3. Kifejlesztettem egy olyan Ti:Sa - excimer hibrid lézerrendszert, amely 30 mJ energiájú UV impulzusok kibocsájtására képes, 300 Hz-es ismétlési frekvencia mellett, több mint 9 W-os átlagteljesítmény elérését téve lehetővé, 300 femtoszekundumos UV optikai impulzusok formájában, 248 nm-es hullámhosszon [81].

Az UV lézerek alkalmazásainak széles körében nem okvetlenül a maximális kimenő energia, hanem az elérhető legnagyobb átlagteljesítmény a legfontosabb paraméter. Mivel az 1. és 2. pontban leírt rendszerek esetében az elérhető legnagyobb ismétlési frekvencia a néhány 10 Hz-es tartományba esett, az átlagteljesítmény a nagy kimenő energia ellenére is csak alacsony értékeket érhetett el. Kihasználva a Ti:Sa rendszerek nyújtotta nagy ismétlési frekvencia elérését biztosító lehetőségeket, olyan Ti:Sa - excimer hibrid rendszert fejlesztettem ki, amely több mint 9 W-os átlagteljesítmény elérésére képes 300Hz-es ismétlési frekvencián. A szükséges magas repetíciós ráta biztosításához egy különleges, nagy teljesítményű excimer lézernek (*NovaLine100, Lambda Physik*) a rövidimpulzusú erősítéshez optimalizált, nagy apertúrájú módosított változatát alkalmaztam. A működési paraméterek optimalizálását többek között a pillanatnyilag tárolt energia mérésével végeztem. Megvizsgáltam a különböző elektromos és működési paraméterek – mint pl. a „peaking" kondenzátorok eredő kapacitása, az erősítőben alkalmazott gáz nyomása – hatását a pillanatnyilag tárolt energiára és azt állapítottam meg, hogy maximális tárolt energia 28.5 nF-os eredő kapacitású „peaking" kondenzátorok esetén, 3.3 bar gáznyomás

esetén érhető el. Ezen kapacitás és nyomás paraméterek mellett, az 1.pontban is alkalmazott - 3 optikai átmenetet használó - „off-axis" elrendezés segítségével 30 mJ-os erősített impulzusokat detektáltam. Az erősített nyaláb impulzushosszát autokorrelációs mérés segítségével 300 fs-nak mértem.

A fent leírt rendszerek nyújtotta lehetőségeket számos felhasználási területen lehet kamatoztatni. Ezek közé tartozik pl. XUV impulzusok generálása frekvencia-sokszorozás segítségével [94], a rövidimpulzusú ablációs mechanizmus vizsgálata [102], különböző anyagok ablációs tulajdonságainak tanulmányozása [106], fémek leválasztása polymer illetve Si minták felületére [26,97], periodikus struktúrák illetve lyukak ablálása a mikron alatti mérettartományban [94,99-102] stb. Az anyagmegmunkálásra vonatkozó kísérletek legfontosabb eredményei a következő pontokban foglalhatók össze:

4. Az ablációs folyamat során bekövetkező morfológiai változásokat az impulzus-időtartam függvényében, nagy hővezető képességű anyagok esetén tanulmányozva megállapítottam, hogy az olvadásos jelenségek mértéke erősen függ a lézerimpulzus hosszától. Nagy pontosságú szubmikronos megmunkáláshoz 5 ps-nál rövidebb impulzusok szükségesek. Hagyományos illetve nanorészecskékből felépülő arany filmek ablációs tulajdonságainak vizsgálatainak során bemutattam, hogy míg az ablált felületek morfológiája megegyezik, a nanorészecskékből felépülő filmek esetében 5-ször nagyobb ablációs sebesség mérhető [102,106].

A vizsgálatok kimutatták, hogy a nagy hővezető képességű anyagok fotomaratása (*ablációja*) során kialakuló struktúrák minősége szorosan függ az alkalmazott impulzus hosszától. A kísérletekben rövid impulzushosszú KrF lézerrendszert használtam, amelyben az impulzushosszt 500 fs és 50 ps között lehetett változtatni. A folyamatok pontos nyomonkövetése érdekében mikron alatti méretű rácsokat és lyukakat abláltam fémes illetve félvezető minták felületére. A minták besugárzását követően a felületi struktúrák körül megfigyelt olvadt réteg vastagsága függ az impulzushossztól, illetve az adott anyagra jellemző elektron-fonon relaxációs időtől és hővezető-képességtől. A vizsgálatok eredménye szerint 50 ps-os impulzusokkal ablált próbák esetében nem kívánt olvadásos jelenségek figyelhetők meg, amelyek többsége kiküszöbölhető 5 ps-os impulzusok

alkalmazásával. Tovább rövidítve az impulzust, jelentős változás már nem figyelhető meg. Az olvadt réteg vastagságának impulzushossztól való függése egyezik a nemzetközi irodalomban közölt elmélettel, mely szerint az olvadt zóna mérete minimálisra csökkenthető, ha $L_{th} = \sqrt{2\kappa\tau} \leq \alpha^{-1}$, ahol L_{th} a hővezetési hossz, κ az anyag hővezetési együtthatója, τ a lézer impulzushossza és α^{-1} a sugárzás behatolási mélysége. Ez a feltétel fémek és félvezetők esetében csak néhány pikoszekundumosnál rövidebb impulzusokra teljesül. Az újra megszilárdult struktúrák formája szintén impulzushosszfüggő. Rövid impulzusok esetén inkább éles formák és apró cseppek, míg hosszú impulzusok esetén széles, sima gyűrődések figyelhetők meg.

Új, nanorészecskékből felépülő arany filmeknek a femtoszekundumos impulzushosszra vonatkozó ablációs tulajdonságait (ablációs küszöb, ablációs sebesség, morfológia) vizsgáltam és összehasonlítottam a hagyományos módon párologtatott arany filmek ablációs jellemzőivel. A kísérletekhez fényforrásként egy 50 mJ-os Ti:Sa - excimer lézerrendszert alkalmaztam. Amíg az ablációs küszöb illetve az ablált felületek morfológiája a két anyag esetében hasonlónak bizonyultak, nanorészecskékből felépülő filmeken végzett kísérletek során mintegy 5-ször magasabb ablációs sebességet figyeltem meg. Az ablációs küszöb és sebesség függött a nanofilmet felépítő részecskék méretétől illetve a párologtatás során alkalmazott nyomástól is.

5. Kísérleti úton megmutattam, hogy UV femtoszekundumos lézerimpulzusokat alkalmazásával acél-minták szubmikronos méretű megmunkálása lehetséges. A szükséges optikai feloldás biztosításához nagy numerikus apertúrájú Schwarzschild-objektívvel képeztem le egy kis méretű amplitúdómaszkot a minták felszínére. Megmutattam, hogy 500 nm-es átmérőjű lyukak fúrhatók a minták felületére, illetve ilyen módon lehetővé válik ~5 μm vastag lemezek átfúrása is. Vastagabb minták esetében előfúrási technikát alkalmazástam [94,100,101].

Az UV femtoszekundumos lézerek nyújtotta lehetőségek kísérleti úton történő demonstrálása céljából nagy hővezető képességű anyagok (pl. fémek, félvezetők) szubmikronos méretű megmunkálási lehetőségeit tanulmányoztam. Ezen anyagok esetében a mikronnál kisebb méretű struktúrák létrehozása hosszú impulzusú lézerekkel az anyagok

besugárzása során fellépő olvadásos folyamatot kísérő jelenségek miatt csak igen korlátozott mértékben vagy egyáltalán nem valósítható meg, amelyet a 4. pontban közölt eredmények is alátámasztanak. Néhány száz nanométeres átmérőjű lyukak különböző típusú fémek felületére történő ablálásához egy egyszerű amplitúdómaszk (12-25 μm átmérőjű kör alakú apertúra) leképezésén alapuló optikai elrendezést használtam. Egy Schwarzschild típusú „reflexiós" objektív segítségével elérhető maximális (kb. 360 nm-es) felbontást kihasználva lehetővé válik az iparilag nagy fontossággal bíró acél mikrométernél nagyobb pontosságú megmunkálása is. Néhány 10 lézerimpulzus alkalmazásával 500 nm-es lyukakat abláltam a minták felületére. Megmutattam, hogy nemcsak felületmegmunkálás válik lehetővé μm-nél nagyobb pontossággal, hanem vékony minták átfúrása is. A vizsgálatok eredménye szerint maximálisan 5 μm-es vastagságú minták átfúrása lehetséges. Vastagabb lemezek esetében azonban – valószínűleg a leképező rendszer nagy numerikus apertúrája és a rövid konfokális tényező miatt – az átfúráshoz megfelelő előfúrási technikák használata szükséges. Egy nagy pontosságú hagyományos (mechanikus) előfúrási technikát alkalmazva szubmikron méretű lyukakat fúrtam 1 mm vastag acél lemezbe.

6. Kísérleti úton bizonyítottam, hogy nagy intenzitású lézerrendszert alkalmazva a felhasznált leképező rendszer a különféle megmunkálási eljárásokra optimalizálható, jelentősen növelve ily módon a folyamat hatásfokát. Megmutattam, hogy a leképező rendszer optimalizálható a különböző felhasználások szabta követelményekhez, mint a) mikron alatti periódusú felületi struktúrák (rácsok, keresztrácsok) létrehozása, b) nagy számú, 300 nm-es minimális átmérőjű lyuk egyidejű fúrása egy speciális interferometrikus technika alkalmazásával, illetve c) mikrométeres méretű lyukakból álló mátrixok ablálása - speciálisan az adott struktúra létrehozására optimalizált - diffrakciós fázismaszkok (DFM) segítségével [99,101,102].

Egy viszonylag egyszerű, nagy optikai feloldást biztosító leképező rendszer felhasználásával (Schwarzschild-objektívvel leképezve egy amplitúdórácsot) mikronnál kisebb periódusú rácsokat abláltam fémek, félvezetők, dieletrikumok, illetve hullámvezető anyagok felületére. Két rácsot keresztezve és maszkként felhasználva keresztrácsok ablálhatók a minták felületére. További kísérletekben Fourier szűrést alkalmaztam, és csak

kiválasztott diffrakciós rendeket használtam fel a képalkotáshoz. Így minimálisan 300 nm-es átmérőjű lyukakból álló mátrixokat sikerült létrehozni, mindössze néhány lövéssel több tízezer lyukat képezve a minta felületére. Olyan mintázatok esetében, ahol a maszk felületének csak viszonylag kis hányada átlátszó, diffrakciós fázismaszkok alkalmazásával jelentősen hatékonyabb megmunkálás érhető el. Kísérletileg bizonyítottam, hogy ilyen fázismaszkok alkalmazásával mikronos méretű struktúrák hozhatók létre különböző fémek felületén. Mindhárom bemutatott eljárás nagy felületek egyidejű megmunkálását teszi lehetővé lényegesen lecsökkentve ezáltal az egységnyi számú lyuk létrehozásához szükséges impulzusok számát.

7. Kidolgoztam egy olyan egylépéses lézeres eljárást, amely kvarc hordozóanyagú fázismaszkok gyors és nagy pontosságú létrehozását teszi lehetővé. A maszkot alkotó pixelek mélységére vonatkozó elvárások enyhítésére immerziós technikát alkalmaztam, melynek segítségével a maszk és a közeg törésmutató-különbsége a pixelmélység által meghatározott értékre illeszthető [99].

Az 5c pontban említett diffrakciós fázismaszkok létrehozása általában igen bonyolult, több lépésből álló, időigényes és nagyon költséges eljárások (pl. maratásos technikák) alkalmazásával valósítható meg. Kísérleti úton bemutattam egy olyan egylépéses lézeres abláción alapuló eljárást, amely lehetővé teszi a maszk hordozóanyagát alkotó kvarc mintáknak egyszerű és gyors megmunkálását, biztosítva a fázismaszk optimális működéséhez szükséges megmunkálási pontosságot. A kvarc hordozóanyag megmunkálása bonyolult feladat, különösen kis mélységű, nagypontosságú, sima struktúrák létrehozása esetén. A fázismaszkok hatékony működéséhez szükséges pixelmélység a $d = \lambda/(2(n_m-n_k))$ egyenlettel adható meg, ahol d a kívánt pixelmélység, λ a maszk megvilágítási hullámhossza (248 nm), n_m a maszk anyagának, n_k pedig a környezet (immerzió) anyagának törésmutatója. Ezen képlet alapján a maszk hatékony működéséhez 244 nm-es mélységű pixelek létrehozása szükséges (kvarc hordozóanyagon, levegőben). Ilyen kis mélységű struktúrák létrehozása igen bonyolult feladatnak bizonyult. A pixelek mélységére vonatkozó elvárások enyhítésére egy immerziós technikát alkalmaztam, amely lehetővé tette a szükséges pixelmélység szabályozását az immerzió törésmutatójának illesztésével. Desztillált vizet használva immerziós folyadékként a kívánt pixelmélység

900 nm. Ilyen mélységű struktúrákat sikerült nagy pontossággal előállítani pixelenként 2 lövéssel, 19 J/cm^2-es energiasűrűségű impulzusokat használva. Az elkészített maszkokat profilométerrel és pásztázó elektronmikroszkóppal vizsgáltam, majd 248 nm-en kísérletileg is teszteltem.

A felsorolt tudományos eredmények hozzájárulnak a KrF-os excimer erősítők fizikai tulajdonságainak tökéletesebb megértéséhez. Kombinálva a szilárdtest lézerek előnyös tulajdonságait az UV excimer erősítők biztosította lehetőségekkel, kis méretű és igen nagy teljesítményű rendszerek létrehozása válik lehetővé. A dolgozatban leírt kis méretű és viszonylag alacsony áron beszerezhető lézerrendszerek új utakat nyithatnak olyan fizikai jelenségek tanulmányozásához, amelyekre korábban csak nagy anyagi ráfordítással, jól felszerelt laboratóriumokban nyílt lehetőség. A kifejlesztett rendszerek és leképezési eljárások segítségével hagyományos eszközökkel nehezen megmunkálható anyagok lézeres megmunkálása is lehetővé válik, akár ipari környezetben is.

List of references

1 Y.R. Shen: “Principles of Nonlinear Optics”, Wiley Interscience New York (1984).

2 M.M. Tilleman and J.H. Jacob: “Short pulse amplification in the presence of absorption”, Appl. Phys. Lett. 50, 121-123 (1987).

3 G. Almasi, S. Szatmari, and P. Simon: “Optimized operation of short-pulse KrF amplifiers by off-axis amplification”, Opt. Comm. 88, 231-329 (1992).

4 D. Strickland and G. Mourou: “Compression of amplified chirped optical pulses”, Opt. Comm. 56, 219-221 (1985).

5 S. Szatmari, F.P. Schäfer, E. Müller-Horsche, and W. Mückenheim: “Hybrid dye-excimer laser system for the generation of 80 fs, 900 GW pulses at 248 nm”, Opt. Comm. 63, 305-309 (1987).

6 S. Szatmari and F.P. Schäfer: “Simplified laser system for the generation of 60 fs pulses at 248 nm”, Opt. Comm. 68, 196-202 (1988).

7 S. Szatmari and F.P. Schäfer: “Picosecond gain dynamics of KrF*”, Appl. Phys B 33, 219-223 (1984).

8 M. Frantz and J.S. Nodvik: “Theory of pulse propagation in a laser amplifier”, J. Appl. Phys. 34, 2346-2350 (1963).

9 P.W. Milloni, R.B. Gibson, and A.J. Taylor: “Ultrashort pulse propagation in KrF laser amplifiers”, J. Opt. Soc. Am. B 5, 1360-1368 (1988).

10 G. Almasi and S. Szatmari: “Optimization of multiple-pass off-axis KrF amplifiers”, Appl. Phys. B 60, 565-570 (1995).

11 H. Jara, K. Boyer, U. Johann, T.S. Luk, I.A. McIntyre, A. McPherson, and C.K. Rhodes: “Dinamic absorption effects in KrF* amplifiers”, Appl. Phys. B 42, 11-15 (1987).

12 S. Szatmari and F.P. Schäfer: “Comparative study of gain dynamics of XeCl and KrF with subpicosecond resolution”, Opt. Soc. of Am. B 4, 1943-1948 (1987).

13 A.J. Taylor, R.B. Gibson, and J.P. Roberts: “Picosecond gain dynamics in KrF amplifiers”, Appl. Phys. Lett. 52, 773-775 (1988).

14 A.J. Taylor, R.B. Gibson, and J.P. Roberts: “2-photon absorption at 248 nm in ultraviolet window materials”, Opt. Lett. 13, 814-816 (1988).

15 P. Simon, H. Gerhardt, and S. Szatmari: “Intensity-dependent loss properties of window materials at 248-nm”, Opt. Lett. 14, 1207-1209 (1989).

16 S. Szatmari, G. Almasi, and P. Simon: “Off-axis amplification scheme for short-pulse amplifiers”, Appl. Phys. B 53, 82-87 (1991).

17 S. Szatmari: “High-brightness ultraviolet excimer lasers”, Appl. Phys. B 58, 211-223 (1994).

18 S. Szatmari and P. Simon: “Interferometric multiplexing scheme for excimer amplifiers”, Opt. Comm. 98, 181-192 (1993).

19 L.A. Rosocha, L.A. Hanlon, J. McLeod, M. Kang, B.L. Kortegaard, M.D. Burrows, and P.S. Bowling: "Aurora multikilojoule Krf laser system prototype for inertial confinement fusion", Fusion Techn. 11, 497-531 (1987).

20 C.J. Pawley, J. Bone, K.J. Kearney, S.P. Obershain, M.S. Pronko, J.D. Sethian, T. Lehecka, A.V. Deniz: CLEO´91, CWF43, Techn. Digest, 276 (1991).

21 I.N. Ross, M.J. Show, C.J. Hooker, M.H. Key, E.C. Harvey, J.M.D. Lister, J.E. Andrew, G.J. Hirst, and P.A. Rodgers: "A high-performance excimer pumped raman laser", Opt. Comm 78, 263-270 (1990).

22 J. Békési, K. Kordás, K. Bali, R. Vajtai, Cs. Beleznai, and L. Nánai: "UV-laser-induced etching and metal seeding on polymers; a surface characterization", App. Surf. Sci. 138-139, 613-616 (1999).

23 K. Kordás, J. Békési, K. Bali, R. Vajtai, L. Nánai, Thomas F. George, and S. Leppävuori: "UV laser-induced liquid phase palladium seeding on polymers", J. Mater. Res. 14, 3690-3694 (1999).

24 K. Kordás, L. Nánai, K. Bali, J. Békési, Thomas F. George, S. Leppävuori, and A. Uusimäki: "Palladium thin film deposition on polyimide by cw Ar+ laser for electroless copper plating", Thin Solid Films 384, 185-188 (2001).

25 K. Kordás, J. Békési, R. Vajtai, L. Nánai, S. Leppävuori, A. Uusimäki, K. Bali, Thomas F. George, and G. Galbács: "Laser-assisted metal deposition from liquid-phase precursors on polymers", Appl. Surf. Sci. 172, 178-189 (2001).

26 K. Kordás, J. Békési, R. Vajtai, M. Jauhianen, J. Remes, A. Uusimäki, S. Leppävuori, T. F. George, and L. Nanai: "Laser-assisted via hole metallization in PCB materials", J. Electron. Mater. 30, 21-24 (2001).

27 R. Vajtai, K. Kordás, B. Q. Wie, J. Békési, S. Leppävouri, T. F. George, and P. M. Ajayan: "Carbon nanotube network growth on palladium seeds", Mat. Sci and Eng. C 19, 271-274 (2002).

28 R. Srinivasan and B. Braren: "Ultraviolet-laser ablation of organic polymers", Chem. Rev. 89, 1303-1316 (1989).

29 M. Bolle, S. Lazare, M. Leblanc, and A. Wilmes: "Submicron periodic structures produced on polymer surfaces with polarized excimer laser ultraviolet-radiation", Appl. Phys. Lett. 60, 674-676 (1992).

30 H.M. Phillips, D.L. Callahan, R. Sauerbrey, G. Szabo, and Z. Bor: "Direct laser ablation of sub-100 nm line structures into polyimide", Appl. Phys. A 54, 158-165 (1992).

31 M. Bolle and S. Lazare: "Submicron periodic structures produced on polymer surfaces with polarized excimer laser ultraviolet-radiation", Appl. Surf. Sci. 65-66, 349-354 (1993).

32 S. Lazare, J. Lopez, and F. Weisbuch: "High-aspect-ratio microdrilling in polymeric materials with intense KrF laser radiation", Appl. Phys. A 69, 1-6 (1999).

33 J. Krüger and W. Kautek: "Femtosecond-pulse laser processing of metallic and semiconducting thin films", SPIE 2403 (1995).

34 C. Momma, S. Nolte, B.N. Chickov, F. von Alvensleben, and A. Tünnermann: "Precise laser ablation with ultrashort pulses", Appl. Surf. Sci. 110, 15-19 (1997).

35 C. Momma, B.N. Chichkov, S. Nolte, F.v. Alvensleben, A. Tünnermann, H. Welling, and B. Wellegehausen: "Short-pulse laser ablation of solid targets", Opt. Commun. 129, 134-142 (1996).

36 H. Kumagai, K. Midorikawa, K. Toyoda, S. Nakamura, T. Okamoto, and M. Obara: “Ablation of polymer films by a femtosecond high-peak-power Ti:sapphire laser at 798 nm”, Appl. Phys. Lett. 65, 1850-1852 (1994).

37 B.N. Chichkov, C. Momma, S. Nolte, F.v. Alvensleben, and A. Tünnermann: “Femtosecond, picosecond and nanosecond laser ablation of solids”, Appl. Phys. A 63, 109-115 (1996).

38 W. Kautek and J. Krüger: “Femtosecond pulse laser ablation of metallic, semiconducting, ceramic, and biological materials”, SPIE 2207, 600-611 (1994).

39 W. Kautek, S. Mitterer, J. Krüger, W. Husinsky, and G. Grabner: “Femtosecond-pulse laser ablation of human corneas”, Appl. Phys. A 58, 513-518 (1994).

40 J. Krüger, W. Kautek, and H. Newesely: “Femtosecond-pulse laser ablation of dental hydroxyapatite and single-crystalline fluoroapatite”, Appl. Phys. A 69 ,403-407 (1999).

41 S. Preuss, A. Demchuk, and M. Stuke: “Sub-picosecond UV laser ablation of metals”, Appl. Phys. A 61, 33-37 (1995).

42 P. Simon and J. Ihlemann: “Machining of submicron structures on metals and semiconductors by ultrashort UV-laser pulses”, Appl. Phys. A 63, 505-508 (1996).

43 K. Chen, J. Ihlemann, P. Simon, I. Baumann, and W. Sohler: “Generation of submicron surface gratings on $LiNbO_3$ by ultrashort UV laser pulses”, Appl. Phys. A 65, 517-518 (1997).

44 P. Simon and J. Ihlemann: “Ablation of submicron structures on metals and semiconductors by femtosecond UV-lasef pulses”, Appl. Surf. Sci. 110, 25-29 (1997).

45 E. Matthias, M. Reichling, J. Siegel, O.W. Käding, S. Petzold, H. Skurk, P. Bizenberger, and E. Neske: “The influence of thermal diffusion on laser ablation of metal films”, Appl. Phys A 58, 129-136 (1994).

46 S. Preuss, E. Mattias, and M. Stuke: “Sub-picosecond UV-laser ablation of Ni films”, Appl. Phys. A 59, 79-82 (1994).

47 B. Wolff-Rottke, J. Ihlemann, H. Schmidt, and A. Scholl: “Influence of the laser spot diameter on photo-ablation rates”, Appl. Phys. A 60, 13-17 (1995).

48 N. Bloembergen: “Pulsed laser interactions with condensed matter”, Mat. Res. Symp. Proc. 51, 3-13 (1986).

49 N. Bloembergen: “Laser-material interactions; fundamentals and applications”, AIP Conf. Proc. 288, 3-10 (1993).

50 S.I. Anisimov, B.L. Kapeliovich, T.L. Perelman: “Electron emission from metal surfaces exposed to ultrashort laser pulses”, Sov. Phys.-JETP 39, 375-377 (1974).

51 P.B. Allen: “Theorie of thermal relaxation of electrons in metals”, Phys. Rev. Lett. 59, 1460-1463 (1987).

52 G.L. Eesley: “Observation of nonequilibrium electron heating in copper” Phys. Rev. Lett. 51, 2140-2143 (1983).

53 G.L. Eesley: “Generation of nonequilibrium electron and lattice temperatures in copper by picosecond laser pulses”, Phys. Rev. B 33, 2144-2151 (1986).

54 J.G. Fujimoto, J.M. Liu, E.P. Ippen, and N. Bloembergen: “Femtosecond laser interaction with metallic tungsten and nonequilibrium electron and lattice temperatures”, Phys. Rev. Lett. 53, 1837-1840 (1984).

55 H.E. Elsayed-Ali, T.B. Norris, M.A. Pessot, and G.A. Mourou: “Time-resolved observation of electron-phonon relaxation in copper”, Phys. Rev.Lett. 58, 1212-1215 (1987).

56 J. Hohlfeld, D. Grosenick, U. Conrad, and E. Matthias: “Femtosecond time-resolved reflection second-harmonic generation on polycrystalline copper”, Appl. Phys. A 60, 137-142 (1995).

57 S.D. Brorson, J.G. Fujimoto, and E.P. Ippen: “Femtosecond electronic heat transport dynamics in thin gold films”, Phys. Rev. Lett. 59, 1962-1965 (1987).

58 C.A. Schuttenmaer, M. Aeschlimann, H.E. Elsayed-Ali, R.J.D. Miller, D.A. Mantell, J. Cao, and Y. Gao: “Time-resolved two-photon photoemission from Cu(111): Energy dependence of electron relaxation”, Phys. Rev. B 50, 8957-8960 (1994).

59 C.-K. Sun, F. Vallée, L.H. Akioli, E.P. Ippen, and J.G. Fujimoto: “Femtosecond tunable measurement of electron thermalization in gold”, Phys. Rev. B 50, 337-348 (1994).

60 J.J. Klossika, U. Gratzke, M. Vicanek, and G. Simon: “Importance of finite speed of heat propagation in metals irradiated by femtosecond laser pulses”, Phys. Rev. B 54, 277-279 (1996).

61 C. Suárez, W.E. Bron, and T. Juhasz: “Dinamics and transport of electronic carriers in thin gold films”, Phys. Rev. Lett. 75, 4536-4539 (1995).

62 J.R. Goldman and J.A. Prybila: “Ultrafast dimamics of laser-excited electron distributions in silicon”, Phys. Rev. Lett. 72, 1364-1367 (1994).

63 U. Hohenester, P. Supancic, P. Kocevar, X.Q. Zhou, W. Kütt, and H. Kurz: “Subpicosecond thermalization and relaxation of highly photoexcited electrons and holes in intrinsic and p-type GaAs and InP”, Phys. Rev. B 47, 233-245 (1993).

64 X.Q. Zhou, H.M. van Driel, and G. Mak: “Femtosecond kinetics of photoexcited carriers in germanium”, Phys. Rev. B 50, 5226-5230 (1994).

65 C.V. Shank, R. Yen, and C. Hirlimann: “Time-resolved reflectivity measurements femtosecond-optical-pulse-induced phase transitions in silicon”, Phys. Rev. Lett. 50, 454-457 (1983).

66 M.C. Downer, R.L. Fork, and C.V. Shank: “Femtosecond imaging of melting and evaporation at a photoexcited silicon surface”, J. Opt. Soc. Am. B2, 595-598 (1985).

67 C.V. Shank, R. Yen, and C. Hirlimann: “Femtosecond-time-resolved surface structural dynamics of optically excited silicon”, Phys. Rev. Lett. 51, 900-902 (1983).

68 D. von der Linde: “Femtosecond time resolved microscopy of laser-induced morphology changes”, Materials Science Forum 173-174, 1-6 (1995).

69 A.E. Faulhaber, B.A. Smith, J.K. Andersen, and J.Z. Zhang: “Femtosecond electronic relaxation dynamics in metal nano-particles: Effects of surface and size confinement”, Mol. Cryst. Liq. Cryst. 283, 25-30 (1996).

70 A. Stella, M. Nisoli, S. De Silvestri, O. Svelto, P. Cheyssac, and R. Kofman: “Size effects in the ultrafast electronic dynamics of metallic tin nanoparticles”, Phys. Rev. B 53, 497-500 (1996).

71 S. Seznec, C. Sauteret, S. Gary, E. Bechir, J.L. Bocher, and A. Migus: “Towards the 10^{19}-10^{20} W/cm^2 regime with amplified chirped pulses - basic limitations and solutions”, Opt. Comm. 87, 331-339 (1992).

72 J.P. Roberts, A.J. Taylor, P.H.Y. Lee, and R.B. Gibson: “High-irradiance 248 nm laser system”, Opt. Lett. 13, 734-736 (1988).

73 A.J. Taylor, C.R. Tallmann, J.P. Roberts, C.S. Lester, T.R. Gosnell, P.H.Y. Lee, and G.A. Kyrala: “High-intensity subpicosecond XeCl laser system”, Opt. Lett. 15, 39-41 (1990).

74 T.S. Luk, A. McPherson, G. Gibson, K. Boyer, and C.K. Rhodes: “Ultrahigh-intensity KrF-star laser system”, Opt. Lett. 14, 1113-1115 (1989).

75 B. Bouma, T.S. Luk, K. Boyer, and C.K. Rhodes: “High-brightness subpicosecond terawatt KrF-asterisk system driven with a frequency-converted self-mode-locked pulse-compressed Tial$_2$O$_3$ laser”, J. Opt. Soc. Am. B 10, 1180-1184 (1993).

76 I.N. Ross, M.J. Show, C.J. Hooker, M.H. Key, E.C. Harvey, J.M.D. Lister, J.E. Andrew, G.J. Hirst, and P.A. Rodgers: “A high-performance excimer pumped raman laser”, Opt. Comm. 78, 263-270 (1990).

77 M.J. Shaw, G. Bialolenker, G.J. Hirst, C.J. Hooker, M.H. Key, A.K. Kidd, J.M.D. Lister, K.E. Hill, G.H.C. New, and D.C. Wilson: “Ultrahigh-brightness laser-beams with low prepulse obtained by stimulated Raman-scattering”, Opt. Lett. 18, 1320-1322 (1993).

78 I.A. McIntire and C.K. Rhodes: “High-power ultrafast excimer lasers”, J.Appl.Phys. 69, 1-19 (1991).

79 S. Szatmari: “Pulse shortening of 5 x 103 by the combined pulse forming of dye oscillators, saturated amplifiers and gated saturable absorbers”, Opt. Quant. Electr. 21, 55-61 (1989).

80 J. Bekesi, G. Marowsky, S. Szatmari, and P. Simon: “A 100 mJ table-top short pulse amplifier for 248 nm using interferometric multiplexing”, Z. für Phys. Chem. 215, 12, 1543-1555 (2001).

81 J. Békési, S. Szatmári, P. Simon, and G. Marowsky: “Table-top KrF amplifier delivering 270 fs output pulses with over 9 W average power at 300 Hz”, Appl. Phys. B 75, 521-524 (2002).

82 P. Simon, H. Gerhardt, and S. Szatmari: “A single-shot autocorrelator for UV femtosecond pulses”, Meas. Sci. Techn. 1, 637-639 (1990).

83 S. Szatmari, G. Kühnle, and P. Simon: “Pulse-compression and traveling-wave excitation scheme using a single dispersive element”, Appl. Opt. 29, 5372-5379 (1990).

84 S. Szatmari, P. Simon, and M. Feuerhake: “Group-velocity-dispersion-compensated propagation of short pulses in dispersive media”, Opt. Lett. 21, 1156-1158 (1996).

85 M. Hentschel, Z. Cheng, F. Krausz, and Ch. Spielmann: “Generation of 0.1-TW optical pulses with a single-stage Ti : sapphire amplifier at a 1-kHz repetition rate”, Appl. Phys. B 70, 161-164 (2000).

86 V. Bagnoud and F. Salin: “Amplifying laser pulses to the terawatt level at a 1-kilohertz repetition rate”, Appl. Phys. B 70, 165-170 (2000).

87 Y. Nabekawa, T. Togashi, T. Sekikawa, S. Watanabe, S. Konno, T. Kojima, S. Fujikawa, and K. Yasui: “All-solid-state high-peak-power Ti:sapphire laser system above 5-kHz repetition rate”, Appl. Phys B 70, 171-179 (2000).

88 J.D. Bonlie, F. Patterson, D. Price, B. White, and P. Springer: "Production of > 10^{21} W/cm^2 from a large-aperture Ti:sapphire laser system", Appl. Phys. B 70, 155-160 (2000).

89 Y. Nabekawa, K. Kondo, N. Sarukura, K. Sajiki, and S. Watanabe: "Terawatt KrF/Ti:sapphire hybrid laser system", Opt. Lett. 18, 1922-1924 (1993).

90 Y. Nabekawa, K. Sajiki, D. Yoshitomi, K. Kondo, and S. Watanabe: "High-repetition-rate high-average-power 300-fs KrF/Ti:sapphire hybrid laser", Opt. Lett. 21, 647-649 (1996).

91 Y. Nabekawa, D. Yashitomi, T. Sekikawa, and S. Watanabe: "50 W average-power, 480-fs KrF excimer laser with gated gain amplification", Opt. Lett. 26, 807-809 (2001).

92 A. McPherson, B. D. Thompson, A. B. Borisov, K. Boyer, and C. K. Rhodes: "Multiphoton-induced X-ray-emission at 4-5 Kev from Xe atoms with multiple core vacancies", Nature 370, 631-634 (1994).

93 U. Teubner, I. Uschmann, P. Gibbon, D. Altenbernd, E. Förster, T. Feurer, W. Theobald, R. Sauerbrey, G. Hirst, M. H. Key, J. Lister, and D. Neely: "Absorption and hot electron production by high intensity femtosecond UV-laser pulses in solid targets", Phys. Rev E 54, 4167-4177 (1996).

94 P. Simon, J. Bekesi, C. Dölle, J.-H. Klein-Wiele, and S. Szatmari: "Ultraviolet femtosecond pulses: Key technology for sub-micron machining and efficient XUV pulse generation", Appl. Phys. B 74, 189-192 (2002).

95 C. Dölle, C. Reinhardt, P. Simon, and B. Wellegehausen: "Generation of 100 μJ pulses at 82.8 nm by frequency tripling of sub-picosecond KrF laser radiation", Appl. Phys. B 75, 629-634 (2002).

96 S. Kranzusch and K. Mann: "Spectral characterization of EUV radiation emitted from a laser-irradiated gas puff target", Opt. Comm. 200, 223-230 (2001).

97 K. Kordás, S. Leppävouri, J. Békési, L. Nánai, J. Remes, R. Vajtai, and S. Szatmári: "Nickel deposition on porous silicon utilizing lasers", Appl. Surf. Sci. 186, 232-236 (2002).

98 I. Zergioti, S. Mailis, N.A. Vainos, P. Papakonstantinou, C. Kalpouzos, C.P. Grigoropoulos, and C. Fotakis: "Microdeposition of metal and oxide structures using ultrashort laser pulses", Appl. Phys. A 66, 579-582 (1998).

99 J. Békési, J.-H. Klein-Wiele, D. Schäfer, J. Ihlemann, P. Simon: "Surface texturing of metals with sub-micron precision using a short pulse UV laser", SPIE 4830, 497-500 (2003).

100 J. Bekesi, P. Simon, and J. Ihlemann: "Femtosecond UV-laser processing of sub-micron holes in steel foils", CLEO Europe 2000, Conf. Dig. 390 (2000).

101 J. Bekesi, J.-H. Klein-Wiele, and P. Simon: "Efficient submicron processing of metals with femtosecond UV pulses", Appl. Phys. A 76, 3, 355-357 (2003).

102 P. Simon, J. Ihlemann, J.-H. Klein-Wiele, and J. Bekesi: "Ablation of solid targets with UV femtosecond pulses", SPIE 3822, 118-124 (1999).

103 M. Feuerhake, J.-H. Klein-Wiele, G. Marowsky, and P. Simon: "Dynamic ablation studies of sub-micron gratings on metals with sub-picosecond time resolution", Appl. Phys. A 67, 603-606 (1998).

104 M. Feuerhake: "Entwicklung specieller Methoden für die Anwendung ultrakurzer UV-Laserpulse in der Materialforschung", Cuvillier Verlag Göttingen (PhD dissertation) (1997).

105 J. Ihlemann, B. Wolff-Rottke, and P. Simon: “Nanosecond and femtosecond excimer laser ablation of fused-silica”, Appl. Phys. A 54, 363-368 (1992).

106 J. Bekesi, R. Vajtai, and P. Simon, L.B. Kiss: “Subpicosecond excimer laser ablation of thick gold film of ultra-fine particles generated by a gas deposition technique”, Appl. Phys. A 69, 385-387 (1999).

107 C.H. Hayashi, R. Uyeda, and A. Tasaki (Eds.): “Ultra-fine particles”, Exploratory Science and Technology (Noyes Publications, Westwood, NJ) (1997).

108 J. Söderlund, L.B. Kiss, G.A. Niklasson, and C.G. Granqvist: “Lognormal size distributions in particle growth processes without coagulation”, Phys. Rev. Lett. 80, 2386-2388 (1998).

109 S. Okuda and F. Tang: “Thermal stability of nanocrystalline gold prepared by gas deposition method”, Nanostruct. Mater. 6, 585-588 (1995).

110 E. Ochs, A. Seeger, H. Stoll, L.B. Kiss, and J. Söderlund: “Electrical noise in nanocrystalline films”, Phys. Status Solidi A 168, 9-10 (1998).

111 S.D. Brorson, J.G. Fujimoto, and E.P. Ippen: “Femtosecond Electronic Heat-Transport Dynamics in Thin Gold-Films”, Phys. Rev. Lett. 59, 1962-1965 (1987).

112 K. Sokolowski-Tinten, J. Bialkowski, A. Cavalleri, D. von den Linde, A. Oparin, J. Meyer-ter-Vehn, and S.I. Anisimov: “Transient states of matter during short pulse laser ablation”, Phys. Rev. Lett. 81, 224-227 (1998).

113 J. Güdde, J. Hohlfeld, J.G. Müller, and E. Matthias: “Damage threshold dependence on electron-phonon coupling in Au and Ni films”, Appl. Surf. Sci. 129, 40-45 (1998).

114 X. Zhu, A.Y. Naumov, D.M. Villeneuve, and P.B. Corkum: “Influence of laser parameters and material properties on micro drilling with femtosecond laser pulses”, Appl. Phys. A 69, 367-371 (1999).

115 X. Zhu, D.M. Villeneuve, A.Y. Naumov, S. Nikumb, and P.B. Corkum: “Experimental study of drilling sub-10 mu m holes in thin metal foils with femtosecond laser pulses”, Appl. Surf. Sci. 152, 138-148 (1999).

116 P.P. Pronko, S.K. Dutta, J. Squier, J.V. Rudd, D. Du, and G. Mourou: “Machining of submicron holes using a femtosecond laser at 800-nm”, Opt. Comm. 114, 106-110 (1995).

117 K: Venkatakrishnan, B. Tan, and B.K.A. Ngoi: “Submicron holes in copper thin film directly ablated using femtosecond pulsed laser”, Opt. Eng. 40, 2892-2893 (2001).

118 S. Nolte, C. Momma, G. Kamlage, A. Ostendorf, C. Fallnich, F. von Alvensleben, and H. Welling: “Polarization effects in ultrashort-pulse laser drilling”, Appl. Phys. A 68, 563-567 (1999).

119 W. Kautek and J. Krüger: “Femtosecond-pulse laser microstructuring of semiconducting materials”, Mat. Sci.Forum 173-174, 17-22 (1995).

120 S. Shoji and S. Katawa: “Photofabrication of three-dimensional photonic crystals by multibeam laser interference into a photopolymerizable resin”, Appl. Phys. Lett. 76, 19, 2668-2670 (2000).

121 J.R. Lankard and G. Wolbold: “Excimer laser ablation of polyimide in a manufacturing facility”, Appl. Phys. A 54, 355-359 (1992).

122 F. Beinhorn, J Ihlemann, P. Simon, and G. Marowsky: “Sub-µm grating formation in Ta_2O_5-waveguides by femtosecond UV-laser ablation”, E-MRS 1998 spring meeting (1998).

123 T. Kondo, S. Matsuo, S. Juodkazis, and H. Misawa: “Femtosecond laser interference technique with diffractive beam splitter for fabrication of three-dimensional photonic crystals”, Appl. Phys. Lett. 79, 725-727 (2001).

124 D. Schäfer, J. Ihlemann, G. Marowsky, B. Burghardt, and M. Timm: “Multifacet Kinoforms for KrF excimer laser”, DOMO 2000, Quebec City, Canada, 18-22.06.2000.

125 F. Wyrowski: “Diffractive optical-elements - iterative calculation of quantized, blazed phase structures”, J. Opt. Soc. Am. A 7. 961-969 (1990).

126 J. Tururen and F. Wyrowski: “Diffractive optics for industrial and commercial application”, Academie Verlag Berlin (1997).

127 G.P. Behrmann and M.T. Duignan: “Excimer laser micromachining for rapid fabrication of diffractive optical elements”, Appl. Opt. 36, 4666-4674 (1997).

128 N.A. Vainos, S. Mailis, S. Pissadakis, L. Boutsikaris, P.J.M. Parmiter, P. Dainty, and T.J. Hall: “Excimer laser use for microetching computer-generated holographic structures”, Appl. Opt. 35, 6304-6319 (1996).

129 X.M. Wang, J.R. Leger, and R.H. Rediker: “Rapid fabrication of diffractive optical elements by use of image-based excimer laser ablation”, Appl. Opt. 36, 4660-4665 (1997).

130 D. Schäfer, J. Ihlemann, K. Mann, and G. Marowsky: “Excimer laser patterned dielectric masks for the fabrication of diffractive optical elements by laser ablation”, Appl. Phys. A 69, 319-322 (1999).

131 J. Ihlemann and D. Schäfer: “Fabrication of diffractive phase elements for the UV-range by laser ablation patterning of dielectric layers”, Appl. Surf. Sci. 197, 856-861 (2002).

132 S. Mailis, L. Boutsikaris, N.A. Vainos, C. Xirouhaki, G. Vasiliou, N. Garawal, G. Kiriakidis, and H. Fritzsche: “Holographic recording in indium-oxide (In2O3) and indium-tin-oxide(In2O3:Sn) thin films”, Appl. Phys. Lett. 69, 2459-2461 (1996).

133 T.V. Kononenko, V.I. Konov, S.M. Pimenov, A.M. Prokhorov, V.S. Pavelyev, V.A. Soifer, B. Lüdge, and M. Duparré: SPIE 4426, 128 (2002).

134 J. Ihlemann, S. Müller, S. Puschmann, D. Schäfer, M. Wei, J. Li, and P.R. Herman: “Fabrication of submicron gratings in fused silica by F2-laser ablation”, Appl. Phys. A (2002) (in press).

Acknowledgement

This study has been carried out at the Laser Laboratorium Göttingen (LLG, Germany) in the scope of a collaboration work between the LLG and the Department of Experimental Physics at the University of Szeged, Hungary.

At this point I would like to thank all those friends and colleges whom without this thesis could not be realized.

First of all I wish to express my gratitude to my supervisor and group leader Dr. Péter Simon who gave me the continuous support and attention during these years to perform this research. The ideas he gave me during the interesting and fruitful discussions greatly contributed to the progress each stages of my work.

I also want to acknowledge Professor Dr. Gerd Marowsky (Laser Laboratorium Göttingen, Germany), who gave me the opportunity to work in the Laser Laboratorium Göttingen.

I am deeply indebted to Professor Dr. Sándor Szatmári (Department of Experimental Physics, University of Szeged, Hungary) who introduced me into this part of the physics and followed my research, giving valuable advises and support during the whole period of time.

I am very grateful to Dr. Jürgen Ihlemann; he was always ready to answer my questions, especially in the field material processing.

Special thanks to Professor László Nánai and Dr. Róbert Vajtai who helped me to take the very first steps in the field of laser physics. I would like to thank my friend and college Dr. Krisztián Kordás for his cooperation, help, and for his valuable contribution to my research. I would also like to thank my coworkers Christopher Dölle and Jan-Hendrik Klein-Wiele for their valuable contribution and technical assistance.

I am very grateful to Professor Imre Hevesi for revising and commenting on the manuscripts.

I wish to thank my family for the education, regard and patience. Finally, my deepest gratitude goes to my wife, who always stood by, and helped me with love and devotion during this beautiful and exciting period of my life.